ISSN: 1949-2421 (Print), 1947-3826 (Online) Volume 1, Number 1, August 2009

Communications and Network

通信與網路 國際期刊

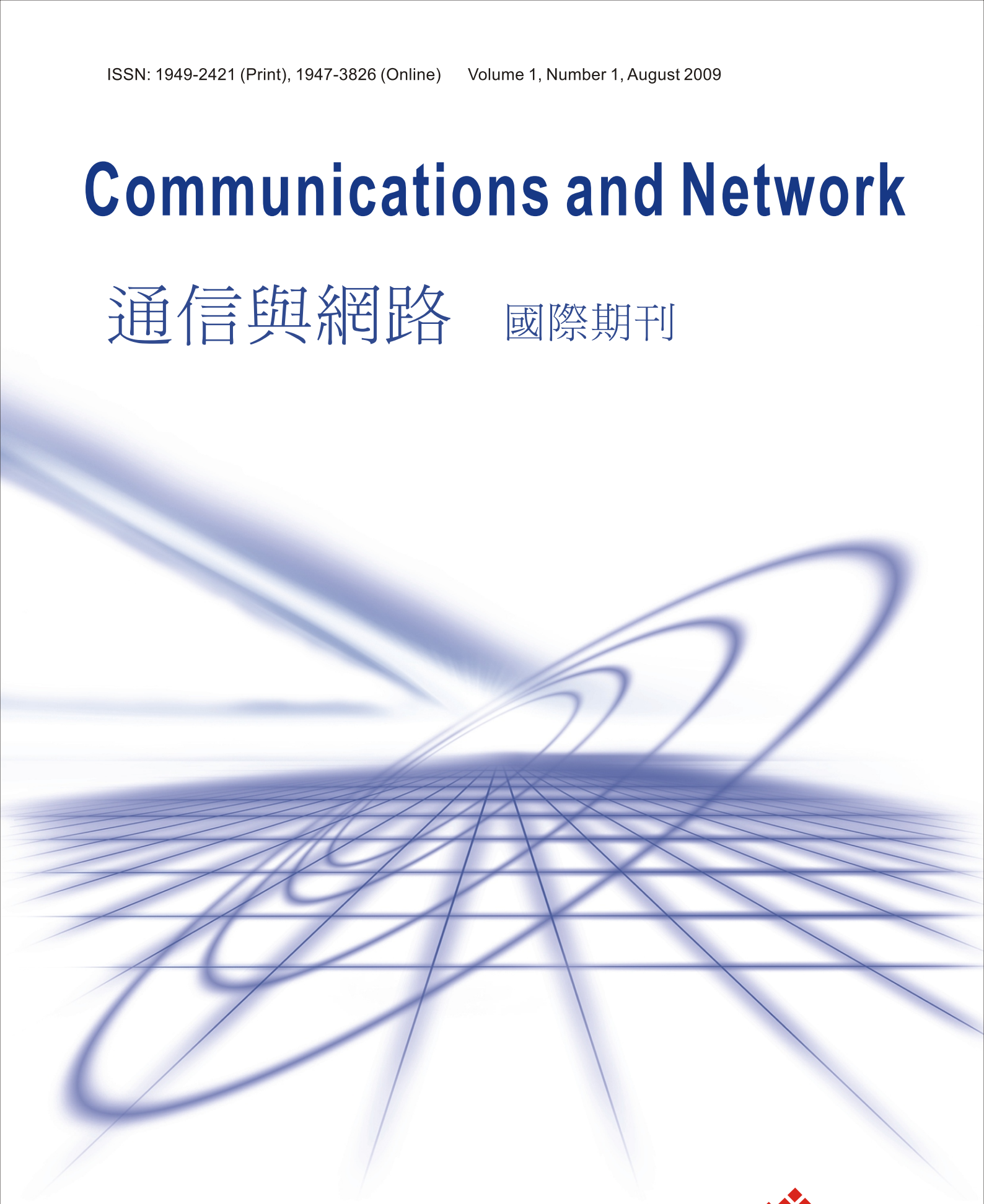

www.scirp.org/journal/cn

Scientific Research

Journal Editorial Board

ISSN: 1949-2421 (Print) ISSN: 1947-3826 (Online)

http://www.scirp.org/journal/cn

Communications and Network, 2009, 01-56
http://www.scirp.org/journal/cn

Scientific Research

Table of Contents

Communications and Network (CN)

Journal Information

SUBSCRIPTIONS

Communications and Network (Online at Scientific Research Publishing, www.SciRP.org) is published quarterly by Scientific Research Publishing, Inc., USA.

E-mail: cn@scirp.org

Subscription rates: Volume 1 2009
Print: $50 per copy.
Electronic: free, available on www.SciRP.org.
To subscribe, please contact Journals Subscriptions Department, E-mail: cn@scirp.org

Sample copies: If you are interested in subscribing, you may obtain a free sample copy by contacting Scientific Research Publishing, Inc. at the above address.

SERVICES

Advertisements
Advertisement Sales Department, E-mail: cn@scirp.org

Reprints (minimum quantity 100 copies)
Reprints Co-ordinator, Scientific Research Publishing, Inc., USA.
E-mail: cn@scirp.org

COPYRIGHT

PRODUCTION INFORMATION

For manuscripts that have been accepted for publication, please contact:
E-mail: cn@scirp.org

Communications and Network, 2009, 01-05
doi:10.4236/cn.2009.11001 Published Online August 2009 (http://www.scirp.org/journal/cn)

The Comparisonal Analysis of the Concept of Rectangular and Hexagonal Pilot in OFDM

Jeanbaptiste YAMINDI[1], Muqing WU[2]
Broadband Communication Network Laboratory, Beijing University of Posts and Telecommunications, Beijing, China
Email: [1]jbyamindi@yahoo.fr, [2]wumuqing@bupt.edu.cn

Abstract: Channel estimation in coherent OFDM by inserting pilot-symbols into two-dimensional time- frequency lattice is a promising candidate for improving channel transmission capacity in future wireless communication systems. This paper proposes a new Cartesian mathematical concept of the Hexagonal Pilot Pattern, Hexagonal Pilot with Virtual and Rectangular Pilot Pattern. The main focus of this work is to compare between the two pilots and by virtue of simulation conclusion which of the two pilots yields a better performance.

Keywords: hexagonal pilot pattern, hexagonal pilot with virtual, rectangular pilot pattern, estimation, interpolation, extrapolation

1. Introduction

One of the most important techniques applied in Physical layer of WiMAX is known as Orthogonal Frequency -Division Multiplexing (OFDM), which is the system for data transmission and the support for channel estimation and synchronization.

Many authors proposed the concept of pilot tones to interpolate the channel response in [1] and [2], recently some literature proposed methods of pilot symbols apart from the existing equi-spaced pilot pattern for OFDM system as described in [4] and [5]. In this paper, we are focusing on a specific pilot subcarriers by doing the analytical description and structural pilot of the two different pilots known as Hexagonal and Rectangular.

The rest of this paper is organized as follows: The graphical representation of Rectangular and Hexagonal Pilot Pattern in Section 2, The Simulation results of the Hexagonal Pilot Pattern, Hexagonal with Virtual and Rectangular Pilot Pattern in Section 3. The analytical evaluation and comparison in Section 4 and the paper is concluded in Section 5.

2. The Rectangular and Hexagonal Pilot Pattern Representative

2.1 The Rectangular Pilot Grid Representation

The rectangular Pilot grid matrix can be expressed by

$$\Pi_{rect} = \begin{pmatrix} \Delta p_f & 0 \\ 0 & \Delta p_t \end{pmatrix} \quad (1)$$

where Δp_f is the distance in frequency and Δp_t is the distance in time direction and this rectangular matrix can be written as:

$$V = V_{RECT} = \begin{pmatrix} N_t & 0 \\ 0 & N_f \end{pmatrix} \quad (2)$$

where N_f subcarriers in the frequency direction and N the OFDM symbols in the time direction that can be arranged as a set given by:

$$P = \left\{ (n_1', k_1'), (n_2', k_2'), ..., \left(n_{N_{tap}}', k_{N_{tap}}'\right) \right\}. \quad (3)$$

And the number of pilot subcarriers in the input block is expressed by

$$N_p = \left\lceil \frac{N_f N_t}{|\det \Pi_{rect}|} \right\rceil \quad (4)$$

The estimation of block contains $\left\lceil \frac{N_t}{\Delta p_t} \right\rceil$ number of OFDM symbols each hosting $\left\lceil \frac{N_f}{\Delta p_f} \right\rceil$ pilot positions.

The total number of pilot positions $N_{p,rect}$ of a rectangular pilot grid is given by

$$N_{p,rect} = \left\lceil \frac{N_f}{\Delta p_f} \right\rceil \times \left\lceil \frac{N_t}{\Delta p_t} \right\rceil \quad (5)$$

Under the condition of

$$N_t < \frac{1}{2(1+N_2) f_{D,\max}} \text{ and } N_f < \frac{N}{CP}. \quad (6)$$

The graphical representation of the rectangular pilot in the coordinate system is depicted below.

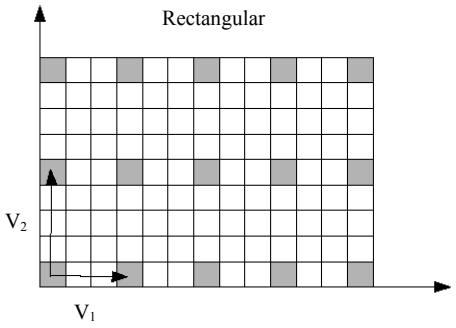

Figure 1. The rectangular pilot grid.

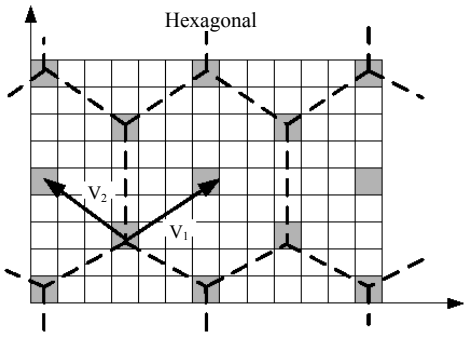

Figure 2. The hexagonal pilot grid.

2.2 Modification of Rectangular Pilot Pattern

The application of Cognitive Radio for optimum channel estimation by using pilot pattern can affect the frequency band by the presence of Licensed User. The pilot pattern in the presence of Licensed User can be classified according to the Bandwidth into Narrowband Licensed User and Wideband Licensed User.

1) The Narrowband Licensed User: It can exchange easily the position of the pilot symbols with data parts. This exchange of the pilot subcarrier is connected to the data subcarrier of the previous or the next subcarrier and we assumed that the application of pilot symbols in the channel estimation process cannot modify the pilot symbol but only one data subcarrier and can lose some throughput so this narrowband interference is depicted.

2) The Wideband Licensed: There are similarities in the process of Narrowband and Wideband, the only difference is on the edge location of the License User signal exchange of two pilot subcarriers with data subcarriers and the number of deactivated subcarriers is depending upon the Licensed User Band.

2.3 The Hexagonal Pilot Grid Representation

The implementation of Hexagonal Pilot is facilitated by the Virtual Pilot in reducing the Pilot Density by the annulment of u_2 =0 and the Pilot Density becomes dp=| u_1 v_2| and the representation of the structure is according to the Hexagonal Pilot spacing. The equation of the Hexagonal Pilot is expressed by

$$V = V_H = \begin{pmatrix} N_t & -N_t \\ N_f & N_f \end{pmatrix} \quad \textbf{(7)}$$

And graphically it can be represented as below.

In both of the two different types of Pilot, the Inter-Symbol Interference is still a big challenge during the process of pilot transmission. This challenge can be resolved by the following techniques.

2.4 Modification of Hexagonal Pilot Pattern

The process of exchanging the position of the pilot subcarrier with the data subcarrier connected to the previous subcarrier and the next subcarrier is done by exchanging the pilot subcarrier with the data subcarrier which lies in the previous subcarrier or in the next subcarrier. By doing this we can still be able to keep the pilot symbols to be used in the channel estimation process, but on the other side we will have to sacrifice one data subcarrier and thus lossing some throughput. This process is almost similar as in Rectangular process, the only difference, at the receiver, the received pilot symbols are processed using the iterative algorithm in order to obtain the virtual pilot symbol. This iterative algorithm introduces the concept of interpolation option which is applied via simple averaging between the received shifted pilot symbols and the received pilot symbols. The received shifted pilot symbols in the next subcarrier or extrapolating the virtual pilot symbols on the position of the Licensed User by the effect of the received pilot symbols.

2.5 The Virtual Pilot

The Virtual Pilot symbols are iterative of the interpolation of contiguous pilot to the position of the virtual. It is defined at first by the pilot spacing in frequency axis, which is smaller than the channel coherence bandwidth, and the second is pilot spacing in time axis, which is smaller than the channel coherence time on the initial computation of the received pilot symbols for each OFDM. The OFDM frames during each time slots, and subcarriers in the frequency domain respectively. Note that this operation must be processed only at the pilot positions as:

$$\hat{H}_{k',n'} = H_{k',n'} + \frac{N_{k',n'}}{S_{k',n'}} \forall \{k',n'\} \in \Omega \quad \textbf{(8)}$$

$S_{k,n}$ is the transmitted symbol, the indexes k, and n indicates the position of each pilot symbol within the OFDM frame. The symbol W is the set of pilot positions within the OFDM sub frame.

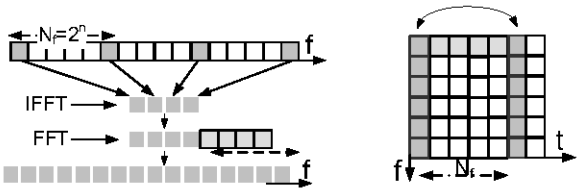

Figure 3. Interpolations processes, (a) the DFT principle for frequency domain interpolation, (b) linear interpolation process over the time domain.

These Interpolations processes are illustrated by the figure above.

By the initial computation of the channel the value can be linearly interpolated i.e. the value of the virtual pilot symbols is expressed by

$$\hat{H}_{n',k'} = \frac{1}{2}\left[\hat{H}_{n',k'-1} + \hat{H}_{n',k'+1}\right] \quad \textbf{(9)}$$

Where $\hat{H}_{n',k'-1}$ and $\hat{H}_{n',k'+1}$ are initial estimates respectively of the previous and the next pilot at this point. The iterative algorithm processing of pilot symbols is expressed as

for n'=1: (p'−1) N_f

for k'=1: (q'−1) N_f

$$\hat{H}_{n',k'} = \frac{1}{2}\left[\hat{H}_{n',k'-1} + \hat{H}_{n',k'+1}\right]$$

end

end

$$p' = 1,2,...\left\lceil \frac{N_c}{N_f} \right\rceil \quad \text{and} \quad q' = 1,2,...\left\lceil \frac{N_s}{N_t} \right\rceil$$

Where N_f, N_t, N_s, N_c are respectively the distance between pilots in frequency direction, distance between pilots in time direction, number of subcarriers and the number of OFDM symbols per frame.

At the positions close to Licensed User's carriers. The estimation process itself is divided into two parts assume that it we can assume that it can also be divided into more than two depending on the number of Licensed User that exist.

The first part is the upper part and the second is the lower part. The part of the spectrum which is occupied in the middle is discarded and not included in the channel estimation calculation. By deploying the virtual pilot concept on certain case for good understanding let us illustrate by band less than 2x distance of pilots, the edge effect of the sliding window can be avoided, hence better channel estimate can be obtained, while the Channel Transfer Function at the position of the Licensed User are discarded.

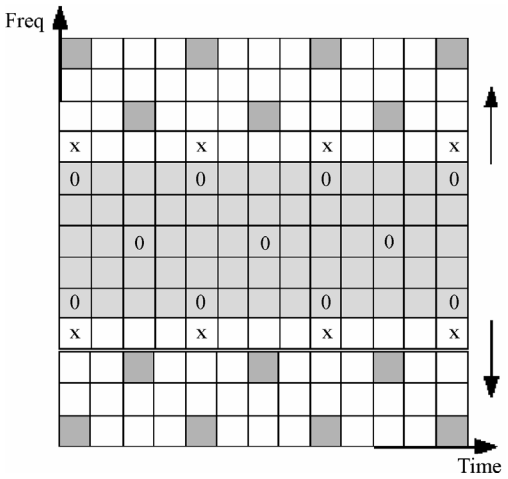

Figure 4. Transmitted modified hexagonal pilot pattern for the wideband Licensed User case.

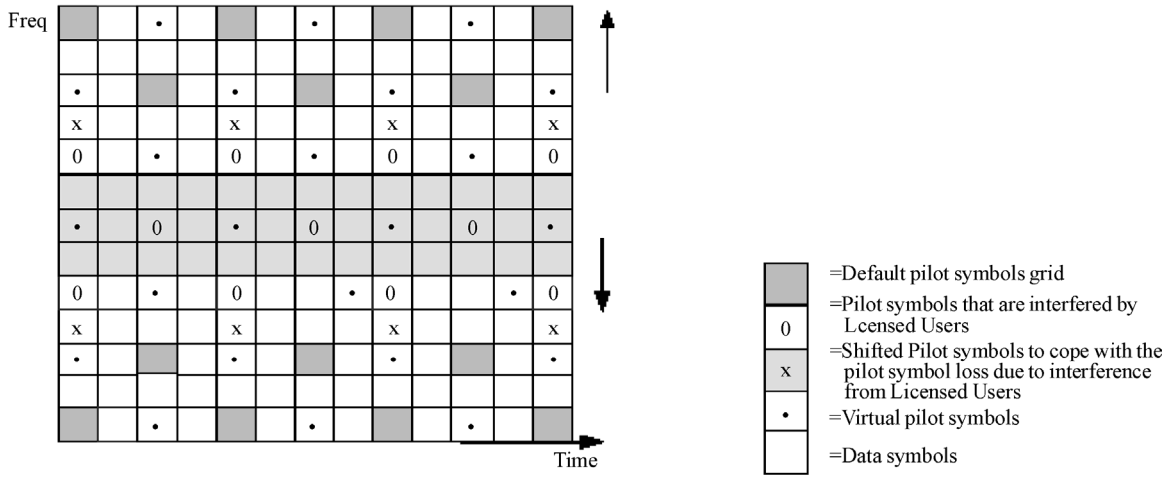

Figure 5. Receiver side hexagonal pilot pattern with virtual pilot symbols obtained from the iterative processing algorithm.

By deploying this scheme, we can still estimate the channel optimally despite of the unloaded subcarriers caused by the Licensed User.

At the receiver, the received pilot symbols are processed using the Iterative algorithm to obtain the virtual pilot symbols like in the case of the Narrowband Interference. The scheme itself can be seen in Figure 5.

3. The Simulation Result

In this section we are going to do the comparison between the Hexagonal Pilot Pattern with the Rectangular Pilot Pattern and the Hexagonal Pilot with Virtual symbols with the Rectangular Pilot Pattern with Virtual Pilot symbols distribution. For this simulation, we consider the different parameters such as subcarriers per OFDM symbol, OFDM symbols per estimator frame and the distance of subcarriers in the frequency direction and the time direction, the total number of pilot subcarrier positions is excessive to be directly employed in the estimation of all the channel transfer factors.

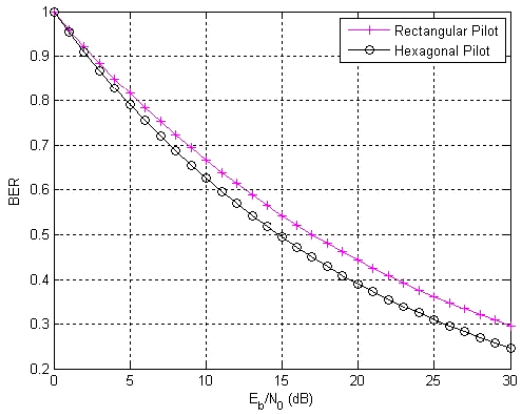

Figure 6. The performance comparison of hexagonal pilot pattern and the rectangular pilot pattern in function of BER in Eb/N0 in dB scale.

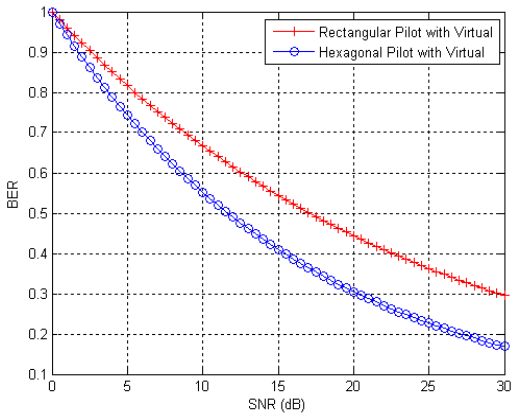

Figure 7. The performance comparison of Hexagonal Pilot with Virtual symbols compared with Rectangular Pilot Pattern with Virtual Pilot symbols in function of BER in SNR in dB scale.

4. The Comparisonal Analysis

This section presents the main goal of our work by making the analytical evaluation and comparison of the Hexagonal Pilot Pattern and Rectangular Pilot Pattern.

Analysis of the effect of having several scattered interferences and the effectiveness of the proposed hexagonal pilot pattern scheme to combat the interferences effects. Here we analyze the effect of increasing number of interferers by using the iterative and exploiting the channel coherence bandwidth property.

The Hexagonal Pilot Pattern is more complicated to be implemented using the 2xl-D Wiener filter. The implementation of Hexagonal Pilot Pattern is easy due to the technique of Hexagonal Pilot Pattern with the Virtual Pilot symbols.

The Hexagonal Pilot Pattern is an optimum sampling. It is the main method which requires 13.3% less samples when compared to the Rectangular Pilot Pattern that represents the same signal and gives a better BER performance, and therefore the Hexagonal Pilot Pattern performs better and more efficient sampling mechanism when compared to the Rectangular Pilot Pattern as shown in Figure 6.

The performance comparison of the Hexagonal Pattern with virtual pilots at high SNR outperforms significantly the other three, the Rectangular, Hexagonal, and Hexagonal with Virtual pilots and interpolation/extrapolation process.

Rectangular Pattern with Virtual Pilots outperforms the Rectangular and Hexagonal Pilot Pattern at high SNR, while at low SNR performance degradation occurs caused by the error of interpolating the noisy initial channel estimates.

5. Conclusions

The simulation shows that Hexagonal Pilot design is better than the rectangular and other pilot design patterns. This better performance is due to the effect of increasing number of interferers by using the iterative and exploiting the channel coherence bandwidth property of Hexagonal Pilot. The technique of combining with Virtual Pilot symbols in the low SNR space is due to the error caused by interpolation of the heavily noisy pilots and the Cognitive Radio is the best support of perform channel estimation. The Hexagonal Pilot is become the most useful in the system of Wireless Network communication thank to the compatibility of the Hexagonal Pilot and Network configuration.

6. Acknowledgments

Special thanks to Engineers from Beijing University of Posts and Telecommunications: Mr. Fenta Adinew, Mr. Mala Umar, my professor Wu Mu-qing and Beijing University of Posts and Telecommunications for the assistance.

REFERENCES

[1] YIN Q Y, ZHANG Y, DING L. A new space diversity technology. Transaction of Xi' an Jiaotong University. 2005, 39(6): 551-557.

[2] SENDONARIS A, ERKIP E, AAZHANG B. Increasing uplink capacity via user cooperation diversity. IEEE Int. Symp. on Information Theory, Cambridge, MA, Aug. 1998, 156.

[3] HASNA M O, ALOUINI M S. Harmonic mean and end-to-end performance of transmission systems with relays. IEEE Transactions on Communications, January 2004, 52(1).

[4] HASNA M O, ALOUINI M S. Performance analysis of two-hop relayed transmission over Rayleigh fading channels. In Proc. IEEE Vehicular Technology Conf. (VTC'02), Vancouver, BC, Canada, Sept. 2002, 1992-1996.

[5] GRADSHTEYN I S, RYZHIK I M. Table of Integrals, Series, and Products.San Diego, CA: Academic Press, fifth ed., 1994.

[6] ABRAMOWITZ M, STEGUN I A. Handbook of mathematical functions with formulas, graphs, and mathematical tables. NY: Dover Publications, New York, 9th Edition, 1970.

[7] IKKI S, AHMED M H, Performance analysis of cooperative diversity wireless networks over nakagamim fading channel. IEEE Communications Letters, April 2007, 11(4).

[8] SIMON M K, ALOUINI M S. Digital communication over fading channels: A unified approach to performance analysis. NEW York: Wiley, 2000.

Communications and Network, 2009, 06-19
doi:10.4236/cn.2009.11002 Published Online August 2009 (http://www.scirp.org/journal/cn)

Principle of Link Evaluation

Jinbao ZHANG[1], Hongming ZHENG[2], Zhenhui TAN[3], Yueyun CHEN[4]
[1,3]*Institution of Electronics and Information, Beijing JiaoTong University, Beijing, China*
[2]*Intel China Research Centre, Beijing, China*
[4]*University of Science and Technology Beijing, Beijing, China*
Email: [1]*jinbao.zhang@gmail.com*, [2]*hongming.zheng@intel.com*, [3]*zhhtan@ bjtu.edu.cn*, [4]*chenyy@ies.ustb.edu.cn*

Abstract: Link Evaluation (LE) is proposed in system evaluation to reduce complexity. It is important to practical systems also for link adaptation. Current algorithms for link evaluation are developed by simulation method, lacking of theoretical description. Although they provide some good accuracy for some scenarios, all of them are not universal. With the help of information theory, a universal principle of link evaluation is proposed in this paper, which explains current algorithms and leads to a universal algorithm to implement link evaluation for common wireless transmissions.

This paper proposes an Extended Received Block Information Rate (ERBIR) algorithm for universal link evaluation, which is extended from current RBIR algorithm by the help of the principle presented in this paper. Mainly the universality and accuracy are highlighted. Simulation results verify all the algorithms mentioned in this paper. Both the principle and ERBIR are validated by simulation with various wireless scenarios.

Keywords: link evaluation, information theory, MIMO, OFDM, WiMAX II

1. Introduction

LINK evaluation aims to estimate the instant performance of transmissions for given channel status information (CSI), by a computational model with reasonable complexity.

As to wireless transmissions, due to macro and micro fading, the CSI is varying within both time and frequency domains, so fading will influence wireless transmission a lot. Consequently, link evaluation is significant to analysis and design for real wireless system.

For that the instant performance for wireless transmissions under given CSI can be computed by link evaluation quite simply and accurately, it is possible for System Level Simulation (SLS) to hold down real coding and decoding procedures, reducing a lot of complexity [1]. Meanwhile, wireless system can dynamically choose the proper transmitting mode with the help of link evaluation to enhance system performance, which is referred as link adaptation [1-3].

Accuracy is very important to link evaluation. For SLS, obviously it directly determines if the simulation results are reasonable. For link adaptation, accurate link evaluation ensures that the transmitting mode is selected properly. If the link performance is overestimated, the transmitter will always choose a mode which can not be supported by instantaneous CSI, introducing too much transmission error; while the link performance is underestimated, potential gain exists. Both of the above cases will lead to loss of system performance.

Currently, there are several algorithms to implement link evaluation, like Effective Exponential Signal-to-noise-ratio Mapping (EESM) [4], Mean Instantaneous Capacity (MIC) [5], Received Block Information Rate (RBIR) [6] and Mean Mutual Information per Bit (MMIB) [7]. Here RBIR and MMIB are Mean mutual Information (MI) based algorithms, with different RBIR calculation. Unfortunately, all of them are just simulation methods, lacking of theoretical analysis. Moreover, when it comes to nonlinear detection, there are still problems with all these algorithms mentioned above.

This paper proposes a universal principle for link evaluation, and extends RBIR to common wireless scenarios. Firstly, background knowledge is introduced, including models of common transmission and link evaluation; a universal principle for link evaluation is proposed; and then RBIR is extended to ERBIR with the help of this principle. Simulation results show that the proposed algorithm provides more accuracy for different scenarios. Finally, conclusions are drawn.

2. Background

To analyze link evaluation, common models of wireless transmission and link evaluation are presented in this section.

2.1 Common Model of Wireless Transmission

Following assumptions are made for analysis in this paper.

1) Multi-Input Multi-Output Orthogonal Frequency Division Multiplexing (MIMO OFDM) is adopted in wireless transmission. NT and NR indicate the number of

transmitting and receiving antennas respectively. NOFDM indicates the number of subcarriers in OFDM symbol. As to SISO or single subcarrier case, there is NT= NR=1 or NOFDM=1;

2) Perfect channel estimation and the channel response is flat fading on each OFDM subcarrier;

3) Detection with interference cancellation is not taken into consideration;

4) Source bits are random and iterative coding and decoding is used, for example Turbo;

5) Link evaluation interests in statistical BLock Error Rate (BLER) [1] for given CSI. Let Nu indicate the number of subcarriers mapped to the interested wireless resource block.

6) Modulation and Coding Scheme (MCS) levels are set to QPSK 1/2, QPSK 3/4, 16QAM 1/2, 16QAM 3/4, 64QAM 1/2, 64QAM 2/3, 64QAM 3/4 and 64QAM 5/6, referred to MCS 1~8 respectively.

Disregarding subcarrier index, MIMO OFDM transmission can be written as [2]

$$\boldsymbol{y} = \boldsymbol{H}_c\boldsymbol{F}\boldsymbol{x} + \boldsymbol{H}_I\boldsymbol{x}_I + \boldsymbol{n} \quad (1)$$

where $\boldsymbol{y}$ is $N_R\times1$ dimensional receiving signal vector; $\boldsymbol{H}_c$ is $N_R\times N_T$ channel response matrix; $\boldsymbol{F}$ is $N_T\times N_S$ transmitting precoding matrix; $\boldsymbol{x}$ is $N_S\times1$ independent transmitting signal vector, with unit transmitting power; $\boldsymbol{H}_I$ is $N_R\times N_S$ interference channel response matrix; $\boldsymbol{x}_I$ is $N_S\times1$ independent interference signal vector, with unit transmitting power; $\boldsymbol{n}$ is $N_R\times1$ AWGN vector, which is consisted of N_R independent AWGN elements with power of $\sigma2$ (given SNR, $\sigma2=10^{-SNR/10}$). So this MIMO OFDM transmission is effective to

$$\begin{gathered}\boldsymbol{y} = \boldsymbol{H}_e\boldsymbol{x} + \boldsymbol{n}_e;\ \|\boldsymbol{H}_e\|_F^2 = 1;\ \mathrm{E}\{\boldsymbol{x}\boldsymbol{x}^H\} = \boldsymbol{I}(N_S);\\ \boldsymbol{H}_e = \boldsymbol{T}^{-1}\boldsymbol{H}_c\boldsymbol{F} / \|\boldsymbol{T}^{-1}\boldsymbol{H}_c\boldsymbol{F}\|_F;\ \boldsymbol{T}\boldsymbol{T}^H = \boldsymbol{H}_I\boldsymbol{H}_I^H + \sigma^2\boldsymbol{I}(N_R);\\ \mathrm{E}\{\boldsymbol{n}_e\boldsymbol{n}_e^H\} = \sigma_e^2\boldsymbol{I}(N_R);\ \sigma_e^2 = 1 / \|\boldsymbol{T}^{-1}\boldsymbol{H}_c\boldsymbol{F}\|_F^2 \quad (2)\end{gathered}$$

See Appendix A for a proof. Here $\boldsymbol{H}e$ is $N_R\times N_S$ effective channel response matrix. $\|\boldsymbol{A}\|_F$ refers to the Frobenius norm of matrix $\boldsymbol{A}$. $\boldsymbol{I}(N)$ is N×N identity matrix. σ_e^2 is effective AWGN power.

2.2 Detection Algorithms

Consider detection at receiver. There are mainly three types of detection algorithms [8]: Minimum Mean Square Error (MMSE), Zero Forcing (ZF) and Maximum Likelihood (ML). Since MMSE and ZF are homologous, MMSE and ML are emphasized, and ZF is similar to MMSE.

For MMSE detection, the output signal is

$$\boldsymbol{x}_o = \boldsymbol{M}\boldsymbol{y} = \boldsymbol{M}(\boldsymbol{H}_e\boldsymbol{x} + \boldsymbol{n}_e) \quad (3)$$

where $\boldsymbol{M}$ is $N_S\times N_R$ dimensional equalizing matrix. Then this MIMO transmission can be divided into NS SISO transmissions with NS different Output Signal to Interference and Noise Ratio (OSINR), written as γ_i, i = 1, 2, … , NS.

$$x_o(i) = x(i) + n(i) \quad (4)$$

where $n(i)$ is independent AWGN with power of $1/\gamma_i$. For MMSE, $\boldsymbol{M}$ and OSINR for each output signal are detailed in Appendix B.

As to ML detection, let $\Omega(\boldsymbol{x})$ mean the vector aggregate of every possible value of $\boldsymbol{x}$, then output signal is

$$\mathbf{x}_o = \arg\max_{x\in\Omega(x)} \frac{P(\mathbf{y}\mid\mathbf{x})}{\sum_{q\in\Omega(x)} P(\mathbf{q})P(\mathbf{y}\mid\mathbf{q})} \quad (5)$$

Note that there is an exception of Alamouti MIMO. Only one symbol can be transmitted by each transmission for Alamouti MIMO. This Alamouti MIMO is effective to SISO transmission [8], where n is AWGN with power of σ^2.

$$y = \|\boldsymbol{H}\|F^2x + n \quad (6)$$

For both linear and nonlinear detection, the iterative coding and decoding is adopted. The implementation of such system is described in reference [9].

2.3 Common Model of Link Evaluation

There have been already several algorithms to carry out link evaluation, such like EESM, MIC, RBIR and MMIB. Common model of link evaluation is shown as the following figure.

Link evaluation follows these procedures:

Step 1: Channel estimation outputs CSI of this block;

Step 2: According link evaluation algorithm, indicator S_k for the k^{th} subcarrier is computed from CSI;

Step 3: Compute average S with all these indicators;

Step 4: Once the relation between S and $BLER$ of this block is definite, $BLER$ is computed from S, without Monte Carlo simulation.

If necessary, Packet Error Rate (PER), Frame Error Rate (FER) and so on can be computed also, using bellowing equation [1]

$$PER \text{ or } FER = 1 - \prod_{m=1}^{N_B}(1 - BLER_m) \quad (7)$$

Here N_B is the number of blocks in the packet or frame.

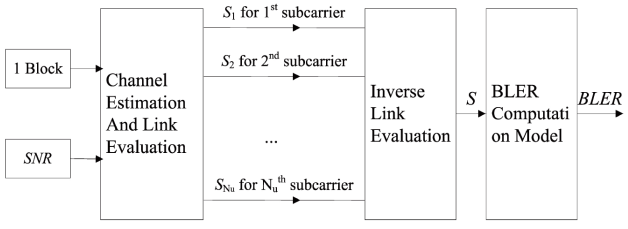

Figure 1. Common model of link evaluation

3. Universal Principle of Link Evaluation

EESM, MIC, RBIR and MMIB algorithms are developed by simulation method, without strict theoretical deduction. A universal principle of link evaluation is proposed in this section, making them clear.

3.1 Mathematical Model of Link Evaluation

Since link evaluation mainly interests in BLER for given CSI, it should be deduced from block transmission error rate. As the transmitting block is consisted of N_u subcarriers, the uncoded BLER is computed as

$$BLER_u = 1 - \prod_{k=1}^{N_u} \left(1 - SER_k\right) = 1 - \left(1 - SER_{\text{ave}}\right)^{N_u} \quad (8)$$

Here $BLER_{\text{u}}$ means the statistical uncoded BLER. With the help of information theory, there is *lemma* 1: When MCS of the transmitted block is given, *BLER* is one-one to the $BLER_{\text{u}}$. Written as

$$BLER = \text{MappingFunction}_{\text{MCS}}(BLER_{\text{u}}) \quad (9)$$

See Appendix C for a proof. Then the universal principle of link evaluation is described as: find a unified and accurate indicator to reflect the BLER of the current transmitting block.

3.2 Current Link Evaluations

Generally speaking, there are three indicators which reflect the Symbol Error Rate (SER) under given CSI. They are OSINR, Channel Capacity and MI. Current link evaluation falls into EESM, MIC and RBIR algorithms.

3.2.1 EESM Link Evaluation

As γ_k is known, the Chernoff limit of SER_k is approximated as [8]

$$SER_k \approx \exp(-\gamma k/\beta) \quad (10)$$

where β is MCS related parameter. Use the mathematical average of all SER_k to approximate SER_{ave} of this block, then

$$SER_{\text{ave}} \approx \frac{1}{N_u}\sum_{k=1}^{N_u} SER_k \approx \exp\left(-\gamma_{\text{eff}}/\beta\right) \quad (11)$$

Then there is

$$BLER_{\text{u}} = 1 - \left[1 - \exp\left(-\gamma_{\text{eff}}/\beta\right)\right]^{N_u} \quad (12)$$

And

$$\gamma_{\text{eff}} = -\beta \log_{\text{e}}\left(\frac{1}{N_u}\sum_{k=1}^{N_u}\exp\left(-\gamma_k/\beta\right)\right) \quad (13)$$

The effective OSINR defined by (13) is exactly the same as in EESM [4]. The mapping function between γ_{eff} and *BLER*, and parameter β can be decided by training data from Link Level Simulation (LLS).

3.2.2 MIC Link Evaluation

Since channel response $\boldsymbol{H}_k$ and *SNR* is given, the channel capacity for this transmission is

$$C_k = \frac{1}{N_R}\log_2\left|\boldsymbol{I} + \frac{1}{\sigma^2}\boldsymbol{H}_k\boldsymbol{H}_k^{H}\right| \quad (14)$$

Here $|\boldsymbol{A}|$ means the determinant of matrix $\boldsymbol{A}$. The capacity decides the lower bound of SER_k [5], so

$$SER_{\text{k}} \le 1 - 2^{AC_k + B} \quad (15)$$

where A and B are MCS related parameters. Then

$$BLER_{\text{u}} \approx 1 - \prod_{k=1}^{N_u}\left(1 - SER_k\right) = 1 - \prod_{k=1}^{N_u}\left(1 - 1 + 2^{AC_k + B}\right)$$

$$= 1 - 2^{A\sum_{k=1}^{N_u} C_k + N_u B} = 1 - 2^{AN_u MIC + N_u B} = 1 - 2^{A_1 MIC + A_2} \quad (16)$$

Here A_1 and A_2 are optimized by training data from LLS, and $A1$ and $A2$ are listed in Table 2. Then,

$$MIC = \frac{1}{N_u}\sum_{k=1}^{N_u} C_k \quad (17)$$

This is exactly the same as [5]. Then MIC is validated by the same LLS data base in previous section.

3.2.3 RBIR Link Evaluation

Let the transmitting symbol is x, and the receiving symbol is y after distortion by fading channel and pollution by interference and noise. Then MI for this symbol is [10]

$$MI = \mathop{\text{E}}_{x,y}\left\{\log_2\frac{P(x,y)}{P(x)P(y)}\right\} = \mathop{\text{E}}_{x,y}\left\{\log_2\left[1 - SER(x,y)\right]\right\} \quad (18)$$

Then consider RBIR of the uncoded block

Table 1. Parameter for EESM

MIMO Scheme	Parameter Values (MCS 1~8)
SISO	[1.6000 1.6000 4.8000 4.9000 12.1000 19.1000 22.1000 25.1000]
2×2 Alamouti	[1.6000 1.6000 4.8000 4.9000 12.1000 19.1000 22.1000 25.1000]
2×2 SM	[1.2000 1.3000 4.3000 7.1000 13.1000 21.1000 22.1000 28.1000]

Table 2. Parameter for MIC

Prameter	Parameter Values
A_1	[−14.3852 −9.1091 −8.0877 −6.6149 −5.2316 −4.3936 −5.3627 −3.3814]
A_2	[18.2503 17.8563 20.6476 24.411 20.5704 22.0257 28.8529 19.8698]

$$RBIR_{\mathrm{u}} = \frac{1}{\mathrm{N_u}}\sum_{k=1}^{\mathrm{N_u}} MI_k = \frac{1}{\mathrm{N_u}}\sum_{k=1}^{\mathrm{N_u}} \mathrm{E}_{x_k,y_k}\left\{\log_2\left[1-SER\left(x_k,y_k\right)\right]\right\} \quad (19)$$

Generally speaking, for multi-subcarriers transmission, each symbol is transmitted independently. So

$$\begin{aligned} RBIR_{\mathrm{u}} &= \mathrm{E}_{\{x_k,y_k\}}\left\{\frac{1}{\mathrm{N_u}}\sum_{k=1}^{\mathrm{N_u}}\log_2\left[1-SER\left(x_k,y_k\right)\right]\right\} \\ &= \mathrm{E}_{\{x_k,y_k\}}\left\{\frac{1}{\mathrm{N_u}}\log_2\prod_{k=1}^{\mathrm{N_u}}\left[1-SER\left(x_k,y_k\right)\right]\right\} \\ &= \mathrm{E}_{\{x_k,y_k\}}\left\{\frac{1}{\mathrm{N_u}}\log_2 BLER_{\mathrm{u}}\left(\{x_k,y_k\}\right)\right\} \end{aligned} \quad (20)$$

Reconsider the uncoded $BLER_{\mathrm{u}}$

$$RBIR_{\mathrm{u}} = \mathrm{E}_{\{x_k,y_k\}}\left\{RBIR_{\mathrm{u}}\left(\{x_k,y_k\}\right)\right\} \quad (21)$$

Compare (20) and (21), $RBIR_{\mathrm{u}}$ is one-one to $RBIR_{\mathrm{u}}$ of the block. From *lemma* 1, *BLER* is one-one to *RBIR*u also.

According to different calculations of $RBIR_{\mathrm{u}}$, there are RBIR and MMIB algorithms.

As to RBIR, $RBIR_{\mathrm{u}}$ is computed by OSINR [6], so there are same problems as EESM, not to support ML scenario. But as it is strictly in accordance to the BLER model, RBIR shows better accuracy than EESM.

As to MMIB, computation of $RBIR_{\mathrm{u}}$ is from bit Log-wise Likelihood Ratio (LLR), which is presented in reference [7], so it can support ML scenario. Also as it is strictly in accordance to the BLER model, MMIB should be of the same accuracy as RBIR.

3.3. Principle of Link Evaluation

There are two parts for the principle of link evaluation, based on previous analysis. Firstly, BLER should be computed from the BLER model presented before; secondly, RBIR is the most accurate indicator of BLER computation.

4. Erbir Link Evaluation

Previous analysis shows that RBIR reflects the transmission error probability accurately. Thus link evaluation should be based on mean mutual information indicator. This section proposes extension for RBIR, obtaining a unified and accurate ERBIR algorithm for common wireless transmissions.

4.1 General Procedures of ERBIR Link Evaluation

ERBIR link evaluation is implemented following these steps:

1) Get instantaneous CSI from channel estimation. The interested CSI indicators are channel response matrixes of [$\boldsymbol{H}_1$, $\boldsymbol{H}_2$, …, $\boldsymbol{H}_{\mathrm{Nu}}$], and AWGN power of *SNR*;

2) According to detection algorithms, normalized MI 'I_k' for each transmitted symbol is computed;

3) Average all the I_k in this block to get RBIR;

4) Finally BLER is computed from RBIR according to RBIR to BLER mapping function which is obtained by LLS.

In Step (2), computation is the same as conventional RBIR when it comes to MMSE detection. While ML detection is used, it is not the same. So ERBIR is extension for RBIR, which is homologous to RBIR and MMIB, but providing more accurate and universal RBIR computation.

4.2 Normalized MI Computation for SISO

For SISO transmission, the received symbol is

$$y = Hx + n;\ \mathrm{E}\{xx^*\} = 1;\ \mathrm{E}\{nn^*\} = 10^{-SNR/10} \quad (22)$$

The normalized MI 'I' is computed as

$$\begin{aligned} I &= \frac{1}{\log_2 \mathrm{N_{QAM}}}\mathrm{E}_{x,y}\left\{\log_2\frac{P(x,y)}{P(x)P(y)}\right\} \\ &= \frac{1}{\log_2 \mathrm{N_{QAM}}} SISO\_\mathrm{MI}\left(10^{-SNR/10}/|H|^2\right) \end{aligned} \quad (23)$$

See Appendix D for details. And the following figure shows that it is accurate for a random selected channel 'H'.

4.3. Normalized MI Computation for MIMO

To simplify analysis, take 2×2 MIMO as example, and analysis is similar for MIMO with more antennas. The received symbol is

$$\begin{bmatrix} y_1 \\ y_2 \end{bmatrix} = \begin{bmatrix} h_{11} & h_{12} \\ h_{21} & h_{22} \end{bmatrix}\begin{bmatrix} x_1 \\ x_2 \end{bmatrix} + \begin{bmatrix} n_1 \\ n_2 \end{bmatrix} \quad (24)$$

Here assume

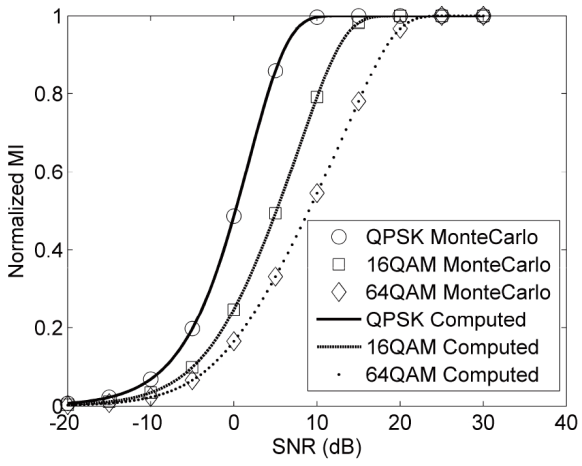

Figure 2. SISO normalized MI computation

$$\left\| \begin{bmatrix} h_{11} & h_{12} \\ h_{21} & h_{22} \end{bmatrix} \right\|_{\mathrm{F}} = 1 \quad \begin{cases} \mathrm{E}\left\{x_1 x_1^*\right\} = \mathrm{E}\left\{x_2 x_2^*\right\} = 1 \\ \mathrm{E}\left\{n_1 n_1^*\right\} \mathrm{E}\left\{n_2 n_2^*\right\} = 10^{-SNR/10} \end{cases}$$

$$\mathrm{E}\left\{x_1 x_2^*\right\} = 0 \quad \mathrm{E}\left\{n_1 n_2^*\right\} = 0 \tag{25}$$

The normalized MI 'I_1' for the 1st transmitted symbol is computed as

$$I_1 = \frac{1}{\log_2 \mathrm{N_{QAM}}} \mathop{\mathrm{E}}_{x,y} \left\{ \log_2 \frac{P(x_1, \boldsymbol{y})}{P(\boldsymbol{x}) P(\boldsymbol{y})} \right\}$$

$$= \frac{\mathrm{VectorMI}\left(\boldsymbol{H}, SNR\right) - \mathrm{SISO\_MI}\left(\dfrac{10^{-SNR/10}}{\left|h_{12}\right|^2 + \left|h_{22}\right|^2} \right)}{\log_2 \mathrm{N_{QAM}}} \tag{26}$$

Similarly

$$I_2 = \frac{\mathrm{VectorMI}\left(\boldsymbol{H}, SNR\right) - SISO\_\mathrm{MI}\left(\dfrac{10^{-SNR/10}}{\left|h_{11}\right|^2 + \left|h_{21}\right|^2} \right)}{\log_2 \mathrm{N_{QAM}}}$$

(27)

This computation is detailed in Appendix E. And Figure 3 shows that it is accurate for a random selected channel '$\boldsymbol{H}$'.

5. Validation by Static LLS

All algorithms for link evaluation are validated by static LLS, based on WiMAX II down link.

5.1 Simulation Configurations

Static LLS means that the CSI is given, and then the block transmission is trialed by a lot of Monte Carlo simulations to get real BLER under the given CSI. Then the CSI and real BLER are stored. The CSI is processed by link evaluation to get computed BLER. Obviously the more different between real and computed BLER, the worse the link evaluation algorithm is. Configuration of static LLS is shown as the following Table 3.

Table 3. Configuration of static LLS

Parameters	Configuration
MIMO Scheme	SISO/MIMO 2×2 Spatial Multiplexing (SM) Vertical EnCoding (VEC)/MIMO 2×2 SM Horizontal EnCoding (HEC)
Frame Duration	5 ms
Bandwidth	10 MHz; NOFDM = 1024
Channel Estimation	Ideal
Channel Model	70% ITU PedB 3kmph and 30% ITU VA 30kmph
Channel Coding	Turbo
MCS	MCS 5
Block Size	16 subcarrier × 6 symbol (Subcarriers are continuously allocated in wireless resource block)
Detection	MMSE/ML
Link Adaptation	Disable

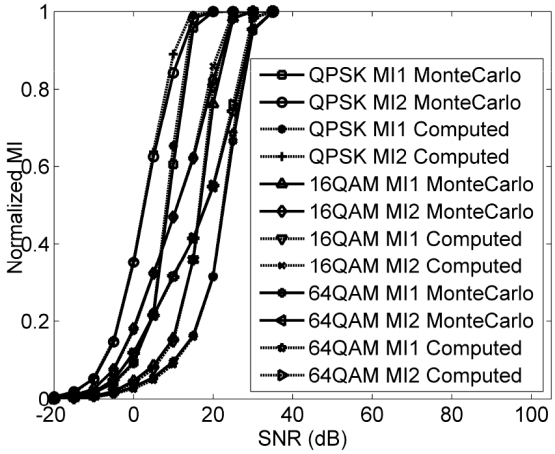

Figure 3. 2×2 Normalized MI computation

5.2 Simulation Results

In these results figures, the black bold curve is the computing function of indicator *S* to BLER obtained by training data from LLS; and the marked point is plotted with real *BLER* and *S* computed by the adopted link evaluation algorithm. The more deviation between the marked point and black bold curve, the more inaccurate is the link evaluation algorithm.

5.2.1 Link Evaluation for SISO

Firstly, SISO transmission with MMSE detection is validated by different link evaluation algorithms, shown as the following figures.

From these figures, it is obvious that although EESM, MIC and MMIB algorithms can obtain accurate enough link evaluation. RBIR/ERBIR algorithm can obtain most accurate link evaluation for simulated transmission Monte Carlo trials. Moreover, RBIR/ERBIR algorithm doesn't need any channel related tuning parameters, which makes RBIR/ERBIR more universal.

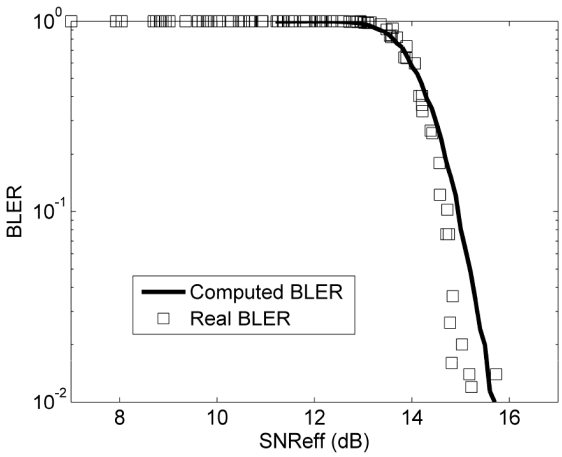

Figure 4(a). EESM LE for SISO MMSE

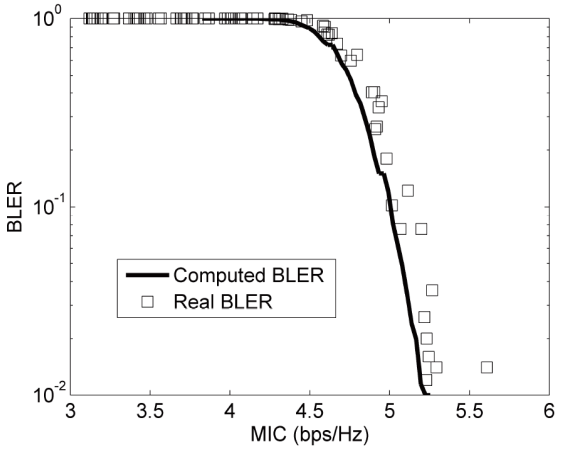

Figure 4(b). MIC LE for SISO MMSE

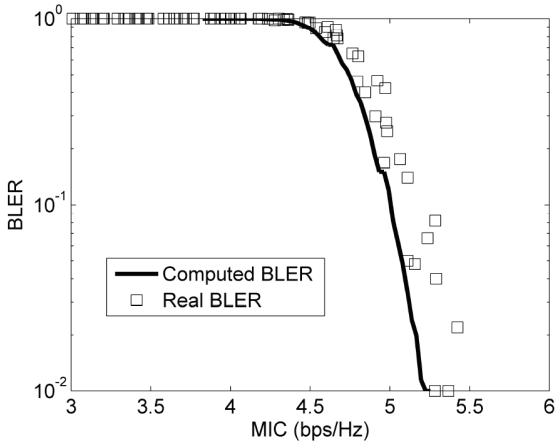

Figure 5(a). MIC LE for SISO ML

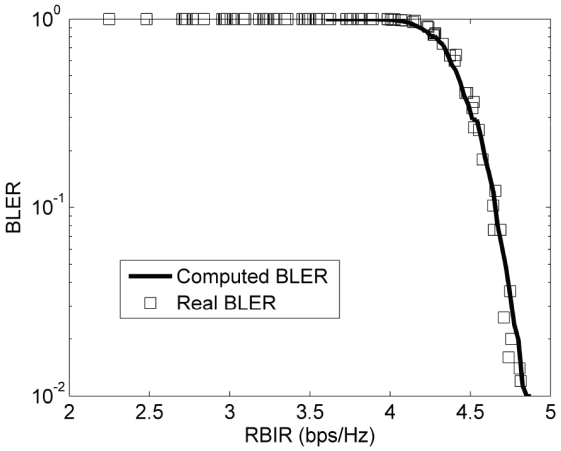

Figure 4(c). RBIR/ERBIR LE for SISO MMSE

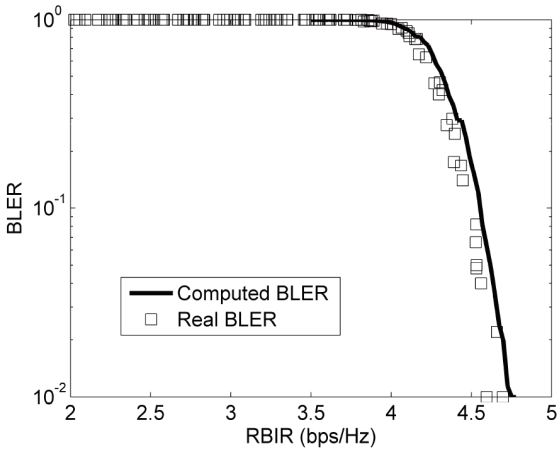

Figure 5(b). MMIB LE for SISO ML

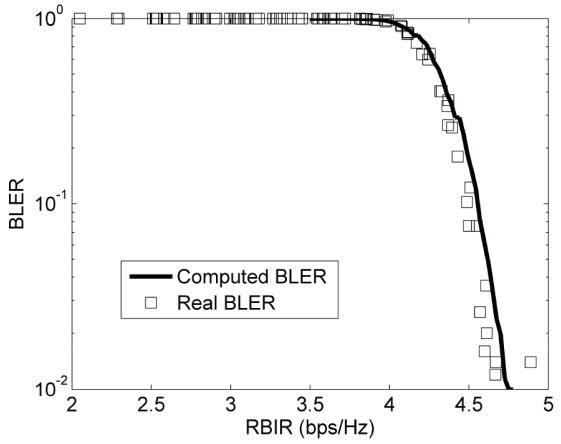

Figure 4(d). MMIB LE for SISO MMSE

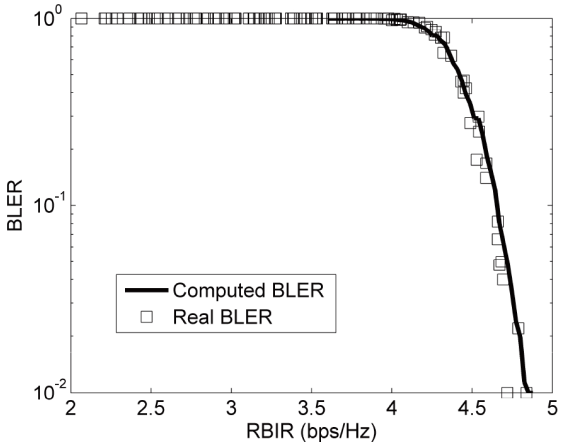

Figure 5(c). ERBIR LE for SISO ML

Then, SISO transmission with ML detection is validated by different link evaluation algorithms, shown as the following figures.

From these figures, it is obvious that EESM and RBIR algorithm is invalid, and MIC algorithm shows too much inaccuracy. MMIB and ERBIR are of accurate enough

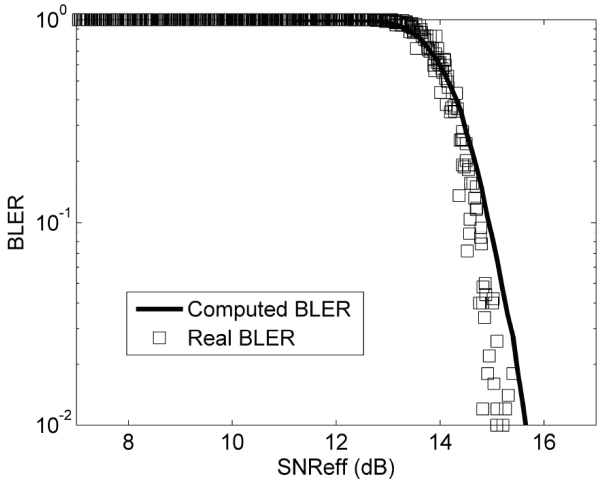

Figure 6(a). EESM LE for VEC MMSE

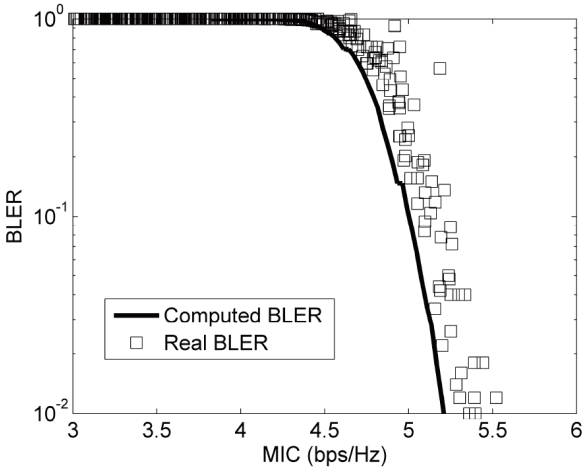

Figure 6(b). MIC LE for VEC MMSE

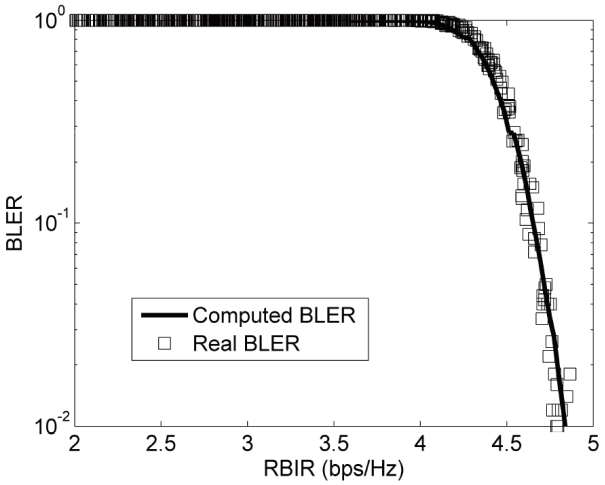

Figure 6(c). RBIR/ERBIR LE for VEC MMSE

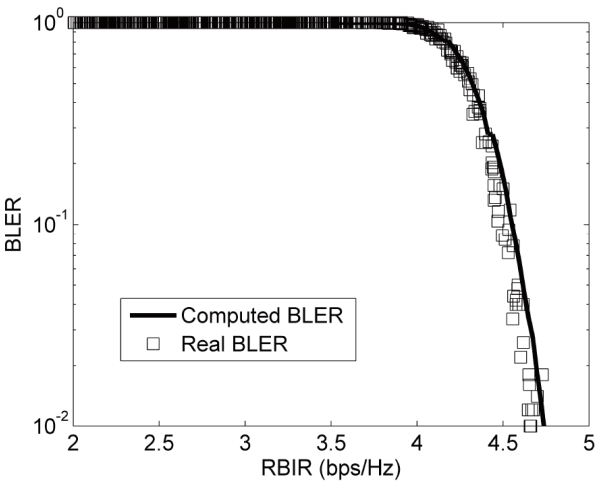

Figure 6(d). MMIB LE for VEC MMSE

results, while ERBIR is a bit better than MMIB.

Here simulation results also validate the theoretical conclusions. MIC chooses the upper bound of SER, so all the real BLER are bigger than computed BLER. And MMIB uses approximation in MI computation, so there is a little inaccuracy.

5.2.2 Link Evaluation for VEC

Firstly, VEC transmission with MMSE detection is validated by different link evaluation algorithms, shown as the following figures.

These figures show that although EESM, MIC and MMIB algorithms can also obtain quite accurate link evaluation, RBIR/ERBIR algorithm is the most accurate. Moreover, RBIR/ERBIR algorithm doesn't need any channel related tuning parameters.

Then, VEC transmission with ML detection is validated by different link evaluation algorithms, shown as the following figures.

Figure 7(a), Figure 7(b) and Figure 7(c) show that EESM and RBIR algorithms are invalid, and MIC and MMIB algorithms show too much inaccuracy. ERBIR algorithm betters the accuracy of link evaluation for VEC ML transmissions a lot, although there is still some inaccuracy.

Here, MIC algorithm only provides the upper bound of wireless transmissions, and it is of the worst accuracy. Although MMIB seems a little better, for the sake of limited parameters presented in reference [7], the RBIR is not very accurate, so MMIB shows worse results than ERBIR.

5.2.3 Link Evaluation for HEC

Firstly, HEC transmission with MMSE detection is validated by different link evaluation algorithms, shown as the following figures.

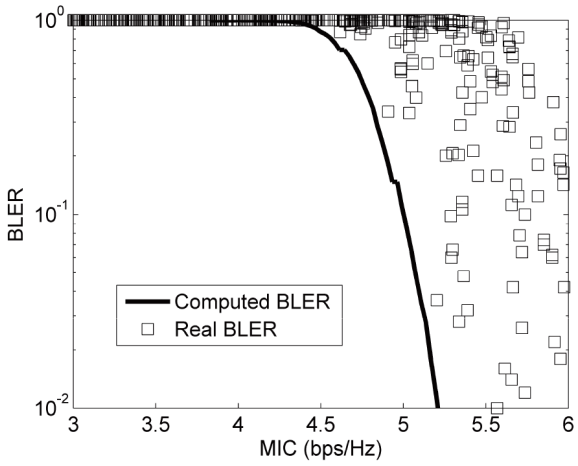

Figure 7(a). MIC LE for VEC ML

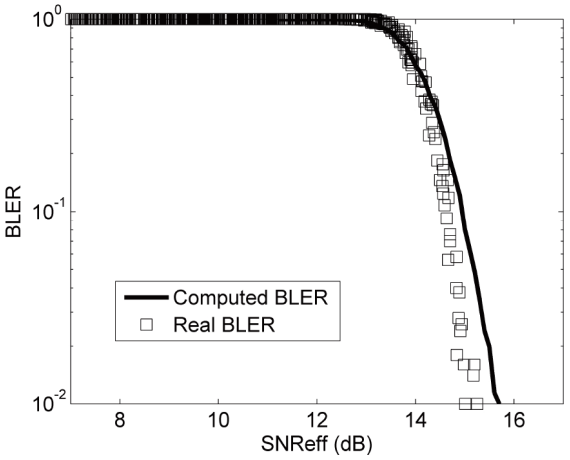

Figure 8(a). EESM LE for HEC MMSE

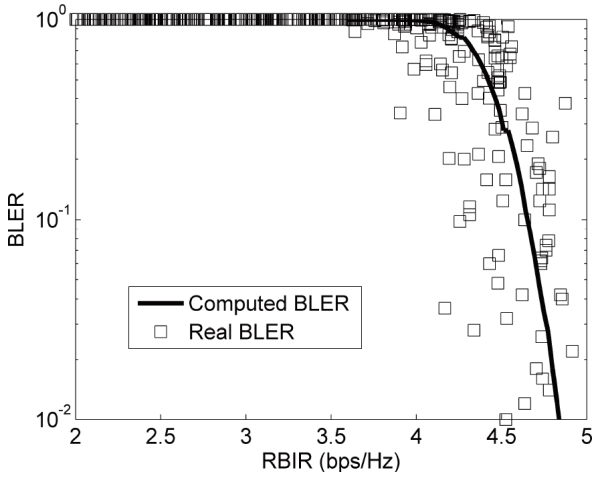

Figure 7(b). MMIB LE for VEC ML

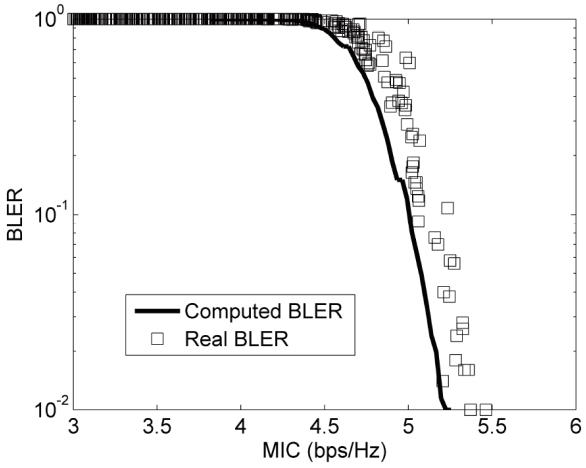

Figure 8(b). MIC LE for HEC MMSE

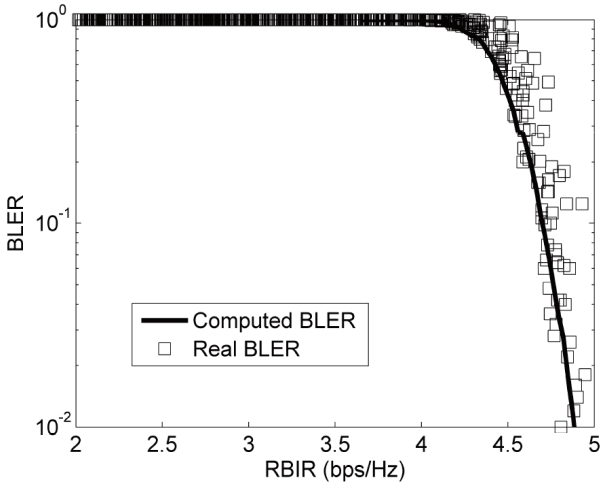

Figure 7(c). ERBIR LE for VEC ML

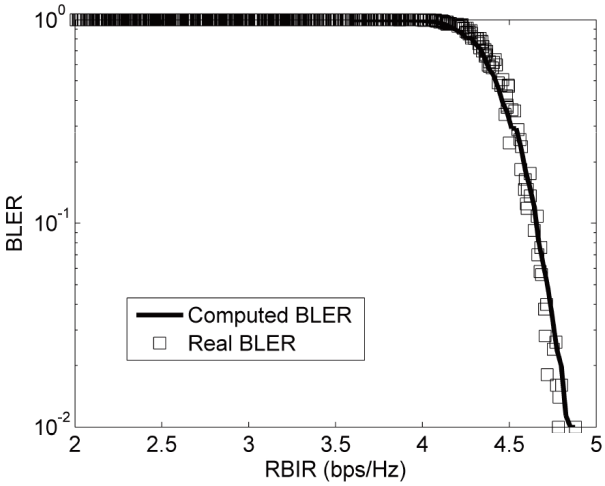

Figure 8(c). RBIR/ERBIR LE for HEC MMSE

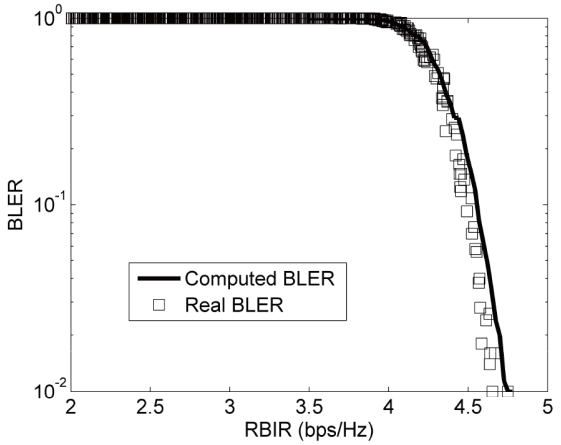

Figure 8(d). MMIB LE for HEC MMSE

These figures show that although EESM, MIC and MMIB algorithms can also obtain quite accurate link evaluation, RBIR/ERBIR algorithm is the most accurate. Moreover, RBIR/ERBIR algorithm doesn't need any channel related tuning parameters.

Then, HEC transmission with ML detection is validated by different link evaluation algorithms, shown as the following figures.

Figure 9 shows that EESM, RBIR, MIC and MMIB algorithms are invalid at all. Only ERBIR algorithm can achieve link evaluation for HEC ML transmissions.

5.3 Further Results Comparisons and Analysis

To ensure the universality of the simulation, more MCS levels are simulated. Following configuration in Table 3, MCS levels are set to MCS 1~8 with different MIMO schemes respectively. And the average difference is listed in the following tables. The average difference is measured by Mean Square Error Root (MSER) between computed and real BLER values.

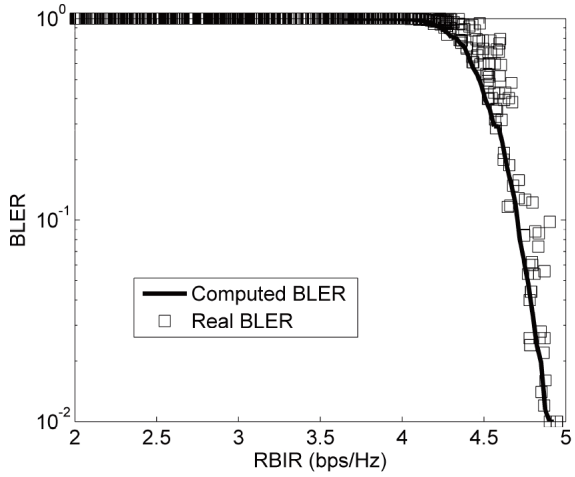

Figure 9. ERBIR LE for HEC ML

Table 4. MSER for EESM link evaluation

Transmission Mode	MSE				
	EESM	MIC	RBIR	MMIB	ERBIR
SISO with MMSE Detection	0.0369	0.1295	0. 0247	0. 0400	0. 0247
SISO with ML Detection	Not Supported	0.1296	Not Supported	0. 0469	0. 0241
VEC with MMSE Detection	0.0547	0.1348	0. 0604	0. 0622	0. 0604
VEC with ML Detection	Not Supported	0.3956	Not Supported	0. 1574	0.0956
HEC with MMSE Detection	0.0256	0.0851	0. 0206	0. 0312	0.0206
HEC with ML Detection	Not Supported	Not Supported	Not Supported	Not Supported	0.0791

As to EESM and RBIR, although they have achieved quite accurate link evaluation for wireless transmissions with MMSE detection, because the computation is based on OSINR, they can not support ML detection scenarios. To solve this problem, MIC and MMIB are developed. Unfortunately, they are not accurate for some levels either.

EESM, MIC and MMIB need MCS and CSI related tuning parameters, while RBIR does not. This makes EESM, MIC and MMIB not universal. RBIR is the most common algorithm for link evaluation, but it can be used for MMSE only. ERBIR can support link evaluation for all scenarios.

Simulation results in Table 4 show that ERBIR can provide more accurate link evaluation and more universality. Moreover, the MCS and CSI related tuning parameters are no longer necessary, which makes ERBIR become a universal and accurate method for link evaluation.

6. Validation by Link Adaptation and SLS

Link evaluations are validated by link adaptation and SLS of WiMAX II down link, profiling the influence caused by inaccuracy of link evaluation. Since previous results show that ERBIR is accurate, and MIC is not, link adaptation and SLS with ERBIR and MIC link evaluations are implemented.

6.1 Validation by Link Adaptation

Basic configuration of dynamical LLS is the same as Table 2, with link adaptation enable, 2×2 Alamouti STBC and MIMO 2×2 SM VEC of all MCS levels adaptation, and ML detection. Receiver dynamically estimates the statistical performance of wireless channel, and chooses the MCS level which can get best Spectrum Efficiency (SE) and acceptable BLER, then feeds it back to the transmitter [1].

Let target BLER is 0.1, SNR is [5 10 15 20] dB. Firstly Hybrid Automatic Repeat reQuest (HARQ) is disabled, and simulation results are listed in the following Table 5.

Table 5. Dynamical LLS results without HARQ

	Extended MI	MIC
BLER	[0.0334, 0.0125, 0.0052, 0.047]	[0.1545, 0.1482, 0.19, 0.2495]
Throughput (10^3 bits)	[0.721, 1.111, 2.007, 3.093]	[0.687, 1.082, 1.819, 2.652]
Total Retransmission Times	[0 0 0 0]	[0 0 0 0]

Then enable HARQ with maximum retransmission times of 3. Simulation results are listed in the following Table 6.

Compare the results of link adaptation with/without HARQ, it is obvious that accurate ERBIR link evaluation will ensure wireless system to choose proper MCS level, obtaining better BLER and throughput, and reducing the retransmission times. While using inaccurate MIC link evaluation, it is shown that MIC will overestimate the link performance, as shown in simulation results in previous section. So BLER and retransmission times increase, and throughput decreases.

6.2 Validation by SLS

Configuration of dynamical SLS is listed in Table 6. In SLS, link evaluation is used to hold down real coding and decoding procedures, reducing SLS complexity, as described in Reference [1]. Because the BLER in SLS is computed by link evaluation, the SLS results will become inaccurate when link evaluation can not provide accurate BLER.

Table 6. Dynamical LLS results with HARQ

	Extended MI	MIC
BLER	[0 0 0 0]	[0 0 0 0]
Throughput (10^3 bits)	[0.747, 1.382, 2.294, 3.476]	[0.725, 1.166, 2.023, 3.245]
Total Retransmission Times	[13, 5, 3, 9]	[53, 86, 46, 53]

Table 7. Configuration of SLS

Parameters	Configuration
MIMO Scheme	Single user, 2×2 Alamouti STBC and MIMO 2×2 SM VEC Adaptation
Frame Duration	5 ms
Bandwidth	10 MHz; NOFDM = 1024
Channel Estimation	ideal
Channel Model	70% ITU PedB 3kmph and 30% ITU VA 30kmph
Channel Coding	Turbo
MCS	QPSK 1/2; QPSK 3/4; 16QAM 1/2; 16QAM 3/4; 64QAM 1/2; 64QAM 2/3; 64QAM 3/4; 64QAM 5/6;
Block Size	16 subcarrier×6 symbol (Subcarriers are continuously allocated in wire- less resource block)
Detection	ML
Link Adaptation	Enable
HARQ	Enable, with maximum retransmission times of 3
Target BLER	0.1
Link Evaluation	ERBIR/MIC
Cell Configuration	3 sectors; omni directional antenna; 10 users per sector; 1.5 km of Cell Radius.
Scheduling	Proportional Fairness Scheduling

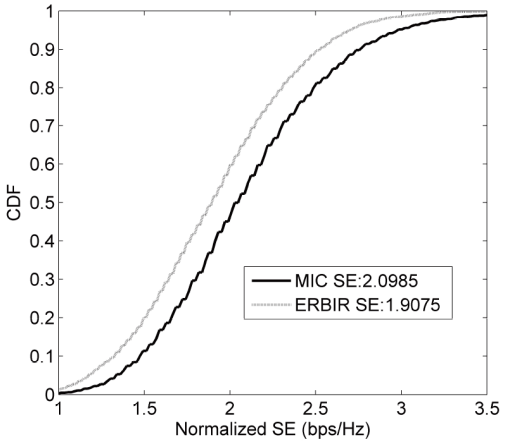

Figure 10. CDF of SLS SE

Figure 10 shows the Cumulative Distribution Function (CDF) of SLS SE results. It is shown that the SLS SE is overestimated by MIC link evaluation by (2.0985 − 1.9075) / 1.9075 × 100% ≈ 10%. It is obvious that inaccurate link evaluation will lead to incredible SLS results.

7. Conclusions

Link evaluation aims to provide a fading insensitive performance metric for common transmissions. It is proven from the view of information theory that RBIR is the most accurate metric, and a method to compute RBIR from CSI is proposed. Simulation results of LLS and SLS show that the proposed ERBIR algorithm works very well for common transmissions, solving the problems existing in current link evaluations.

8. Acknowledgments

Thanks to Tan Zhenhui, Zheng Hongming, and Chen Yueyun for their great support.

This work is supported in part by the Hi-tech research and development program of China (2007AA01Z277), National Natural Science Foundation of China (6077 2035), University Doctorial Foundation of China (2007 0004010), and Intel China Research Centre.

REFERENCES

[1] IEEE 802.16 Broadband Wireless Access Working Group. Draft IEEE 802.16m Evaluation Methodology Document. http:// ieee802.org/16/.July 18th, 2008.

[2] HE X, NIU K, HE Z Q, *et al*. Link layer abstraction in MIMO-OFDM system. International Workshop on Cross Layer Design, IWCLD'07, Sept. 20-21, 2007: 41-44.

[3] AKYILDIZ F, LEE W Y, AND VURAN M C, *et al*. A survey on spectrum management in cognitive radio networks. IEEE Communication Magazine, Apr. 2008, 46(4): 40-48.

[4] 3GPP TSG-RAN-1 Meeting #35, Effective SIR Computation for

OFDM System-Level Simulations.

[5] WiMAX Forum. Mobile WiMAX-Part I: A Technical Overview and Performance Evaluation. white paper, August 2006.

[6] Ericsson. A Fading-Insensitive Performance Metric for a Unified Link Quality Model.

[7] SAYANA K, ZHUANG J. Link performance abstraction based on mean mutual information per bit (MMIB) of the LLR channel. http://ieee802.org/16/. May 2nd, 2008.

[8] PAULRAJ A. Introduction to space-time wireless communications. 1st Edition. Cambridge University Press, England, 2003: 86-88, 178-198.

[9] CHUL H K, SUNGWOO P, MOON J, et al. Iterative joint detection and decoding for MIMO-OFDM wireless communications. Fortieth Asilomar Conference on Signals, Systems and Computers, ACSSC'06. Oct.-Nov. 2006, 1752-1756.

[10] SHANNON C. E. A mathematical theory of communication. The Bell System Technical Journal, July, October, 1948, 27: 379-423, 623-656.

[11] LEE J. W, BLAHUT R. E. Generalized EXIT chart and BER analysis of finite-length turbo codes. Global Telecommunication Conference, Dec. 2003, 4(1-5): 2067-2072.

APPENDIX

1. Effective MIMO Transmission

The original wireless transmission is

$$\boldsymbol{y} = \boldsymbol{H}_c\boldsymbol{F}\boldsymbol{x} + \boldsymbol{H}_I\boldsymbol{x}_I + \boldsymbol{n};\ \mathrm{E}\{\boldsymbol{x}\boldsymbol{x}\mathrm{H}\} = \boldsymbol{I}(\mathrm{NS});\ \mathrm{E}\{\boldsymbol{x}_I\boldsymbol{x}_I^{\mathrm{H}}\} = \boldsymbol{I}(\mathrm{N_S});$$

$$\mathrm{E}\{\boldsymbol{n}\boldsymbol{n}^{\mathrm{H}}\} = \sigma^2\boldsymbol{I}(\mathrm{N_R}) \quad (28)$$

Because receiver knows nothing about interference symbol but the correlation, and $\boldsymbol{H}_I$ is consisted of correlated Gaussians, $\boldsymbol{H}_I\boldsymbol{x}_I + \boldsymbol{n}$ is approximated as correlated Gaussians. Assume $\boldsymbol{R}_I$ is known to the receiver.

$$\mathrm{E}\{(\boldsymbol{H}_I\boldsymbol{x}_I + \boldsymbol{n})(\boldsymbol{H}_I\boldsymbol{x}_I + \boldsymbol{n})^{\mathrm{H}}\} = \boldsymbol{R}_I + \sigma^2\boldsymbol{I}(\mathrm{N_R}) \quad (29)$$

Let $\mathrm{E}\{\boldsymbol{n}_1\boldsymbol{n}_1^{\mathrm{H}}\} = \boldsymbol{I}(\mathrm{N_R})$, and $\boldsymbol{T}\boldsymbol{T}^{\mathrm{H}} = \boldsymbol{R}_I + \sigma^2\boldsymbol{I}(\mathrm{N_R})$. So

$$\mathrm{E}\{(\boldsymbol{T}\boldsymbol{n}_1)(\boldsymbol{T}\boldsymbol{n}_1)^{\mathrm{H}}\} = \mathrm{E}\{(\boldsymbol{H}_I\boldsymbol{x}_I + \boldsymbol{n})(\boldsymbol{H}_I\boldsymbol{x}_I + \boldsymbol{n})^{\mathrm{H}}\} \quad (30)$$

This means $\boldsymbol{T}\boldsymbol{n}_1$ is effective to $\boldsymbol{H}_I\boldsymbol{x}_I + \boldsymbol{n}$, so the original wireless transmission is effective to

$$\boldsymbol{y} = \boldsymbol{H}\mathrm{c}\boldsymbol{F}\boldsymbol{x} + \boldsymbol{T}\boldsymbol{n}_1;\ \mathrm{E}\{\boldsymbol{x}\boldsymbol{x}^{\mathrm{H}}\} = \boldsymbol{I}(\mathrm{N_S});\ \mathrm{E}\{\boldsymbol{n}_1\boldsymbol{n}_1^{\mathrm{H}}\} = \boldsymbol{I}(\mathrm{N_R}) \quad (31)$$

Consider identical transform, it is effective to

$$\boldsymbol{y} = (\boldsymbol{T}^{-1}\boldsymbol{H}_c\boldsymbol{F}\boldsymbol{x} + \boldsymbol{n}_1) / \|\boldsymbol{T}^{-1}\boldsymbol{H}_c\boldsymbol{F}\|_{\mathrm{F}} = \boldsymbol{H}_e\boldsymbol{x} + \boldsymbol{n}_e \quad (32)$$

Where

$$\boldsymbol{H}_e = \boldsymbol{T}^{-1}\boldsymbol{H}_c\boldsymbol{F} / \|\boldsymbol{T}^{-1}\boldsymbol{H}_c\boldsymbol{F}\|_{\mathrm{F}};\ \mathrm{E}\{\boldsymbol{n}_e\boldsymbol{n}_e^{\mathrm{H}}\} = \sigma_e^2\boldsymbol{I}(\mathrm{N_R});$$

$$\sigma_e^2 = 1 / \|\boldsymbol{T}^{-1}\boldsymbol{H}_c\boldsymbol{F}\|_{\mathrm{F}} \quad (33)$$

This identity between (28) and (33) is proven from the view of capacity. Let $|\boldsymbol{A}|$ means the determinant of matrix $\boldsymbol{A}$. Channel capacity of the original transmission is

$$C_1 = \log_2|\pi\mathrm{e}\mathrm{E}\{\boldsymbol{y}\boldsymbol{y}^{\mathrm{H}}\}| - \log_2|\pi\mathrm{e}\mathrm{E}\{(\boldsymbol{H}_I\boldsymbol{x}_I + \boldsymbol{n})(\boldsymbol{H}_I\boldsymbol{x}_I + \boldsymbol{n})^{\mathrm{H}}\}|$$

$$= \log_2\left|\frac{\mathrm{E}\left\{\left(\boldsymbol{H}_c\boldsymbol{F}\boldsymbol{x} + \boldsymbol{H}_I\boldsymbol{x}_I + \boldsymbol{n}\right)\left(\boldsymbol{H}_c\boldsymbol{F}\boldsymbol{x} + \boldsymbol{H}_I\boldsymbol{x}_I + \boldsymbol{n}\right)^{\mathrm{H}}\right\}}{\mathrm{E}\left\{\left(\boldsymbol{H}_I\boldsymbol{x}_I + \boldsymbol{n}\right)\left(\boldsymbol{H}_I\boldsymbol{x}_I + \boldsymbol{n}\right)^{\mathrm{H}}\right\}}\right|$$

$$= \log_2\left|\frac{\boldsymbol{H}_c\boldsymbol{F}\boldsymbol{F}^{\mathrm{H}}\boldsymbol{H}_c^{\mathrm{H}} + \boldsymbol{R}_I + \sigma^2\boldsymbol{I}\left(\mathrm{N}_R\right)}{\boldsymbol{R}_I + \sigma^2\boldsymbol{I}\left(\mathrm{N}_R\right)}\right|$$

$$= \log_2\left|\frac{\boldsymbol{T}^{-1}\left[\boldsymbol{H}_c\boldsymbol{F}\boldsymbol{F}^{\mathrm{H}}\boldsymbol{H}_c^{\mathrm{H}} + \boldsymbol{R}_I + \sigma^2\boldsymbol{I}\left(\mathrm{N_R}\right)\right]\left(\boldsymbol{T}^{\mathrm{H}}\right)^{-1}}{\boldsymbol{T}^{-1}\left[\boldsymbol{R}_I + \sigma^2\boldsymbol{I}\left(\mathrm{N_R}\right)\right]\left(\boldsymbol{T}^{\mathrm{H}}\right)^{-1}}\right|$$

$$= \log_2|\boldsymbol{I}(\mathrm{N_R}) + (\boldsymbol{T}^{-1}\boldsymbol{H}_c\boldsymbol{F})(\boldsymbol{T}^{-1}\boldsymbol{H}_c\boldsymbol{F})^{\mathrm{H}}| \quad (34)$$

Then the channel capacity of the effective transmission is

$$C2 = \log_2|\boldsymbol{I}(\mathrm{N_R}) + (\boldsymbol{T}^{-1}\boldsymbol{H}_c\boldsymbol{F})(\boldsymbol{T}^{-1}\boldsymbol{H}_c\boldsymbol{F})^{\mathrm{H}}| \quad (35)$$

Equation (34) and (35) indicates that the two transmissions are effective.

2. OSINR Computation for MMSE

Consider transmission as

$$\boldsymbol{y} = \boldsymbol{H}_e\boldsymbol{x} + \boldsymbol{n}_e;\ \mathrm{E}\{\boldsymbol{x}\boldsymbol{x}^{\mathrm{H}}\} = \boldsymbol{I}(\mathrm{N_S});\ \mathrm{E}\{\boldsymbol{n}_e\boldsymbol{n}_e^{\mathrm{H}}\} = \sigma_e^2\boldsymbol{I}(\mathrm{N_R}) \quad (36)$$

Let $\boldsymbol{x}_o = \boldsymbol{M}\boldsymbol{y} = \boldsymbol{M}(\boldsymbol{H}_e\boldsymbol{x} + \boldsymbol{n}_e)$, where

$$\boldsymbol{M} = \arg\min_{M}\mathrm{E}\left\{\left\|x_o - x\right\|_{\mathrm{F}}^2\right\} \quad (37)$$

According to orthogonality principle,

$$\mathrm{E}\{(\boldsymbol{x}_o - \boldsymbol{x})\ \boldsymbol{y}^{\mathrm{H}}\} = \boldsymbol{0} \quad (38)$$

$$\mathrm{So},\ \boldsymbol{M} = \boldsymbol{H}_e^{\mathrm{H}}(\boldsymbol{H}_e\boldsymbol{H}_e^{\mathrm{H}} + \sigma_e^2\boldsymbol{I})^{-1} \quad (39)$$

Let, $\boldsymbol{D} = \mathrm{diag}(\boldsymbol{M}\boldsymbol{H}_e)$, $\boldsymbol{N} = \mathrm{diag}(\sigma_e^2\boldsymbol{M}\boldsymbol{M}^{\mathrm{H}})$ and $\boldsymbol{I}_f = \boldsymbol{M}\boldsymbol{H}_e - \boldsymbol{D}$, then OSINR for each symbol in the transmitting signal vector is

$$\gamma_i = (\boldsymbol{D}\boldsymbol{D}^{\mathrm{H}})_{ii} / [(\boldsymbol{I}_f\boldsymbol{I}_f^{\mathrm{H}})_{ii} + (\boldsymbol{N})_{ii}];\ i = 1, 2, \ldots, \mathrm{N_S} \quad (40)$$

$(\boldsymbol{A})_{ii}$ means the i^{th} row and i^{th} column element of matrix $\boldsymbol{A}$.

3. Proof of Lemma 1

According to Equation (20) and (21), BLER is one-one to RBIR. Then consider the uncoded block, there is

$$BLER_{\mathrm{u}} = \mathrm{RBIRtoBLER}(RBIR_{\mathrm{u}}) \quad (41)$$

Since the MCS is given, it is pointed out that Extrinsic Information Transfer (EXIT) is definite [11]. So RBIR for the coded block after iterative decoding is determined by

$$RBIR = \mathrm{EXIT}_{\mathrm{MCS}}(RBIR_{\mathrm{u}}) \quad (42)$$

So there is

$$\begin{aligned} BLER &= \mathrm{RBIRtoBLER}(RBIR) \\ &= \mathrm{RBIRtoBLER}[\mathrm{EXIT}_{\mathrm{MCS}}(RBIR_{\mathrm{u}})] \\ &= \mathrm{RBIRtoBLER}\{\mathrm{EXIT}_{\mathrm{MCS}}[\mathrm{InversRBIRtoBLER}(BLER_{\mathrm{u}})]\} \\ &= \mathrm{MappingFunction}_{\mathrm{MCS}}(BLER_{\mathrm{u}}) \end{aligned} \quad (43)$$

This is referred to *lemma* 1.

4. Normalized MI for SISO

For SISO transmission, the received symbol is

$$y = Hx + n;\ \mathrm{E}\{xx^*\} = 1;\ \mathrm{E}\{nn^*\} = \sigma^2 = 10^{-SNR/10} \quad (44)$$

I is computed as

$$I = \frac{1}{\log_2 \mathrm{N}_{\mathrm{QAM}}} \mathop{\mathrm{E}}_{x,y}\left\{\log_2 \frac{P(y \mid x)}{P(y)}\right\} = \frac{MI}{\log_2 \mathrm{N}_{\mathrm{QAM}}} \quad (45)$$

Since x is random selected from the constellation, then

$$P(x=q_i)=1/\mathrm{N}_{\mathrm{QAM}} \quad (46)$$

Where q_i is the i^{th} mapping point in the modulation constellation, and NQAM is the number of points in the constellation. So

$$MI = \frac{\sum_{i=1}^{\mathrm{N}_{\mathrm{QAM}}} \mathop{\mathrm{E}}_{y}\left\{\log_2 \mathrm{N}_{\mathrm{QAM}} P(y \mid q_i) / \sum_{i=1}^{\mathrm{N}_{\mathrm{QAM}}} P(y \mid q_k)\right\}}{\mathrm{N}_{\mathrm{QAM}}} \quad (47)$$

Then consider the probability of $P(y \mid x)$,

$$\begin{aligned} P(y \mid x) &= P(n = y - Hx) \\ &= P\left(n_{\mathrm{real}} = (y - Hx)_{\mathrm{real}}\right) P\left(n_{\mathrm{imag}} = (y - Hx)_{\mathrm{imag}}\right) \\ &= \frac{1}{\sqrt{\pi}\sigma} \exp\left(-\frac{(y - Hx)_{\mathrm{real}}^{\ 2}}{\sigma^2}\right) \frac{1}{\sqrt{\pi}\sigma} \exp\left(\frac{(y - Hx)_{\mathrm{imag}}^{\ 2}}{\sigma^2}\right) \\ &= \frac{1}{\sqrt{\pi}\sigma} \exp\left(-\frac{|y - Hx|^2}{\sigma^2}\right) \end{aligned} \quad (48)$$

Let $\Delta_{i,k} = q_i - q_k$,

$$MI = \frac{\sum_{i=1}^{\mathrm{N}_{\mathrm{QAM}}} \oint_n p(n) \log_2 \dfrac{\mathrm{N}_{\mathrm{QAM}} \exp\left(-\dfrac{|n|^2}{\sigma^2}\right)}{\sum_{i=1}^{\mathrm{N}_{\mathrm{QAM}}} \exp\left(-\dfrac{|H\Delta_{i,k} + n|^2}{\sigma^2}\right)} dn}{\mathrm{N}_{\mathrm{QAM}}} \quad (49)$$

Here

$$p(n) = \exp(-|n|^2 / \sigma^2) / \pi\sigma^2 \quad (50)$$

Let $n_{\mathrm{e}} = n/H$, and $\sigma_{\mathrm{e}}^{\ 2} = \sigma^2/|H|^2$ then

$$p(n_{\mathrm{e}}) = \exp(-|n_{\mathrm{e}}|^2 / \sigma_{\mathrm{e}}^{\ 2}) / \pi\sigma_{\mathrm{e}}^{\ 2} \quad (51)$$

So

$$MI = \frac{\sum_{i=1}^{\mathrm{N}_{\mathrm{QAM}}} \oint_n p(n_{\mathrm{e}}) \log_2 \dfrac{\mathrm{N}_{\mathrm{QAM}} \exp\left(-\dfrac{|n_{\mathrm{e}}|^2}{\sigma_{\mathrm{e}}^{\ 2}}\right)}{\sum_{i=1}^{\mathrm{N}_{\mathrm{QAM}}} \exp\left(-\dfrac{|H\Delta_{i,k} + n_{\mathrm{e}}|^2}{\sigma^2}\right)} dn_{\mathrm{e}}}{\mathrm{N}_{\mathrm{QAM}}}$$

$$= \mathrm{SISO\_MI}(10^{-SNR/10} / |H|^2) \quad (52)$$

So

$$I = \frac{1}{\log_2 \mathrm{N}_{\mathrm{QAM}}} \mathrm{SISO\_MI}(10^{-SNR/10} / |H|^2) \quad (53)$$

5. Normalized MI for 2×2 MIMO

2×2 MIMO received symbol is

$$y = \begin{bmatrix} y_1 \\ y_2 \end{bmatrix} = \boldsymbol{Hx} + \boldsymbol{n} = \begin{bmatrix} h_{11} & h_{12} \\ h_{21} & h_{22} \end{bmatrix} \begin{bmatrix} x_1 \\ x_2 \end{bmatrix} + \begin{bmatrix} n_1 \\ n_2 \end{bmatrix} \quad (54)$$

Where

$$\begin{cases} \mathrm{E}\{x_1 x_1^*\} = \mathrm{E}\{x_2 x_2^*\} = 1 \\ \mathrm{E}\{n_1 n_1^*\} = \mathrm{E}\{n_2 n_2^*\} = \sigma^{/2} = 10^{-SNR/10} \\ \mathrm{E}\{x_1 x_2^*\} = 0 \quad \mathrm{E}\{n_1 n_2^*\} = 0 \end{cases} \quad (55)$$

For example, the normalized MI of x_1 is

$$I_1 = \frac{1}{\log_2 \mathrm{N}_{\mathrm{QAM}}} \mathop{\mathrm{E}}_{x,y}\left\{\log_2 \frac{P(x_1, \boldsymbol{y} \mid \boldsymbol{x})}{P(\boldsymbol{y})}\right\} \quad (56)$$

Since x_1 and x_2 are random selected from the constel-

lation,

$$P(x_1 = q_{1,i},\ x_2 = q_{2,j}) = 1 / \mathrm{N_{QAM}}^2 \quad (57)$$

Here $q_{1,i}$ and $q_{2,j}$ are the i^{th} and j^{th} mapping points in the constellation for x_1 and x_2 respectively. $\mathrm{N_{QAM}}$ is the number of points in the constellation. Given transmitting vector,

$$\boldsymbol{q}_l = [q_{1,i},\ q_{2,j}]^{\mathrm{T}};\ l = 1,2,\ldots,\mathrm{N_{QAM}}^2;\ i,j = 1,2,\ldots,\mathrm{N_{QAM}} \quad (58)$$

Let $\boldsymbol{\Delta}_{l,m} = \boldsymbol{H}(\boldsymbol{q}_l - \boldsymbol{q}_m)$,

$$P(y) = \frac{\sum_{m=1}^{\mathrm{N_{QAM}}^2} \exp\left(-\left\|H(\boldsymbol{q}_1 - \boldsymbol{q}_m) + \boldsymbol{n}\right\|_{\mathrm{F}}^2 / \sigma^2\right)}{\mathrm{N_{QAM}}^2 \pi^2 \sigma^2}$$

$$= \frac{\sum_{m=1}^{\mathrm{N_{QAM}}^2} \exp\left(-\left\|\Delta_{l,m} + \boldsymbol{n}\right\|_{\mathrm{F}}^2 / \sigma^2\right)}{\mathrm{N_{QAM}}^2 \pi^2 \sigma^4} \quad (59)$$

$$P(q_{1,i}, \boldsymbol{y} \mid \boldsymbol{q}_l) = \frac{\sum_{t=1}^{\mathrm{N_{QAM}}} \exp\left(-\left\|\boldsymbol{H}\begin{bmatrix} q_{1,i} - q_{1,i} \\ q_{2,j} - q_{2,t} \end{bmatrix} + \begin{bmatrix} n_1 \\ n_2 \end{bmatrix}\right\|_{\mathrm{F}}^2 / \sigma^2\right)}{\mathrm{N_{QAM}} \boldsymbol{\pi}^2 \boldsymbol{\sigma}^4}$$

$$= \frac{\sum_{t=1}^{\mathrm{N_{QAM}}} \exp\left(-\left\|H\begin{bmatrix} 0 \\ q_{2,j} - q_{2,t} \end{bmatrix} + \begin{bmatrix} n_1 \\ n_2 \end{bmatrix}\right\|_{\mathrm{F}}^2 / \sigma^2\right)}{\mathrm{N_{QAM}} \pi^2 \sigma^4} \quad (60)$$

Then

$$I_1 = \frac{\sum_{l=1}^{\mathrm{N_{QAM}}^2} \oint_n p(\boldsymbol{n}) \log_2 \frac{p(q_{1,i}, \boldsymbol{y} \mid \boldsymbol{q}_l)}{p(\boldsymbol{y})} d\boldsymbol{n}}{\mathrm{N_{QAM}}^2 \log_2 \mathrm{N_{QAM}}}$$

$$= \frac{\sum_{l=1}^{\mathrm{N_{QAM}}^2} \oint_n p(\boldsymbol{n}) \log_2 \frac{p(q_{1,i}, \boldsymbol{y} \mid \boldsymbol{q}_l) / p(\boldsymbol{n})}{p(\boldsymbol{y}) / p(\boldsymbol{n})} d\boldsymbol{n}}{\mathrm{N_{QAM}}^2 \log_2 \mathrm{N_{QAM}}}$$

$$= \frac{\frac{1}{\mathrm{N_{QAM}}^2} \sum_{l=1}^{\mathrm{N_{QAM}}^2} \oint_n p(\boldsymbol{n}) \log_2 \frac{p(\boldsymbol{n})}{p(q_{1,i}, \boldsymbol{y} \mid \boldsymbol{q}_l)} d\boldsymbol{n}}{\log_2 \mathrm{N_{QAM}}}$$

$$= \frac{1}{\log_2 \mathrm{N_{QAM}}} (MI_c - MI_2) \quad (61)$$

Consider MI_{c},

$$MI_{\mathrm{c}} = \frac{1}{\mathrm{N_{QAM}}^2} \sum_{l=1}^{\mathrm{N_{QAM}}^2} \oint_n p(\boldsymbol{n}) \log_2 \frac{p(\boldsymbol{n})}{p(\boldsymbol{y})} d\boldsymbol{n}$$

$$\frac{\sum_{l=1}^{\mathrm{N_{QAM}}^2} \oint_n p(\boldsymbol{n}) \log_2 \frac{\mathrm{N_{QAM}}^2 \exp\left(-\left\|\boldsymbol{n}\right\|_{\mathrm{F}}^2 / \sigma^2\right)}{\sum_{m=1}^{\mathrm{N_{QAM}}^2} \exp\left(-\left\|\Delta_{l,m} + \boldsymbol{n}\right\|_{\mathrm{F}}^2 / \sigma^2\right)} d\boldsymbol{n}}{\mathrm{N_{QAM}}^2}$$

$$\frac{\sum_{l=1}^{\mathrm{N_{QAM}}^2} \oint_n p(\boldsymbol{n}) \log_2 \frac{\mathrm{N_{QAM}}^2}{\sum_{m=1}^{\mathrm{N_{QAM}}^2} \exp\left(-\frac{\left\|\Delta_{l,m}\right\|_{\mathrm{F}}^2 + \Delta_{l,m}{}^H \boldsymbol{n} + \boldsymbol{n}^H \Delta_{l,m}}{\sigma^2}\right)} d\boldsymbol{n}}{\mathrm{N_{QAM}}^2} \quad (62)$$

Let $n_{\mathrm{e}} = (\boldsymbol{\Delta}_{l,m}{}^{\mathrm{H}}\boldsymbol{n} + \boldsymbol{n}^{\mathrm{H}}\boldsymbol{\Delta}_{l,m}) / \| \boldsymbol{\Delta}_{l,m} \|_{\mathrm{F}}$, so

$$n_{\mathrm{e}} \sim \mathrm{N}(0, 2\sigma^2) \quad (63)$$

Then

$$MI_c = \frac{\sum_{l=1}^{\mathrm{N_{QAM}}^2} \oint_n p(n_{\mathrm{e}}) \log_2 \frac{\mathrm{N_{QAM}}^2}{\sum_{m=1}^{\mathrm{N_{QAM}}^2} \exp\left(-\frac{\left\|\Delta_{l,m}\right\|_{\mathrm{F}}^2 + \left\|\Delta_{l,m}\right\|_{\mathrm{F}} n_e}{\sigma^2}\right)} dn}{\mathrm{N_{QAM}}^2}$$

Then define approximation as

$$\Delta_l = \sqrt{-\sigma^2 \log_{\mathrm{e}}\left(\frac{1}{\mathrm{N_{QAM}}^2} \sum_{m=1}^{\mathrm{N_{QAM}}^2} \exp\left(-\frac{1}{\beta} \frac{\left\|\Delta_{l,m}\right\|_{\mathrm{F}}^2}{\sigma^2}\right)\right)} \quad (64)$$

Here the tuning parameter is

Table 8. Tuning parameter for 2×2 MIC

SNR/dB	[−8	−5	−2	1	4	7]
β	[2	2.1	2.2	2.3	2.4	2.55]

Then

$$MI_c = \frac{\log_2 \mathrm{e}}{\sigma^2 \mathrm{N_{QAM}}^2} \sum_{l=1}^{\mathrm{N_{QAM}}^2} \Delta_l^2 = \mathrm{VectorMI}(\boldsymbol{H}, SNR) \quad \textbf{(65)}$$

Then compute MI_2, and let $\Delta_{2,j,t} = q_{2,j} - q_{2,t}$,

$$MI_2 = \frac{1}{\mathrm{N_{QAM}}^2} \sum_{t=1}^{\mathrm{N_{QAM}}} \sum_{j=1}^{\mathrm{N_{QAM}}} \oint_n p(\boldsymbol{n}) \log_2 \frac{p(\boldsymbol{n})}{P(x_1, \boldsymbol{y} \mid \boldsymbol{x})} d\boldsymbol{n}$$

$$= \frac{1}{\mathrm{N_{QAM}}} \sum_{j=1}^{\mathrm{N_{QAM}}} \oint_n p(\boldsymbol{n}) \log_2 \frac{\exp\left(-\frac{|n_1|^2 + |n_2|^2}{\sigma^2}\right)}{|h_{12}\Delta_{2,j,t} + n_1|^2} d\boldsymbol{n}$$

$$\sum_{t=1}^{\mathrm{N_{QAM}}} \exp\left(-\frac{|h_{22}\Delta_{2,j,t} + n_2|^2}{\sigma^2}\right) \quad \textbf{(66)}$$

Here

$$\left(|h_{12}\Delta_{2,j,t} + n_1|^2 + |h_{22}\Delta_{2,j,t} + n_2|^2\right) / \left(|h_{12}|^2 + |h_{22}|^2\right)$$

$$= |\Delta_{2,j,t}|^2 + \frac{|n_1|^2 + |n_2|^2}{|h_{12}|^2 + |h_{22}|^2} + 2\{\Delta_{2,j,t} \frac{h_{12}n_1^* + h_{22}n_2^*}{|h_{12}|^2 + |h_{22}|^2}\}_{\mathrm{real}} \quad \textbf{(67)}$$

Let $n_\mathrm{e} = (h_{12}n_1^* + h_{22}n_2^*) / (|h_{12}|^2 + |h_{22}|^2)$, so

$\mathrm{E}\{n_\mathrm{e}\} = 0$; $\mathrm{E}\{n_{\mathrm{e,real}} n_{\mathrm{e,imag}}\} = 0$; $\mathrm{E}\{|n_\mathrm{e}|^2\} = \sigma_\mathrm{e}^2$;

$$\sigma_\mathrm{e}^2 = \sigma^2 / (|h_{12}|^2 + |h_{22}|^2) \quad \textbf{(68)}$$

Then

$$T_2 = \frac{1}{\mathrm{N_{QAM}}} \sum_{j=1}^{\mathrm{N_{QAM}}} \oint_{n_\mathrm{e}} p(n_\mathrm{e}) \log_2 \frac{\exp\left(-\frac{|n_\mathrm{e}|^2}{\sigma_\mathrm{e}^2}\right)}{\sum_{t=1}^{\mathrm{N_{QAM}}} \exp\left(-\frac{|\Delta_{2,j,t} + n_\mathrm{e}|^2}{\sigma_\mathrm{e}^2}\right)} dn_\mathrm{e}$$

$$T_2 = \frac{1}{\mathrm{N_{QAM}}} \sum_{j=1}^{\mathrm{N_{QAM}}} \oint_{n_\mathrm{e}} p(n_\mathrm{e}) \log_2 \frac{\exp\left(-\frac{|n_\mathrm{e}|^2}{\sigma_\mathrm{e}^2}\right)}{\sum_{t=1}^{\mathrm{N_{QAM}}} \exp\left(-\frac{|\Delta_{2,j,t} + n_\mathrm{e}|^2}{\sigma_\mathrm{e}^2}\right)} dn_\mathrm{e}$$

$$= \mathrm{SISO\_MI}\left(\frac{10^{-SNR/10}}{|h_{12}|^2 + |h_{22}|^2}\right) \quad \textbf{(69)}$$

The computation of I_1 and I_2 are similar, so

$$I_1 = \frac{\mathrm{VectorMI}(\boldsymbol{H}, SNR) - \mathrm{SISO\_MI}\left(\frac{10^{-SNR/10}}{|h_{12}|^2 + |h_{22}|^2}\right)}{\log_2 \mathrm{N_{QAM}}}$$

$$I_2 = \frac{\mathrm{VectorMI}(\boldsymbol{H}, SNR) - \mathrm{SISO\_MI}\left(\frac{10^{-SNR/10}}{|h_{11}|^2 + |h_{21}|^2}\right)}{\log_2 \mathrm{N_{QAM}}} \quad \textbf{(70)}$$

Communications and Network, 2009, 20-24
doi:10.4236/cn.2009.11003 Published Online August 2009 (http://www.scirp.org/journal/cn)

Comparison and Design of Decoder in B3G Mobile Communication System

Mingxiang GUAN[1], Mingchuan YANG[2]
[1]*Department of Electronic Communication Technology, Shenzhen Institute of Information Technology, Shenzhen, China*
[2]*School of Electronic and Information Technology, Harbin Institute of Technology, Harbin, China*
Email: [1]*gmx*2020@126.*com*; [2]*yangmingchuan@hit.edu.cn*

Abstract: Turbo code has been shown to have ability to achieve performance that is close to Shannon limit. It has been adopted by various commercial communication systems. Both universal mobile telecommunications system (UMTS) TDD and FDD have also employed turbo code as the error correction coding scheme. It outperforms convolutional code in large block size, but because of its time delay, it is often only used in the non-real-time service. In this paper, we discuss the encoder and decoder structure of turbo code in B3G mobile communication System. In addition, various decoding techniques, such as the Log-MAP, Max-log-MAP and SOVA algorithm for non-real-time service are deduced and compared. The performance results of decoder and algorithms in different configurations are also shown.

Keywords: decoder, beyond 3G mobile communication system, decoding algorithm

1. Introduction

A turbo code can be thought as a refinement of the concatenated encoding structure and an iterative algorithm for decoding the associated code sequence [1]. The codes are constructed by applying two or more component codes to different interleaved versions of the same information sequence [2][3]. In literature [4], for any single traditional code, the final step at the decoder yields hard-decision decoded bits (or, more generally, decoded symbols). In order for a concatenated scheme such as a turbo code to work properly, the decoding algorithm should not limit itself to pass hard decisions among the decoders [5]. To best exploit the information learned from each decoder, the decoding algorithm must effect an exchange of soft rather than hard decisions [6]. For a system with two component codes, the concept behind turbo decoding is to pass soft decisions from the output of one decoder to the input of the other, and to iterate this process several times to produce better decisions [7].

2. Principle of Iterative Decoding

For the first decoding iteration of the soft input/soft output decoder in Figure 1, one generally assumes the binary data to be equally likely, yielding an initial a priori LLR value of L(d) =0 for the third term in [8]. The channel pre-detection LLR value, Lc(x) , is measured by forming the logarithm of the ratio of λ_1 and λ_2, seen in Figure l. The output $L(\hat{d})$ of the Figure 2 decoder is made up of the LLR from the detector, $L'(\hat{d})$, and the extrinsic LLR output. $L_e(\hat{d})$, representing knowledge gleaned from the decoding process. As illustrated in Figure 2, for iterative decoding the extrinsic likelihood is fed back to the decoder input, to serve as a refinement of the a priori value for the next iteration.

Consider the two-dimensional code (product code) depicted in Figure 2. The configuration can be described as

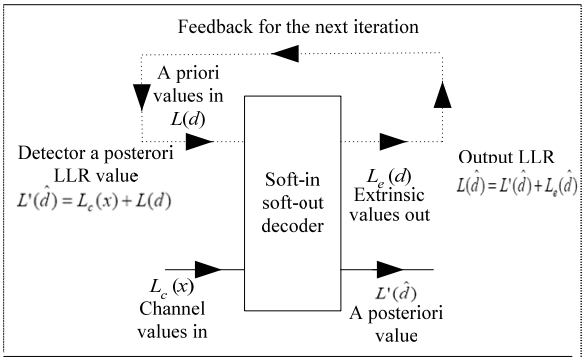

Figure 1. Soft input/soft output decoder

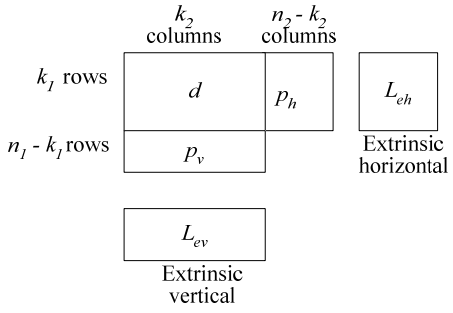

Figure 2. Two-dimensional product code

This paper supported by the 3rd natural science foundation of institute (No. LG-08010).

a data array made up of k_1 rows and k_2 columns. Each of the k_1 rows contains a code vector made up of k_2 data bits and n_2-k_2 parity bits. Similarly, each of the k_2 columns contains a code vector made up of k_1 data bits and n_1-k_1 parity bits. The various portions of the structure are labeled d for data, p_h for horizontal parity (along the rows), and p_v for vertical parity (along the columns). Additionally, there are blocks labeled L_{eh} and L_{ev} , which house the extrinsic LLR values learned from the horizontal and vertical decoding steps, respectively. Notice that this product code is a simple example of a concatenated code. Its structure encompasses two separate encoding steps, horizontal and vertical. The iterative decoding algorithm for this product code proceeds as follows:

1) Set the a priori information

$$L(d)=0 \quad (1)$$

2) Decode horizontally, obtain the horizontal extrinsic information as shown below:

$$L_{eh}(\hat{d}) = L(\hat{d}) - L_c(x) - L(d) \quad (2)$$

3) Set

$$L(d) = L_{eh}(\hat{d}) \quad (3)$$

4) Decode vertically, obtain the vertical extrinsic information as shown below:

$$L_{ev}(\hat{d}) = L(\hat{d}) - L_c(x) - L(d) \quad (4)$$

5) Set

$$L(d) = L_{ev}(\hat{d}) \quad (5)$$

6) If there have been enough iterations to yield a reliable 7 decision, go to step 7; otherwise, go to step 2;

7) The soft output is:

$$L(\hat{d}) = L_c(x) + L_{eh}(\hat{d}) + L_{ev}(\hat{d}) \quad (6)$$

3. B3G Mobile System Decoder Design

The algorithms for decoders can be divided into two categories: (1) Log-MAP: Log-Maximum A Posteriori, (2) SOVA: Soft Output Viterbi Algorithm.

3.1. Log-MAP Algorithm

Before explaining the MAP decoding algorithm, we assume some notations:

$s_k^S(e)$ starting stage of the edge e.

$s_k^E(e)$ ending stage of the edge e.

$d_k(e)$ the information word containing k_0 bits.

u_i stands for individual information bits.

$x_k(e)$ codeword containing n_0 bits.

We assume here that the received signal is $y_k=x_k+n$ (transmitted symbols + noise).

The metric at time k is

$$M_k(e) = p(s_k^E(e), y_k \mid x_k^E(e)) = \sum_{x_k} p(s_k^E(e) \mid s_k^S(e)) p(x_k \mid s_k^S(e)) p(y_k \mid x_k) \quad (7)$$

$p(s_k^E(e) \mid s_k^S(e))$ a priori information of the information bit.

$p(x_k \mid s_k^S(e))$ indicating the existence of connection between edges $s_k^S(e)$, $s_k^E(e)$

$p(y_k \mid x_k)$ probability of receiving y_k if x_k was transmitted.

$A_k(.)$ and $B_k(.)$ is forward and backward path metrics.

$$A_k(s) = p(s_k^E(e) = s, y_1^k) = \sum_{e:s_k^E(e)=s} A_{k-1}(s_k^S(e)) M_k(e), k = 1,...,N-1 \quad (8)$$

$$B_k(s) = p(y_1^k \mid s_{k+1}^S(e) = s) = \sum_{e:s_k^E(e)=s} B_{k+1}(s_{k+1}^S(e)) M_{k+1}(e), k = N,...,1 \quad (9)$$

Suppose the decoder starts and ends with known states

$$A_0(s) = \begin{cases} 1, s = S_0 \\ 0, otherwise \end{cases}, \quad B_N(s) = \begin{cases} 1, s = S_N \\ 0, otherwise \end{cases} \quad (10)$$

If the final state of the trellis is unknown:

$$B_N(s) = \frac{1}{2^m}, \forall s \quad (11)$$

The joint probability at time k is:

$$\sigma_k(e) = p(e, y_1^N) = A_{k+1}(s_k^S(e)).M_k(e).B_k(s_k^E(e)) \quad (12)$$

3.2. Output Viterbi Algorithm (SOVA)

There are two modifications compared to the classical Viterbi algorithm. One is the path metric modified to account the extrinsic information. This is similar to the metric calculation in Log-MAP algorithm. The other is the algorithm modified to calculate the soft bit. For each state in the trellis the metric $M(\underline{s}_k^S)$ is calculated for both merging paths, the path with the highest metric is selected to be the survivor, and for the state (at this stage) a pointer to the previous state along the surviving path is stored. The information to give $L(u_k|\underline{y})$ is stored, the difference $\Delta_k^{s_i}$ between the discarded and surviving path. The binary vector containingδ+1 bits, indicating last δ+1 bits that generated the discarded path. After ML path is found the update sequences and metric differences are used to calculate $L(u_k|\underline{y})$. For each bit u_k^{ML} in the ML path, we try to find the path merging with ML path that had compared to the u_k^{ML} in ML different bit value u_k at state k and this path should have minimal distance with ML path. We go trough δ+1 merging paths that follow

stage k i.e. the $\Delta_k^{s_i}$ $i = k,\ldots, (k+\delta)$, for each merging path in that set we calculate back to find out which value of the bit u_k generated this path. If the bit u_k in this path is not u_k^{ML} and $\Delta_k^{s_i}$ is less than current $\Delta_k^{\min}$, we set $\Delta_k^{\min} = \Delta_k^{s_i}$.

$$L(u_k \mid \underline{y}) \approx u_k \min_{\substack{i=k\ldots k+\sigma \\ u_k^{ML} \neq u_k^i}} \Delta_i^{S_i} \quad \textbf{(13)}$$

4. Comparison of the Decoding Algorithms

SOVA the ML path is found. The recursion used is identical to the one used for calculating of α in Log-MAP algorithm. Along the ML path hard decision on the bit u_k is made. $L(u_k|\underline{y})$ is the minimum metric difference between the ML path and the path that merges with ML path and is generated with different bit value u_k. In $L(u_k|\underline{y})$ calculations accordingly to Log-MAP one path is ML path and other is the most likely path that gives the different u_k. In SOVA the difference is calculated between the ML and the most likely path that merges with ML path and gives different u_k. This path but the other may not be the most likely one for giving different u_k. Compared to Log-MAP output (SOVA does not have bias), the output of SOVA is just much noisier. The SOVA and Log-MAP have the same output. The magnitude of the soft decisions of SOVA will either be identical of higher than those of Log-MAP. If the most likely path that gives the different hard decision for u_k, has survived and merges with ML path the two algorithms are identical. If that path does not survive the path on what different u_k is made is less likely than the path which should have been used.

The forward recursion in Log-MAP and SOVA is identical but the trace-back depth in SOVA is either less than or equal to the backward recursion depth. Log-MAP is the slowest of the three algorithms, but has the best performance among these three algorithms. In our TD-CDMA simulation, we implemented the Log-MAP and SOVA decoder to get best performance (with Log-MAP) or fastest speed (with SOVA). Figure 3 gives the performance comparison between Log-MAP and SOVA and it shows that Log-MAP is 1.2dB better than SOVA at the BER of 10^{-2}, with the code block size of 260 bits and 7 iterations.

The code block size or interleaver size is also affect the decoding performance, the BER performance comparison of various code block size is shown in Figure 4. The longer is the code block, the better is the performance, but the big code block size makes more computing time, and the computing complexity increases by exponential.

Table 1. Comparison of complexity of different decoding algorithms

Operations	MAP	Log-MAP	SOVA
additions	$4\times2^M+6$	$12\times2^M+6$	$4\times2^M+9$
max-ops		$4\times2^M-2$	$2\times2^M-1$
multiplications	$10\times2^M+8$	8	4
look-ups	4(exp)	$4\times2^M-2$	

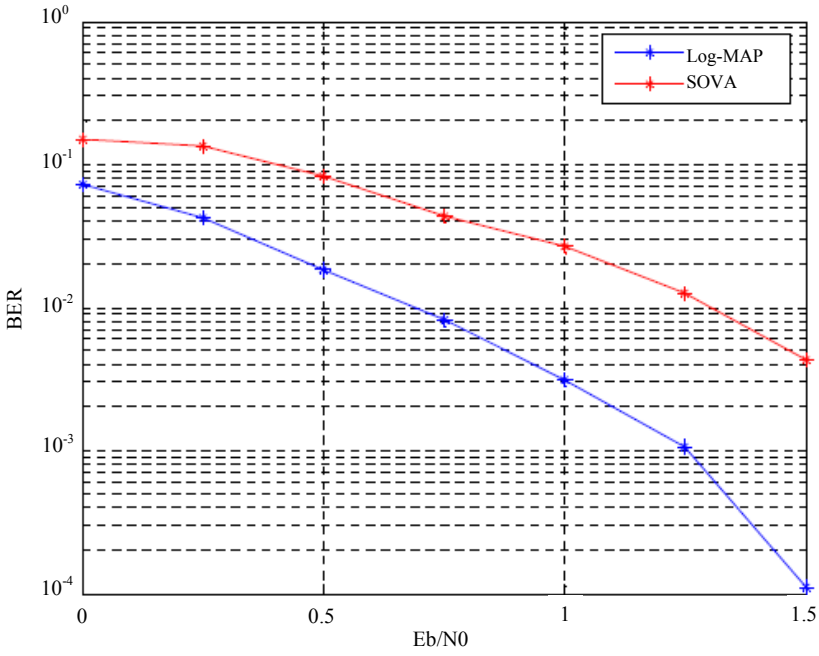

Figure 3. BER performance of Log-MAP algorithm VS SOVA algorithm

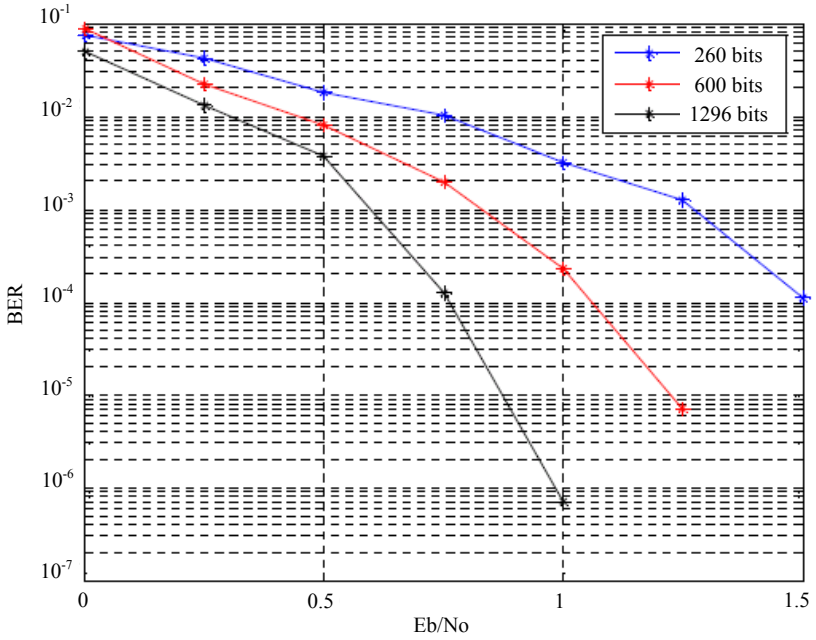

Figure 4. Measured BER performance of the Log-MAP algorithm for various block sizes

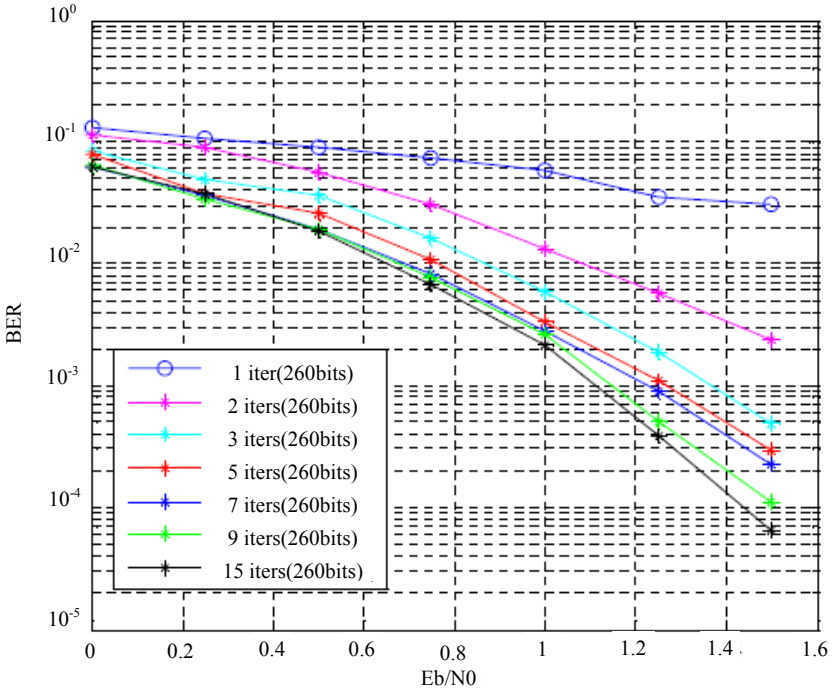

Figure 5. Measured BER performance of Log-MAP algorithm with increasing iteration count

Turbo decoder is the iterative decoder, and decoding performance is also impacted by the number of iteration. Figure 5 shows that the BER performance improves as the number of turbo iteration increased. However, the required computation also increases. It is shown that no significant performance improvement is observed after the sixth iteration.

5. Conclusions

We illustrate the turbo decoder principle, and the derivation of Log-MAP, and SOVA algorithms. Log-MAP algorithm is shown to achieve the best performance with good complexity tradeoff. SOVA algorithm has less computation complexity with about 1.2dB performance

degradation compared with Log-MAP at the BER of 10^{-2}. We also demonstrate that the performance of turbo code is directly proportional to the interleaver size and number of iteration in the turbo decoder. Finally, it is also shown that the performance is affected by the scale of the input soft bits power but the effect is negligible when the scaling factor is larger than 0.8.

6. Acknowledgments

The author would like to thank Dr. Li Lu to help to design simulation platform, and Prof. Gu Xuemai for his revision of the text, and the editor and the anonymous reviewers for their contributions that enriched the final paper.

REFERENCES

[1] PIETROBON S S. Implementation and performance of a turbo/ MAP decoder. Int. J. Satellite Communication, 1998, 16: 23-46.

[2] KAZA J, CHAKRABARTI C. Design and implementation of low-energy turbo decoders. IEEE Transactions on Very Large Scale Integration (VLSI) Systems, 2004, 12(9): 968-977.

[3] HAGH M, SALEHI M, ET AL. Implementation issues in turbo decoding for 3GPP FDD receiver. Wireless Personal Communications, 2006, 39(2): 165-182.

[4] LEE D-S, PARK I.-C. Low-power log-MAP decoding based on reduced metric memory access. IEEE Transactions on Circuits and Systems, 2006, 53(6): 1244-1253.

[5] BOUTILLON E, GROSS W J, GULAK P G. VLSI architectures for the MAP algorithm. IEEE Transactions on Communications, 2003, 51(2): 175-185.

[6] ANANTHARAM V E Y. Iterative decoder architectures. IEEE Communications Magazine, 2003, 41(8): 132-140.

[7] KWON T-W, CHOI J-R. Implementation of a two-step SOVA decoder with a fixed scaling factor. IEICE Transactions on Communications, E86-B(6): Jun. 2003, 1893-1900.

[8] CHEN Y, PARHI K K. On the performance and implementation issues of interleaved single parity check turbo product codes. Journal of VLSI Signal Processing Systems for Signal, Image, and Video Technology, 2005, 39(1): 35-47.

Communications and Network, 2009, 25-34
doi:10.4236/cn.2009.11004 Published Online August 2009 (http://www.scirp.org/journal/cn)

Approximate Analysis of Power Offset over Spatially Correlated MIMO Channels

Guangwei YU, Xuzhen WANG
School of Information and Communication Engineering, Beijing University of Posts and Telecommunications, Beijing, China
Email: {*yuguangwei*1982, *Gxitao*}*@gmail.com*

Abstract: Power offset is zero-order term in the capacity versus signal-to-noise ratio curve. In this paper, approximate analysis of power offset is presented to describe MIMO system with uniform linear antenna arrays of fixed length. It is assumed that the number of receive antenna is larger than that of transmit antenna. Spatially Correlated MIMO Channel is approximated by tri-diagonal toeplitz matrix. The determinant of tri-diagonal toeplitz matrix, which is fitted by elementary curve, is one of the key factors related to power offset. Based on the curve fitting, the determinant of tri-diagonal toeplitz matrix is mathematically tractable. Consequently, the expression of local extreme points can be derived to optimize power offset. The simulation results show that approximation above is accurate in local extreme points of power offset. The proposed expression of local extreme points is helpful to approach optimal power offset.

Keywords: MIMO, multiplexing gain, power offset, high snr region, toeplitz matrix

1. Introduction

Multiple-input multiple-output (MIMO) system is widely used in wireless communication to improve the performance. The spectral efficiency of MIMO channel is much higher than that over the conventional signal antenna channel. The research of MIMO includes two different perspectives: the first one concerns performance analysis in terms of error performance of practical systems, the second one concerns the study of channel capacity.

The design of communication schemes was mainly considered in the former perspectives with the aid of theoretical analysis and simulation [1][2], and [3]. For the latter, important parameters such as diversity gain [4], multiplexing gain [5][6] (referred to degree of freedom in other literatures), and power offset [7-9], and [10] were emphatically analyzed in the high signal-to-noise ratio (SNR) region. Furthermore, diversity and multiplexing tradeoff has been proposed in [11][12], and [13], that is to say diversity and multiplexing tradeoff can be obtained for a given multiple antenna channel. It is worth pointing out in [11] that the diversity and multiplexing tradeoff is essentially the tradeoff between the error probability and the data rate of a given system.

The multiplexing gain is not sufficient to accurately characterize the property of MIMO capacity. A more accurate representation of high SNR behavior in SNR-capacity curve is provided by an affine approximation to capacity, which includes both the multiplexing gain (i.e. slope) and power offset (i.e. zero-order term) [7]. High SNR power offset has been analyzed in [8] over multiple antenna Ricean channels. It was shown in [8] that the impact of the Ricean factor at high SNR region could be conveniently quantified through the corresponding power offset. In [9], high SNR power offset in multiple antenna communication was derived in detail. Achievable throughput was compared between the optimal strategy of dirty paper coding and suboptimal linear precoding techniques (zero-forcing and block diagonalization) in [10] on application of power offset. Hence, power offset is an important parameter in multiple antenna communication.

In many practical environments, signal correlation among the antenna array exists due to the scattering. Fading correlation and its effect on the capacity of multielement antenna system has been studied in [14]. Hence, analysis of spatially correlated MIMO channels has been another topic in the past few years, which necessitates the model of correlated channel. A general space-time correlation model for MIMO systems in mobile fading channel has been presented in [15]. The model in [15] was flexible and mathematically tractable. In [16], the correlated model of [15] has been used to investigate the capacity of spatially correlated MIMO Rayleigh-fading channels.

Recently, application of different antenna arrays in MIMO system has also been exploited. With the consideration of physical constraints imposed by maximum size of the antenna array, uniform linear array of fixed length has been used in [17] to analyze the asymptotic capacity of MIMO systems.

The uniform linear array of fixed length is also used in this paper to analyze the power offset of MIMO system over spatially correlated channel. On application of curve fitting, the determinant of tri-diagonal toeplitz matrix is mathematically tractable. Over spatially correlated chan-

nel, the main result of this paper is the derived expression of local extreme points of power offset, using the uniform linear array of fixed length. To the best of our knowledge, the main result has not been presented in other literatures.

The rest parts are organized as follows. In Section 2, the basic definitions of multiplexing gain and power offset are presented. System model and correlation model are given in Section 3. Approximate analysis of power offset by fitting determinant curve of tri-diagonal toeplitz matrix is put forward in Section 4. Section 5 shows the simulation results. Finally, a brief conclusion is given in Section 6.

Notation: In the following context, matrices and vectors are denoted by boldface upper case symbols and boldface lower case symbols, respectively. The transpose and Hermitian transpose are denoted by $(\bullet)^T$ and $(\bullet)^H$, respectively. The expected value is represented by $E[\bullet]$. $\|\bullet\|$ is used for the Euclidian norm.

2. Basic Definition

In the high SNR region, the capacity of single-user MIMO system of coherent reception is given by [18][19]

$$C(SNR) = \min(n_T, n_R)\log_2 SNR + o(1) \quad (1)$$

where n_T, n_R denote the number of transmit and receive antenna elements , respectively. SNR is the signal to noise ratio. The MIMO capacity in high SNR region is a linear function of $\min(n_T, n_R)$, i.e. the stationary slope in SNR-capacity curve. In other words, any increase in $\max(n_T, n_R)$ is immaterial, i.e. without any impact to the slope. The slope is the so-called maximum multiplexing gain (degree of freedom).

If n_T is fixed to a given value (generally speaking, n_T is less than six, expressed as $\widehat{n_T}$ in the following context), and $n_R \geq n_T$, the multiplexing gain equals to a fixed value without consideration of correlation of channel response and the number of receive antenna elements. So power offset is introduced to compare the impact of channel property with the same value of multiplexing gain, and (1) is replaced by [9]

$$\begin{aligned} C(SNR) &= S_\infty(\log_2(SNR) - L_\infty) + o(1) \\ &= S_\infty\left(\frac{SNR_{dB}}{3dB} - L_\infty\right) + o(1) \end{aligned} \quad (2)$$

where S_∞ is multiplexing gain and L_∞ is power offset in 3-dB units. When $SNR \to \infty$, the multiplexing gain and power offset can be computed by

$$S_\infty = \lim_{SNR\to\infty} \frac{C(SNR)}{\log_2(SNR)} \quad (3)$$

$$L_\infty = \lim_{SNR\to\infty}\left(\log_2(SNR) - \frac{C(SNR)}{S_\infty}\right) \quad (4)$$

In the high SNR region, SNR-capacity curve is approximately determined by multiplexing gain and power offset. Most channels, having the same multiplexing gain, may have very different capacities because of various values of the power offset. Hence, power offset is an important parameter to describe the capacity behavior in high SNR region.

3. System Model and Correlation Mode

The system model and channel correlation model are defined in this section. For MIMO system, the general baseband model is given by

$$\mathbf{y} = \mathbf{H}\mathbf{x} + \mathbf{n} \quad (5)$$

where $\mathbf{H}$ is the channel response matrix, and $\mathbf{x} = [x_1\ x_2 \cdots x_{\widehat{n_T}}]^T$ is the input complex signal vector whose spatial covariance matrix normalized by the energy per dimension can be expressed as

$$\mathbf{\Phi} = \frac{E(\mathbf{x}\mathbf{x}^H)}{1/\widehat{n_T} \times E[\|\mathbf{x}\|^2]} \quad (6)$$

while $\mathbf{y} = [y_1\ y_2 \cdots y_{n_R}]^T$ and $\mathbf{n} = [n_1\ n_2 \cdots n_{n_R}]^T$ are the output vector and additive white Gaussian noise vector, respectively. Because of normalization and assumption of isotropic input, $tr(\mathbf{\Phi}) = \widehat{n_T}$ and $\mathbf{\Phi} = \mathbf{I}_{\widehat{n_T}}$, where $\mathbf{I}_n$ is $n \times n$ identity matrix.

Kronecker model [16] is used to describe the correlation of channel response. On the assumption of rich scattering environments and having no line of sight, the correlated channel response matrix is denoted by

$$\mathbf{\Sigma}_H = \mathbf{\Sigma}_T \otimes \mathbf{\Sigma}_R \quad (7)$$

where $\otimes$ is Kronecker product, $\mathbf{\Sigma}_T$ and $\mathbf{\Sigma}_R$ are correlated matrix of transmit and receive antenna, respectively. So the channel response matrix $\mathbf{H}_\Sigma$ is given by

$$\mathbf{H}_\Sigma = \mathbf{\Sigma}_R^{1/2}\mathbf{H}\mathbf{\Sigma}_T^{1/2} \quad (8)$$

where $\mathbf{H}$ is channel response matrix whose elements are independent and identical distribution random variables. Without loss of generality, we assume that the distance between transmit antenna elements is large enough to neglect the correlation at the transmit node. Consequently, without considering the antenna correlation at the transmit node, the correlation matrix $\mathbf{\Sigma}_T$ is identity matrix, and the receive antenna correlation model $\mathbf{\Sigma}_R$ is given by [15][16].

$$\mathbf{\Sigma}_R(i,j)=\frac{I_0\left(\sqrt{\eta^2-4\pi^2 d_{ij}^2+j4\pi\eta\sin(\mu)d_{ij}}\right)}{I_0(\eta)} \quad (9)$$

where $\eta\in[0,\infty)$ is the so-called AOA(angle of arrival), $\mu\in[-\pi,\pi)$ is average value of AOA, d_{ij} is normalized distance between antenna array elements, that is to say $d_{ij}=\widehat{d_{ij}}/\lambda$, $\widehat{d_{ij}}$ is the factual distance between i and j antenna array element, λ is wave length, $I_n(\cdot)$ is n-order modified Bessel function. It is obvious that $\mathbf{\Sigma}_R(i,j)$ is real symmetric toeplitz matrix.

On the assumption of isotropic scattering, the correlation matrix at the receive node is simplified to

$$\mathbf{\Sigma}_R(i,j)=J_0(2\pi d_{ij}) \quad (10)$$

where $J_n(\cdot)$ is n order Bessel function, and $\mathbf{\Sigma}_R(i,j)$ can be simplified to tri-diagonal toeplitz matrix through the simulation results illustrated by Figure 1 and Figure 2.

$$\mathbf{\Sigma}_R=\begin{bmatrix}1 & \alpha & & & \\ \alpha & \ddots & \ddots & & \\ & \ddots & \ddots & \ddots & \\ & & \ddots & \ddots & \alpha \\ & & & \alpha & 1\end{bmatrix}_{n_R\times n_R} \quad (11)$$

where

$$\alpha=J_0\left(2\pi\frac{L_R}{n_R-1}\right),\quad 1\le L_R\le 10 \quad (12)$$

where L_R is the fixed length of receive antenna array normalized by λ. In this paper, L_R is assumed to be in the range from 1 to 10.

In the Figure 1 and 2, power offset approximation based on tri-diagonal, five-diagonal, and seven-diagonal toeplitz matrix is obtained versus the number of receive antenna with various value of L_R. Furthermore, power offset over independent channel is also provided as lower bound for numerical comparison. It can be seen from Figure 1 and 2 that tri-diagonal toeplitz matrix can be used to approximate the correlation model at the receive node.

4. Approximate Analysis of Power Offset

Depending on the discussion in Section 3, tri-diagonal toeplitz matrix can be used to approximate the correlation model at the receive node. In this section, the determinant curve of tri-diagonal toeplitz matrix is fitted by an elementary function, which simplifies the approximate analysis of power offset.

Expression of power offset for MIMO system over correlated channel is derived in [9], and the expression is given by

$$L_\infty=\log_2\widehat{n_T}-\frac{1}{\widehat{n_T}\ln 2}E(\ln\det(\mathbf{W}^H\mathbf{\Lambda}_R\mathbf{W}))-\frac{1}{\widehat{n_T}}\log_2\det(\mathbf{\Lambda}_T\mathbf{P}) \quad (13)$$

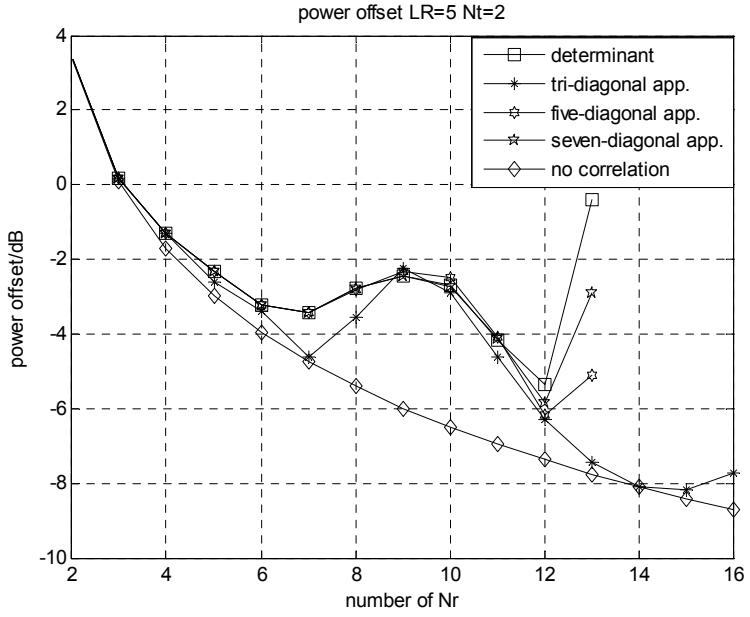

Figure 1. Approximate analysis of power offset based on 3, 5, and 7 diagonal toeplitz matrix with $L_R=5$, $\widehat{n_T}=2$

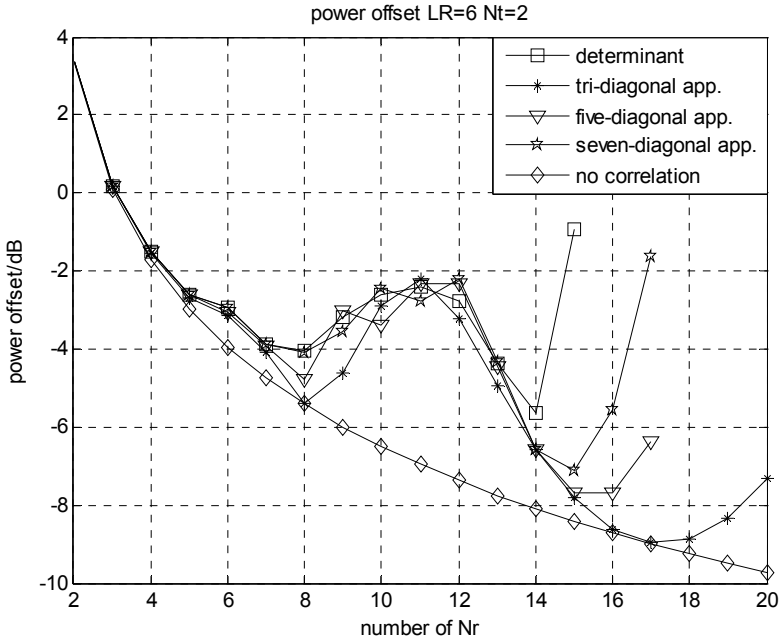

Figure 2. Approximate analysis of power offset based on 3, 5, and 7 diagonal toeplitz matrix with $L_R = 6$, $\widehat{n_T} = 2$

where $\mathbf{\Lambda}_T$ and $\mathbf{\Lambda}_R$ are diagonal matrix whose elements are eigenvalues of $\mathbf{\Sigma}_T$ and $\mathbf{\Sigma}_R$, respectively. $\mathbf{P}$ is also diagonal matrix whose elements are eigenvalues of normalized spatial covariance matrix $\mathbf{\Phi}$, so $\mathbf{P}$ is identity matrix and $1/\widehat{n_T}\log_2\det(\mathbf{\Lambda}_T\mathbf{P})$ is constant zero. $\mathbf{\Lambda}_R$ can be derived from (11). It is obvious that $\mathbf{\Lambda}_R$ is full rank matrix, and then (13) is simplified to

$$L_\infty = \log_2 \widehat{n_T} + (f(n_R) + g(n_R)) \tag{14}$$

where $f(n_R)$ and $g(n_R)$ can be described by

$$f(n_R) = -\frac{E(\ln\det(\mathbf{W}^H\mathbf{W}))}{\widehat{n_T}\ln 2} \tag{15}$$

$$g(n_R) = -\frac{\ln\det(\mathbf{\Lambda}_R)}{\widehat{n_T}\ln 2} \tag{16}$$

Because $\mathbf{W}^H\mathbf{W}$ is wishart matrix and nonsingular with probability 1, $f(n_R)$ is reduced to [9]

$$\begin{aligned} f(n_R) &= -\frac{1}{\widehat{n_T}\ln 2}E(\log_e\det(\mathbf{W}^H\mathbf{W})) \\ &= -\frac{1}{\widehat{n_T}\ln 2}\sum_{l=0}^{\widehat{n_T}-1}\psi(n_R - l) \end{aligned} \tag{17}$$

where $\psi(\cdot)$ is digamma function and the definition of digamma function is

$$\psi(n) = -\gamma + \sum_{l=1}^{n-1}\frac{1}{l} \tag{18}$$

where γ is Euler-Mascheroni constant, and

$$\gamma = \lim_{n\to\infty}\left(\sum_{l=1}^{n}\frac{1}{l} - \log_e n\right) \approx 0.5772 \tag{19}$$

When it comes to function $g(n_R)$, the derivation of $g(n_R)$ can be expressed as

$$g(n_R) = -\frac{1}{\widehat{n_T}\ln 2}\ln\det(\mathbf{\Lambda}_R) = -\frac{1}{\widehat{n_T}\ln 2}\ln\det(\mathbf{\Sigma}_R) \tag{20}$$

It can be found from (20) that $g(n_R)$ is only determined by the determinant of $\mathbf{\Sigma}_R$, and the determinant of n_R order tri-diagonal toeplitz matrix $\mathbf{\Sigma}_R$ can be computed by [20].

$$\det\mathbf{\Sigma}_R = \begin{cases} \dfrac{\left(1+\sqrt{1-4\alpha^2}\right)^{n_R+1} - \left(1-\sqrt{1-4\alpha^2}\right)^{n_R+1}}{2^{n_R+1}\sqrt{1-4\alpha^2}} \\ \left(1-4\alpha^2 \neq 0\right) \\ \dfrac{n_R+1}{2^{n_R}} \\ \left(1-4\alpha^2 = 0\right) \end{cases} \tag{21}$$

With the aid of numerical computation and mathematical analysis, the curve of the determinant of tri-diagonal toeplitz matrix can be fit by some tractable elementary

function. When $1-4\alpha^2 \neq 0$ in (21), $\det \mathbf{\Sigma}_R$ can be approximated by the fitted curve as follow:

$$h(n_R) = 1-5\alpha^2 = 1-5J_0(2\pi \frac{L_R}{n_R-1})^2 \quad \textbf{(22)}$$

The approximation between the fitted curves and determinant curves of tri-diagonal toeplitz matrix are illustrated in Figure 3 and Figure 4. From Figure 3 and 4, we can find that the fitting curve can exactly approach the extreme points of the determinant of tri-diagonal toeplitz matrix. However, the expression is much simpler. In other words, the further derivation using the fitted curve is tractable using well-known mathematical software such as WOLFRAM MATHEMATICA.

In the following context, power offset is analyzed in detail. The approximate analysis of power offset is based on the piecewise function of n_R. The condition $1-5\alpha^2 > 0$ in (22) is necessary due to $\det \mathbf{\Sigma}_R > 0$, so the number of receiver antenna n_R can not be large than $4L_R+1$. Moreover, it shows from the conclusion in [21] that the effect of correlation can be neglected when the normalized length of receive antenna array L_R is larger than one wave length, that is to say $n_R > L_R+1$. Hence, the considered range of the number of receive antenna is $L_R+1 < n_R < 4L_R+1$.

With the discussion above, when $n_R \leq L_R+1$, the normalized length of receive antenna array L_R is large than one wave length and the effect of correlation can be neglected, that is to say $g(n_R)=0$ and the power offset is expressed as

$$L_\infty = \log_2 \widehat{n_T} - \frac{1}{\widehat{n_T}\ln 2}\sum_{l=0}^{\widehat{n_T}-1}\psi(n_R-l) \quad \textbf{(23)}$$

When it comes to the range of $L_R+1 < n_R < 4L_R+1$, the normalized length of receive antenna array L_R is smaller than one wave length and the effect of correlation can not be neglected. In other words, $g(n_R) \neq 0$. However, for a given value of $\widehat{n_T}$, the first-order derivative ($f(n_R)$ is assumed to be continuous) of $f(n_R)$ is obtained by

$$\begin{aligned}\frac{df(n_R)}{dn_R} &= \left(-\frac{1}{\widehat{n_T}\ln 2}\sum_{l=0}^{\widehat{n_T}-1}\psi(n_R-l)\right)' \\ &= -\frac{1}{\widehat{n_T}\ln 2}\sum_{l=0}^{\widehat{n_T}-1}\psi_1(n_R-l) \approx 0\end{aligned} \quad \textbf{(24)}$$

where $\psi_1(\cdot)$ is trigamma function. Hence, it shown from (24) that $f(n_R)$ approximately equal to the constant C (approximation accuracy is related to the value of $\widehat{n_T}$). The power offset is expressed as

$$L_\infty \approx \log_2 \widehat{n_T} + g(n_R) + C \quad \textbf{(25)}$$

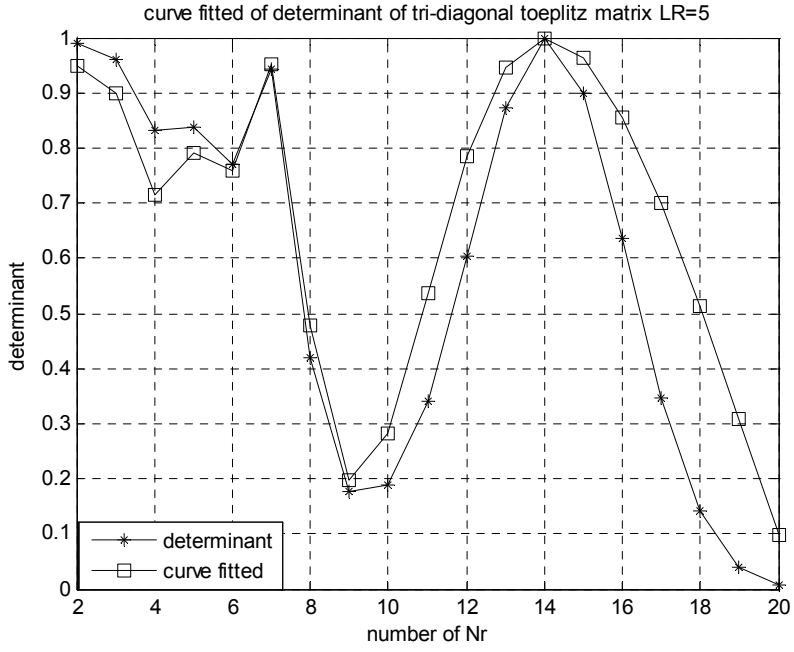

Figure 3. Approximation of determinant of tri-diagonal toeplitz matrix by curve fitting and $L_R = 5$

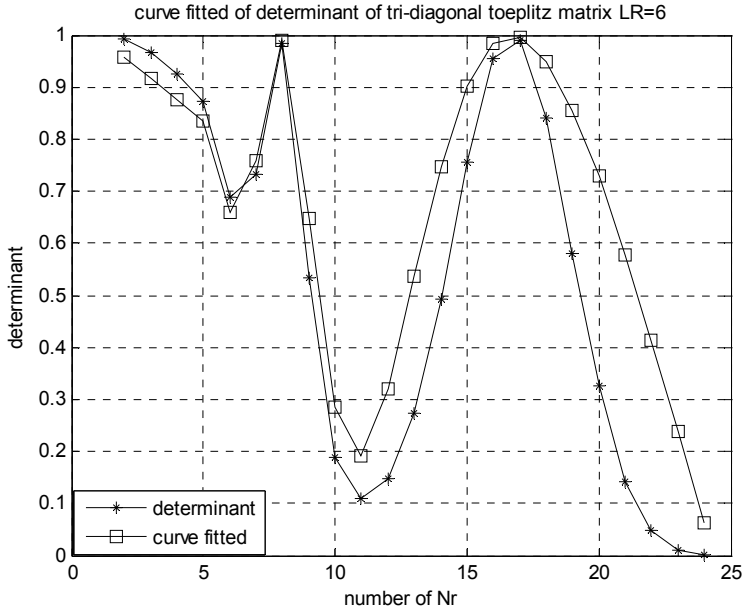

Figure 4. Approximation of determinant of tri-diagonal toeplitz matrix by curve fitting and $L_R = 6$

Without loss of generality, the constant C can be neglected in the approximate computation. Hence, the power offset in (25) is only determined by $g(n_R)$. From (22), the curve of the determinant of tri-diagonal toeplitz matrix can be fitted by $h(n_R) = 1 - 5\alpha^2$, where $\alpha = J_0(\frac{2\pi L_R}{n_R - 1})$. The first order derivative ($h(n_R)$ is assumed to be continuous) of $h(n_R)$ can be computed by

$$\frac{dh(n_R)}{dn_R} = -\frac{4\pi L_R J_0(\frac{2\pi L_R}{n_R-1}) J_1(\frac{2\pi L_R}{n_R-1})}{(n_R-1)^2} \quad \textbf{(26)}$$

where $L_R + 1 < n_R < 4L_R + 1$, that is to say $\frac{\pi}{2} < \frac{2\pi L_R}{n_R - 1} < 2\pi$. In the range above, function $J_0(\frac{2\pi L_R}{n_R-1})$ in (26) has two zero points, i.e. $P_1 = \frac{2\pi L_R}{n_R - 1} = 2.4048$ and $P_2 = \frac{2\pi L_R}{n_R - 1} = 5.5201$, and function $J_1(\frac{2\pi L_R}{n_R-1})$ only has one zero point, i.e. $P_3 = \frac{2\pi L_R}{n_R - 1} = 3.8317$. Consequently, $h(n_R)$ has three extreme points in the range of $\frac{\pi}{2} < \frac{2\pi L_R}{n_R - 1} < 2\pi$, described by $P_i,\ i = 1,2,3$.

And then, the second-order derivative of $h(n_R)$ can be computed by

$$\begin{aligned}\frac{d^2h(n_R)}{dn_R^2} &= \frac{8\pi L_R J_0(\frac{2\pi L_R}{n_R-1}) J_1(\frac{2\pi L_R}{n_R-1})}{(n_R-1)^3} \\ &\quad - \frac{8\pi^2 L_R{}^2 J_1(\frac{2\pi L_R}{n_R-1})^2}{(n_R-1)^4} \\ &\quad + \frac{4\pi^2 L_R{}^2 J_0(\frac{2\pi L_R}{n_R-1})\left[J_0(\frac{2\pi L_R}{n_R-1}) - J_2(\frac{2\pi L_R}{n_R-1})\right]}{(n_R-1)^4}\end{aligned} \quad \textbf{(27)}$$

Using (27), the second-order derivative in points $P_i,\ i = 1,2,3$ is obtained as follow:

$$P_1 : \left.\frac{d^2h(n)}{dn_R^2}\right|_{\frac{2\pi L_R}{n_R-1}=2.4048} = -\frac{4.51}{\pi^2 L_R{}^2} < 0 \quad \textbf{(28)}$$

$$P_2 : \left.\frac{d^2h(n)}{dn_R^2}\right|_{\frac{2\pi L_R}{n_R-1}=5.5201} = -\frac{53.75}{\pi^2 L_R{}^2} < 0 \quad \textbf{(29)}$$

$$P_3 : \left.\frac{d^2h(n)}{dn_R^2}\right|_{\frac{2\pi L_R}{n_R-1}=3.8317} = \frac{17.48}{\pi^2 L_R{}^2} > 0 \quad \textbf{(30)}$$

With the discussion above, it is obvious that point P_1 and P_2 are local maximum points of $h(n_R)$ and point

P_3 is local minimum point. Furthermore, it is obvious from (20) that the extreme points of $h(n_R)$ is same as ones of $g(n_R)$. Consequently, in the range of $L_R+1<n_R<4L_R+1$, the extreme points of power offset in (25) can be approximately computed by

$$\widehat{n_R}=\begin{cases}\arg\min\limits_{n_R\in\Pi}(L_\infty), & \text{for local minimal point}\\ \arg\max\limits_{n_R\in\Pi}(L_\infty), & \text{for local maximum point}\end{cases} \quad \textbf{(31)}$$

where Π is defined as follows:

$$\Pi=\left\{\left\lfloor\frac{2\pi L_R}{P_i}+1\right\rfloor,\left\lceil\frac{2\pi L_R}{P_i}+1\right\rceil\right\},i=1,2,3 \quad \textbf{(32)}$$

where $\lfloor x\rfloor$ and $\lceil x\rceil$ denote the maximum integer smaller than x and minimum integer larger than x, respectively. P_i, $i=1,2,3$ is the extreme points computed above. (31) can be used to approximately compute the number of receive antenna, in order to achieve the optimal power offset.

5. Simulation Results

In the Figure 1 and 2, with the assumption of $\widehat{n_T}=2$, power offset is approximately analyzed based on tri-diagonal, five-diagonal, and seven-diagonal toeplitz versus the number of receive antenna, with $L_R=5$ in Figure 1 and $L_R=6$ in Figure 2. Furthermore, power offset in independent channel is also provided as lower bound for numerical comparison. The approximation trend can be found from Figure 1 and 2. The tri-diagonal toeplitz matrix can be assumably used to characterize the property of power offset over spatially correlated channel. Hence, tri-diagonal toeplitz matrix can be used to approximate the correlation model at the receive node.

The approximation of fitting the curve of tri-diagonal toeplitz matrix determinant is illustrated in Figure 3 and Figure 4 to compare the difference between fitted curves and determinant curves, with $L_R=5$ in Figure 3 and $L_R=6$ in Figure 4. From Figure 3 and 4, we can find that the fitting curve can exactly approach the extreme points of the determinant of tri-diagonal toeplitz matrix. However, the expression is mathematically tractable.

With the same assumption of $\widehat{n_T}=2$, approximation of power offset is shown in Figure 5 and 6, with $L_R=5$ in Figure 5 and $L_R=6$ in Figure 6. From Figure 5 and 6, we can find the position of two local minimal points and one local maximum point. With the condition of $L_R=5$ and $\widehat{n_T}=2$, the local extreme points computed by (31) is $n_R=9$ for local maximum point and $n_R=7,\ 15$ for local minimal points. With the condition of $L_R=6$ and $\widehat{n_T}=2$, the local extreme points computed by (31) is $n_R=11$ for local maximum point and $n_R=8,\ 16$ for local minimal points. The computation results based on (31) coincide with the illustration results in Figure 5 and 6. Hence, all the approximation in this paper is reasonable, including approximation of correlation model and approximation of determinant of tri-diagonal toeplitz matrix.

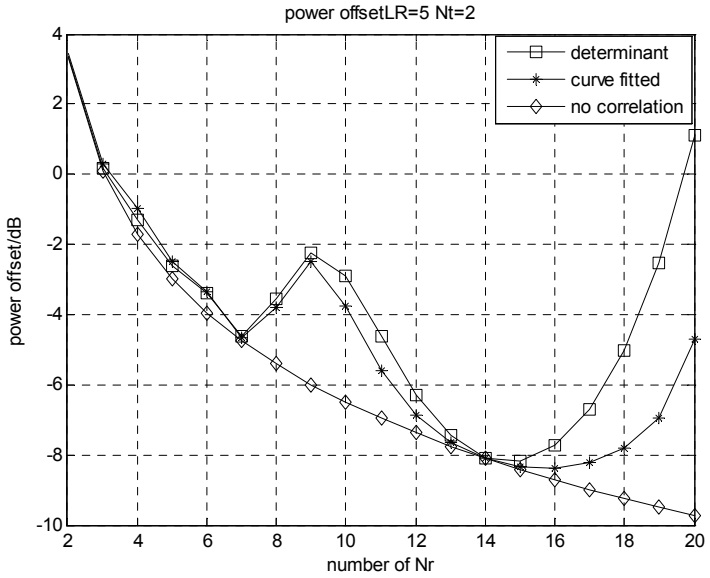

Figure 5. Power offset comparation between accurate and approximate determinant of toeplitz matrix with $L_R=5$, $\widehat{n_T}=2$

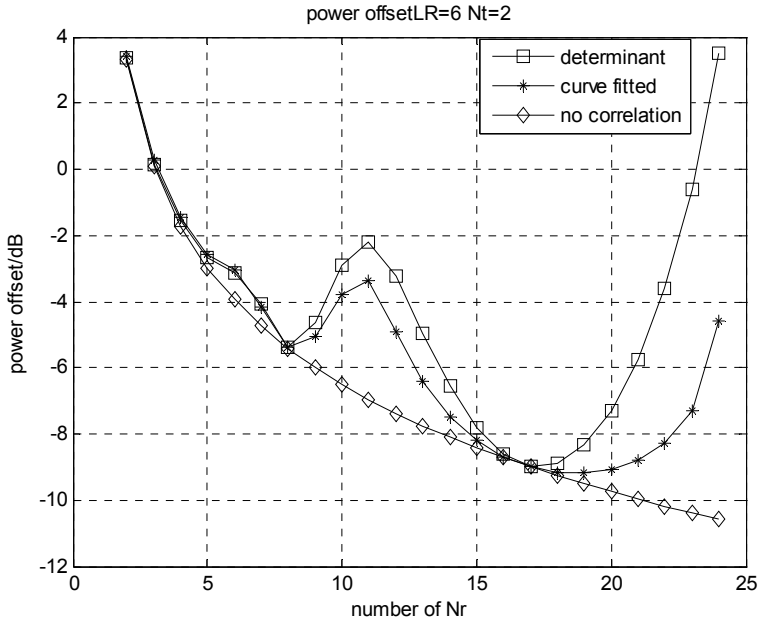

Figure 6. Power offset comparation between accurate and approximate determinant of toeplitz matrix with $L_R = 6$, $\widehat{n_T} = 2$

Similar results are presented in Figure 7 and 8, with the assumption of $\widehat{n_T} = 4$ and $L_R = 5$ in Figure 7 while $L_R = 8$ in Figure 8. With the condition of $L_R = 5$ and $\widehat{n_T} = 4$, the local extreme points computed by (31) is $n_R = 9$ for local maximum point and $n_R = 7,\ 15$ for local minimal points. With the condition of $L_R = 8$ and $\widehat{n_T} = 4$, the local extreme points computed by (31) is $n_R = 14$ for local maximum point and $n_R = 10,\ 22$ for local minimal points. The computation results based on (31) coincide with the illustration results in Figure 7 and 8.

Consequently, it is presented in Figure 5 and 7 that the effect caused by the number $\widehat{n_T}$ can be neglected. In other words, for small value of $\widehat{n_T}$ and in the range of number of receive antenna $L_R + 1 < n_R < 4L_R + 1$, the assumption of $f(n_R) \approx C$ is tenable with neglectable loss of precision. The extreme points of power offset is only determined by $g(n_R)$.

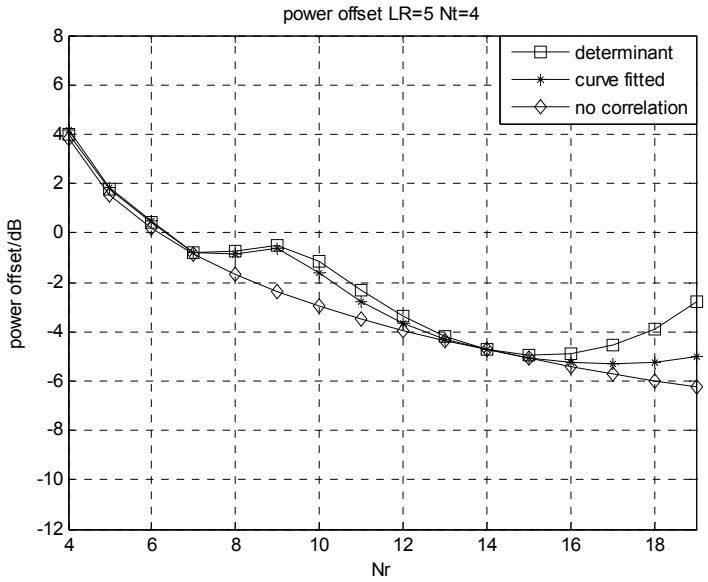

Figure 7. Power offset comparation between accurate and approximate determinant of toeplitz matrix with $L_R = 5$, $\widehat{n_T} = 4$

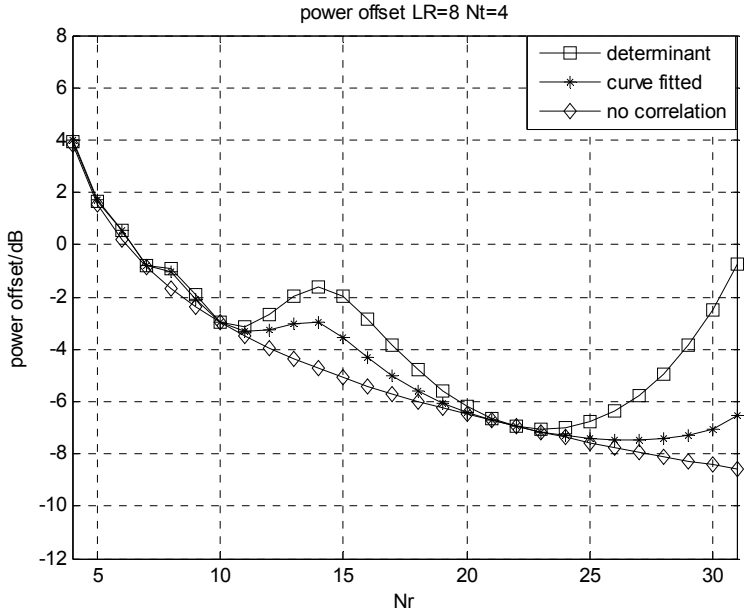

Figure 8. Power offset comparation between accurate and approximate determinant of toeplitz matrix with $L_R = 8$, $\widehat{n_T} = 4$

6. Conclusions

Approximate analysis of power offset over spatially correlated channel is proposed to optimize the number of receive antenna with antenna array of fixed length. Antenna correlation matrix is approximated by tri-diagonal toeplitz matrix. The determinant of tri-diagonal toeplitz matrix is reduced to simple style by curve fitting with neglectable loss of precision. Based on the approximation above, the expression of local extreme points of power offset is derived. Simulation results shows that the derived expression is accurate in the local extreme points of power offset, that is to say, all the approximation in this paper is reasonable.

REFERENCES

[1] TAROKH V, JAFARKHANI H, CALDERBANK A R. Space-time block code from orthogonal designs. IEEE Transactions on Information Theory, Jul. 1999, 45(5): 1456-1467.

[2] BOUBAKER N, LETAIEF K B, MURCH R D. Performance of BLAST over frequency-selective wireless communication channles. IEEE Transactions on Communication, Feb. 2002, 50(2): 196-199.

[3] LOZANO A, PAPADIAS C. Layered space-time receivers for frequency-selective wireless channels. IEEE Transactions on Communication, Jan. 2002, 50(1): 65-73.

[4] BAKIR L, FROLIK J. Diversity gains in two-ray fading channels. IEEE Transactions on Wireless Communications, Feb. 2009, 8(2): 968-977.

[5] POON A, BRODERSEN R, TSE D. N. C. Degrees of freedom in multiple-antenna channels: A signal space approach. IEEE Transactions on Information Theory, Feb. 2006, 51(2): 523-536.

[6] JAFAR S A, SHAMAI S. Degrees of freedom region of the MIMO X channel. IEEE Transactions on Information Theory, Jan. 2008, 54(1): 151-170.

[7] JINDAL N. High SNR analysis of MIMO broadcast channels. ISIT'05, 2005, 2310-2314.

[8] TULINO A M, LOZANO A, VERDU S. High-SNR power offset in multi-antenna Ricean channels. ICC'05, 2005, 683-687.

[9] LOZANO A, TULINO A M, VERDU S. High-SNR power offset in multi-antenna communication. IEEE Transactions on Information Theory, Dec. 2005, 51(12): 4134-4151.

[10] LEE J, JINDAL N. High SNR analysis for MIMO broadcast channels: Dirty paper coding versus linear precoding. IEEE Transactions on Information Theory, Dec. 2007, 53(12): 4787-4792.

[11] ZHENG L Z, TSE D N C. Diversity and multiplexing: A fundamental tradeoff in multiple-antenna channels. IEEE Transactions on Information Theory, May 2003, 49(5): 1073-1096.

[12] TSE D N C, VISWANATH P, ZHENG L Z. Diversity multiplexing tradeoff in multiple-access channels. IEEE Transactions on Information Theory, Sep. 2004, 50(9): 1859-1874.

[13] WAGNER J, LIANG Y C, ZHANG R. On the balance of multiuser diversity and spatial multiplexing gain in random beamforming. IEEE Transactions on Wireless Communication, Jul. 2008, 7(7): 2512-2525.

[14] SHIU D, FOSCHINI G J, GANS M J, ET AL. Fading correlation and its effect on the capacity of multielement antenna system. IEEE Transactions on Communication, Mar. 2000, 48(3): 502-513.

[15] ABDI A, KAVEH M. A space-time correlation model for multielement antenna systems in mobile fading channels. IEEE J. Select. Areas Communication, Apr. 2002, 20: 550-560.

[16] CHIANI M, WIN M Z, ZANELLA A. On the capacity of spatially correlated MIMO Rayleigh Fading channels. IEEE Transactions on Information Theory, Oct. 2003, 49(10): 2363-2371.

[17] WEI S, GOECKEL D, JANASWAMY R. On the asymptotic capacity of MIMO systems with antenna arrays of fixed length. IEEE Transactions on Wireless Communications, Jul. 2005, 4(4): 1608-1621.

[18] TELATAR I E. Capacity of multi-antenna Gaussian channel. Europe Transactions on Telecommunication, Nov./Dec. 1999, 10: 585-595.

[19] FOSCHINI G J, GANS M J. On the limits of wireless communications in a fading environment when using multiple antenna. Wireless Personal Communication, 1998, 6(3): 315-335.

[20] XU Z, ZHANG K Y, LU Q. Fast algorithm based on toeplitz matrix. Xi'an: Northwest Industrial University, 1999.

[21] ZHUANG Z M, CAI C Q, ET AL. Space-time correlation analysis for MIMO fading channel based on geometric model. Journal of Shantou University, 2008, 23(1): 48-53.

Communications and Network, 2009, 35-41
doi:10.4236/cn.2009.11005 Published Online August 2009 (http://www.scirp.org/journal/cn)

A Cross-Layer Scheme for Handover in 802.16e Network with F-HMIPv6 Mobility

Yi ZHENG, Yong ZHANG, Yinglei TENG, Mei SONG
Beijing University of Posts and Telecommunications, Beijing, China
Email: {zhengyibupt, bjzhangyong, lilytengtt}@gmail.com; Songm@bupt.edu.cn

Abstract: IEEE802.16e is the major global cellular wireless standard that enables low-cost mobile Internet application. However, existing handover process system still has latency affects time-sensitive applications. In this paper, the handover procedures of 802.16e and Fast Handover for Hierarchical MIPv6 (F-HMIPv6) are reconstructed to achieve a better transmission performance. The concept of cross layer design is adopted to refine the existing handover procedure specified in 802.16e MAC layer and F-HMIPv6. More specifically, layer2 and layer3 signaling messages for handover are analyzed and combined/interleaved to optimize the handover performance. Extensive simulations show that the proposed scheme in this paper is superior to the other scheme proposed by IETF.

Keywords: handover, cross layer, 802.16e, F-HMIPv6

1. Introduction

Recently, wireless access technologies have been evolving for diverse capabilities and services. The Third Generation Partnership Project (3GPP) has been defining Universal Terrestrial Radio Access (UTRA) for 3G radio access，as well as the optimization of the network architecture with HSxPA [1]. The CDMA2000 mobile communication system also has been evolved into 1xEV-Dx for high speed data services. As one of wireless access technologies, Mobile WiMAX was successfully adopted by ITU as one of the IMT-2000 technologies in November 2007. Since then mobile WiMAX (IP-OFDMA) has officially become a major global cellular wireless standard along with 3GPP UMTS/HSPA and 3GPP2 CDMA/EVDO [2].

Mobile WiMAX is a fast growing broadband access technology that enables low-cost mobile Internet applications, and realizes the convergence of mobile and fixed broadband access in a single air interface and network architecture. The IEEE802.16e provides high bandwidth, low-cost, scalable solutions that extend services from backbone networks to wireless users. Because of a larger coverage area, portability and mobility have become significant issues for providing high quality application, as it is crucial to minimize handover latency and maintain session continuity. The IEEE 802.16e standard only defines a frame work in MAC layer (L2) without considering upper layer handover performance. But from the IP based service point of view, simply reducing the L2 latency does not adequately reduce the overall handover latency. The whole handover procedure shall not include L2 only but also the IP layer. So in order to improve the IP layer (L3) handover performance, a number of standards of MIPv6 are proposed by IETF. Fast Handovers for Mobile IPv6 (FMIPv6) [3], aim to reduce the handover latency by configuring new IP addresses before entering the new subnet. Hierarchical MIPv6 mobility management (HMIPv6) [4] introduces a hierarchy of mobile agents to reduce the registration latency and the possibility of an outdated care-of address. FMIPv6 and HMIPv6 can also be used together as suggested in [5] to reduce the latency related to Movement Detection and CoA configuration/Verification and cut down the signaling overhead and delay concerned with Binding Update (BU). Fast Handover for Hierarchical MIPv6 (F-HMIPv6) [5] also introduces the Mobility Anchor Point (MAP) to provide a better solution for micro mobility.

In order to provide seamless services during handover, in this paper, we study the process that shall be performed in L2 and L3 and the related message of 802.16e and F-HMIPv6 to propose a cross layer handoff scheme. In order to speed up the total handover process, we also use the proposed scheme in [6] to optimize the 802.16e network entry procedure and reduce the L2 handover delay. This paper is organized as follows. In Section 2 we briefly introduce the relevant protocols and related proposals. In Section 3 we present our cross-layer handover scheme, while Section 4 validates its performance. We finally conclude the paper in Section 5.

2. Background and Related Works

2.1 Handover Process of 802.16e

Figure 1 shows the handover process of 802.16e. The 802.16e handover (HO) procedure includes several phases, namely, network topology acquisition and advertisement, target BS scanning procedure, HO decision and initiation, and network re-entry [7]. We provide details about these

stages, explaining what is their role in the overall MAC-layer HO latency.

In network topology acquisition stage, a BS periodically broadcasts the system information of the neighboring BSs using Neighbour Advertisement message. The Serving BS may unicast MOB_NBR-ADV message based on the cell types of neighbor cells, in order to achieve overhead reduction and facilitate scanning priority for MS. Then MS may use any unavailable intervals assigned by the serving BS to perform scanning. The BS or MS may prioritize the neighbor BSs to be scanned based on various metrics, such as cell type, loading, RSSI and location. MS measures the selected scanning candidate BSs and reports the measurement result back to the serving BS by using Neighbour Advertisement message.

The handover algorithm is a network-controlled, MS-assisted handover. Although handover procedure may be initiated by either MS or BS, the final HO decision and target BS(s) selection are performed by the serving BS or the network. MS executes the HO as directed by the BS or cancels the HO procedure through HO cancellation message. The network re-entry procedure with the target BS may be optimized by target BS possession of MS information obtained from serving BS over the backbone network. MS may also maintain communication with serving BS while performing network re-entry at target BS as directed by serving BS.

2.2 Fast Handover for Hierarchical MIPv6 (F-HMIPv6)

The handover process of 802.16e mainly deals with layer2 hop-by-hop connection issues. However, fast Handover for Hierarchical MIPv6 (F-HMIPv6) protocol takes the advantage of FMIPv6 and HMIPv6, which is the most popular layer3 protocol. The HMIPv6 introduces the Mobility Anchor Point (MAP) to reduce the signaling overhead and delay concerned with Binding Update for micro mobility. Therefore HMIPv6 still needs a further handover enhancement to support the real-time applications. Currently FMIPv6 is the typical protocol to reduce the handover latency. Then F-HMIPv6 integrates these two protocols and provides a scheme for effective integration. Figure 2 illustrates the generic procedures for F-HMIPv6 operations.

Based on L2 handover anticipation, the mobile node (MN) sends RtSolPr message to MAP. The RtSolPr should include information about the link layer address or identifier of the concerned New Access Router (NAR). In response to the RtSolPr message, the MAP sends the PrRtAdv message contain information about New on-link Care of Address (NLCoA) to the MN. At this time, MAP

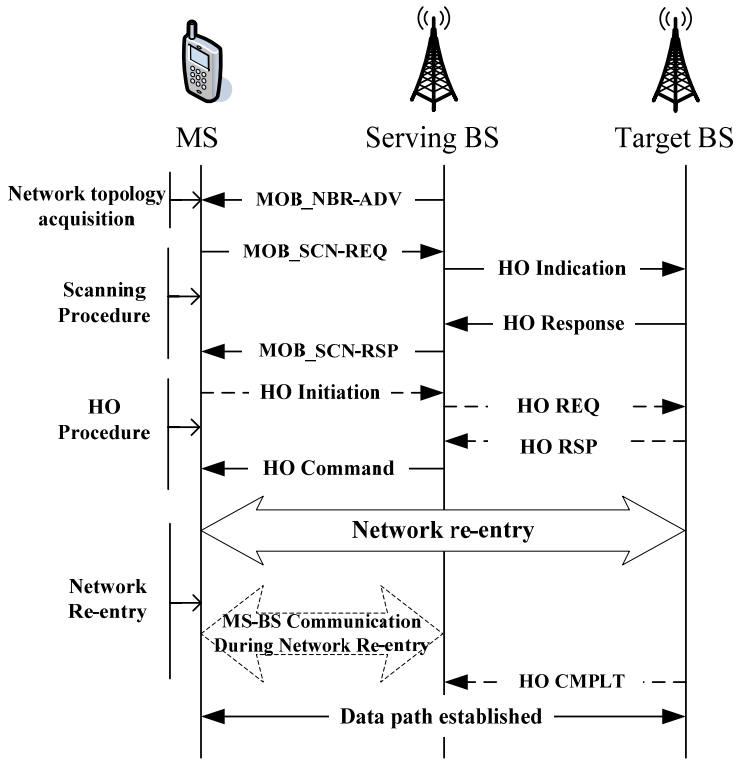

Figure 1. A general flow for HO

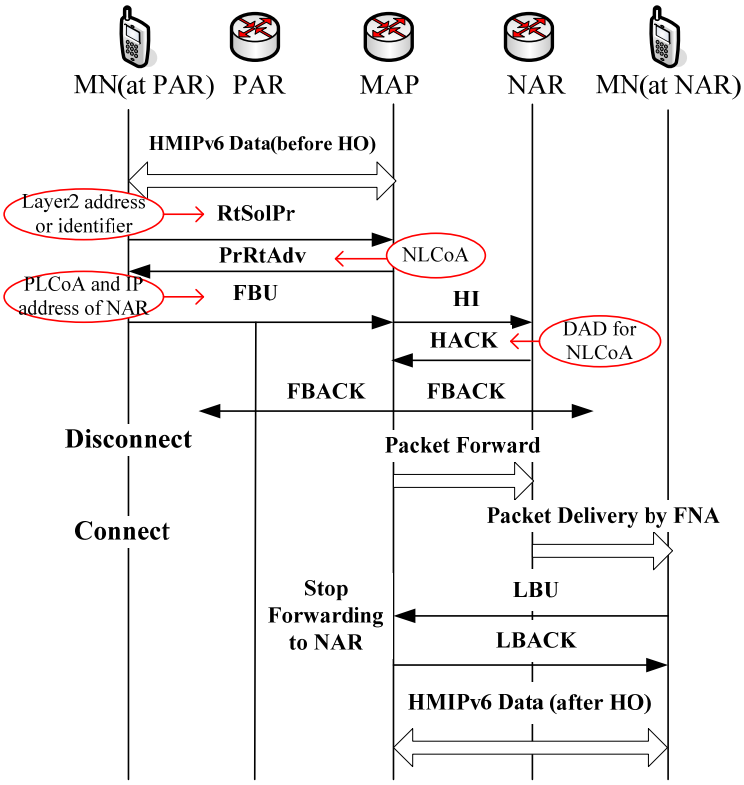

Figure 2. Procedures of F-HMIPv6

has already known the network prefix and link layer address of the associated NAR. Subsequently, MN will update MAP by sending Fast Binding Update (FBU) message which contains previous on-link CoA (PLCoA) and IP address of the NAR. After receiving the FBU message from MN, the MAP will send a Handover Initiate (HI) message to the NAR so as to establish a bi-directional tunnel. If Handover Acknowledgement (HACK) message from NAR indicates the validity of new NLCoA by Duplicate Address Detection (DAD) procedure, the bi-directional tunnel between MAP and NAR will set up. All data packets are intercepted by MAP and delivered over this tunnel. The MN sends Fast Neighbor Advertisement (FNA) messages to NAR, when it detects that it is moved in the link layer, and the NAR delivers the buffered data packets to the MN over NLCoA. When the MAP receives the new Local Binding Update with NLCoA from the MN, it will stop the packet forwarding to NAR and then clear the tunnel established for fast handover. When MN sends Local Binding Update (LBU) to MAP, MAP will respond with Local Binding ACK (LBACK), and forward packet directly to the MN (at NAR).

3. Proposed Cross-Layer Handover Scheme

In this section, we propose our cross layer handover scheme (CLHS). The CLHS achieves seamless handover by exploiting the L2 handover indicators and designing an efficient interleaving scheme of the 802.16e and the F-HMIPv6 handover procedures. The basic idea of CLHS is as follows: 1) integrate the correlated messages of 802.16e and F-HMIPv6. 2) reorder/combine L2 and L3 signaling messages and minimize the required control flow. Thus we can get shorter handover latency and higher throughput.

Figure 3 shows network architecture of CLFS in 802.16e.To achieve hierarchical handover, we propose a MAP in ASN (Access Service Network) Gateway. The MAP acts as an aggregation mobile anchor residing in ASN Gateway and connecting with Access Router (AR). If MN moves between subnets in the same MAP domain, it should be in intra-MAP handover status. If MN moves from one MAP domain to another, it should be in inter-MAP handover status. If MN moves between subnets in the same AR domain, it should be in L2 handover status.

Identical with HMIPv6 scheme, a MN has two CoAs, on-link CoA (LCoA) and Regional CoA (RCoA).When MN enters a new MAP domain, firstly it performs the HMIPv6 registrations procedures with HA and MAP. Then MN will bind its LCoA with an address on the MAP's RCoA. If the MN changes its current address within a local MAP domain (LCoA), such as from AR1 to AR2, it only needs to register the new address with the

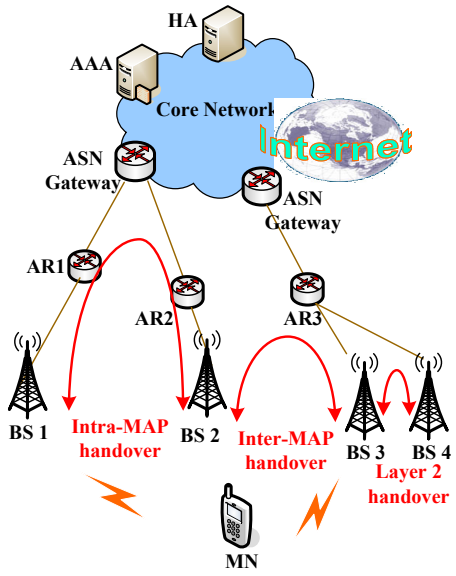

Figure 3. Network architecture of CLFS in 802.16e

MAP, following the Local Binding Update procedures of HMIPv6. As long as MN moves from AR2 to AR3 in the picture, the Regional CoA (RCoA) needs to be registered with correspondent nodes and the HA. When MN moves from BS3 to BS4, it only needs the MAC Layer handover.

In Figure 4, we design F-HMIPv6 handover information integrate with 802.16e and make some modifications. The "MOB_NBR_ADV" message is periodically sent by BS and its function is similar to the "PrRtAdv" message in F-HMIPv6. So, these two periodical advertisement messages can be combined together. We can deliver the L3 information of target network which MN moves to in MOB_NBR_ADV message, and RtSol/RtAdv messages can be omitted. By combining 802.16e with F-HMIPv6, and employing the former's new BS discovery ability with the RtSol/RtAdv messages, MN movement could be detected. In addition to modifying these two messages, we can make a little modification and combine the message of FBU in layer 3 and the message of MOB_HO_IND in layer 2. It is indicate that L2'handover when MS sends MOB_HO_IND message; And FBU message is to inform MAP for the initiation of L3' handover. Therefore, it's reasonable to send MOB_HO_IND together with FBU.

In the first place, S-BS shall broadcast a MOB_NBR-ADV including L3 information of RtSol/RtAdv to MN periodically. If the MN discovers a new neighbor BS in this message, it may perform scanning for the T-BS. When the MN decides to change links based on its policy such as the degrading signal strength or increasing packet loss rate, it will initiate handover by sending a MOB_MSHO-REQ to the BS and will receive a MOB_BSHO-RSP from the BS as a response. Alternatively, the BS may initiate handover by sending a MOB_BSHO-REQ to the MN. Then MN sends MOB_ HO_IND together with FBU to S-BS, and S-BS will forward FBU message to MAP. After that, messages of HI and HACK occur between the MAP and NAR to implement DAD and establish a bi-directional tunnel. As soon as the tunnel is set up, MAP sends FBACK messages over previous LCoA (PLCoA) and new LCoA (NLCoA), and intercepting packets destined for the MN to NAR over this tunnel. After switching links, the MN synchronizes

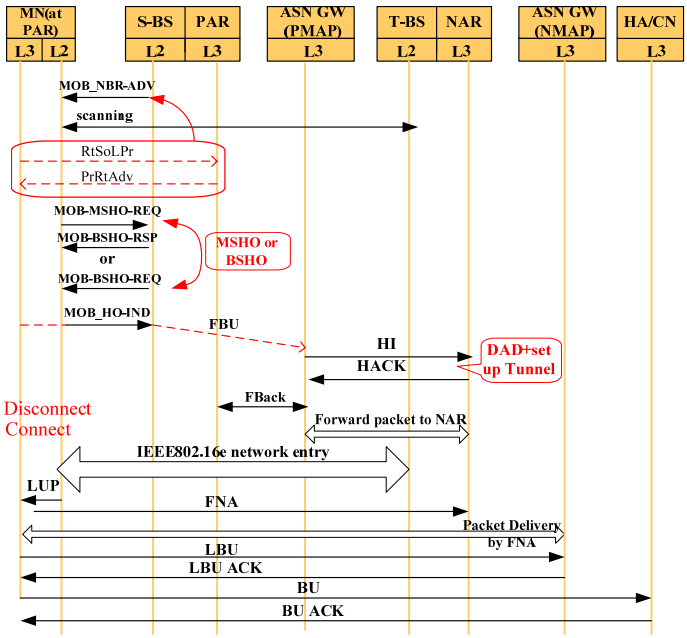

Figure 4. CLFS mechanism for 802.16e

with the target BS and performs the 802.16e network entry procedure. In this process, MN will acquaint of NCoA by Fast_DL_MAP_IE message [7]. Once the network entry procedure is completed, the L2 signals L3 with a LINK_UP (LUP) which report MN establish L2 connection with T-BS. In this stage, MN issues an FNA to NAR by using NLCoA as a source IP address. When the NAR receives the FNA from MN, it delivers the buffered packets to the MN through the tunnel. Then MN sends LBU message to NMAP to bind the NRCoA and NLCoA, and NMAP replies LBACK. In the end, NMAP delivers the buffered packets to MN through the tunnel. Thus, the whole handover operation is completed.

The above is the general flow of CLFS mechanism, in practice, different cases need different processes. When MN from one AR to another with micro mobility, there will be only needs to register the new address with the MAP, following the Local Binding Update procedures of HMIPv6. Therefore, we don't detail here.

4. Performance Analysis

In this section, we provide a performance analysis for the concept described in Section 3. The performance evaluation here provided is performed by means of simulations carried out with Matlab.

4.1 Analytical Models

In this paper, we consider that the handover latency starts with MN send MOB_HO_IND together with FBU, and completes with MN can normally communicate with CN. To analyze the performance of proposed scheme, we define some parameters in the Table 1 as following:

If we assume T_{L2} is the L2 handover delay, the conventional L2 handover delay is

$$T_{L2(c)} = T_{sync} + T_{cont\_resol} + T_{rng} + T_{auth} + T_{reg} + T_{frame} \quad (1)$$

In Formula (1), T_{sync} can be done within 2 frames. T_{cont_resol} typically needs minimum of 6 frames roundtrip delay plus a random handling duration. T_{auth} needs 2 frames plus a handling duration of about 100ms. T_{reg} always needs 2 frames plus a handling duration of about 10ms. And T_{frame} means the duration of MN send MOB_HO_IND together with FBU message which takes 1 frame.

Table 1. Notations of performance parameters

Symbol	Descriptions
T_{a_b}	Delay between node a and node b;
T_{frame}	Frame duration of IEEE802.16e PHY
T_{DAD}	Average delay of the DAD procedure;
$T_{tunnel\ a\_b}$	Latency for Tunneled packets;
T_{hop}	Delay of each hop in a wired backbone network
N_{a_b}	Number of hops between node a and node b;
T_{sync}	Average time required to synchronize with new downlink;
T_{cont_resol}	Average time required for contention resolution procedure;
T_{rng}	Average time required for ranging process during HO;
T_{auth}	Average time required for re-authorization during HO;
T_{reg}	average time required for re-registration;

We also give the L2 and L3 total handover delay T_{total} of conventional FMIPv6 in [8] as follow:

$$\begin{aligned} T_{total(FMIPv6)} &= 2T_{PAR\_NAR} + T_{DAD} + T_{tunnelPAR\_NAR} + T_{L2(c)} \\ &\quad + 2T_{MN\_HA} + 2T_{MN\_CN} + 3T_{MN\_AR} \\ &= 2(N_{PAR\_NAR} + N_{NAR\_HA} + N_{NAR\_CN}) \times T_{hop} \\ &\quad + T_{DAD} + T_{tunnelPAR\_NAR} + T_{L2(c)} + 7T_{MN\_AR} \end{aligned} \quad (2)$$

From the Formula (1), we may see that it takes a long time for handover procedures in conventional L2 scheme. That's mainly because, in case of network entry produce, MS fails to receive Fast RNG_IE and conducts contention based ranging. The MS performs random backoff and sends CDMA codes instead of RNG-REQ message on the link. Furthermore, the MS should perform re-authorization and re-registration processes. If we use the proposed scheme in [8], the downlink packet could be transmitted just after synchronization to the new downlink and total L2 handover delay is cut down. So we can get optimized L2 handover delay as follow:

$$T_{L2(o)} = T_{sync} + T_{frame} \quad (3)$$

The total handover latency of the CLHSmechanism is calculated as follow:

$$\begin{aligned} T_{total(CLFS)} &= \max(T_{L2(o)}, T_{DAD} + 2T_{PMAP\_NAR} \\ &\quad + T_{PMAP\_PAR} + T_{tunnelMAP\_AR}) \\ &\quad + T_{MN\_NAR} + 2T_{MN\_NMAP} + 2T_{MN\_HA} \\ &= \max(T_{L2(o)}, T_{DAD} + 2(N_{PAR\_NAR} + N_{MAP\_AR} - 1) \\ &\quad \times T_{hop} + T_{tunnelMAP\_AR}) + T_{MN\_NAR} \\ &\quad + 2T_{MN\_NMAP} + 2T_{MN\_HA} \end{aligned} \quad (4)$$

Then we list the delay period and packet disruption time with CLFS based 802.16e in Figure 5. Apart from handover disruption and delay period, we also note how the time point of trigger influences these operations, as well as the time point at which CN can send packet directly to MN.

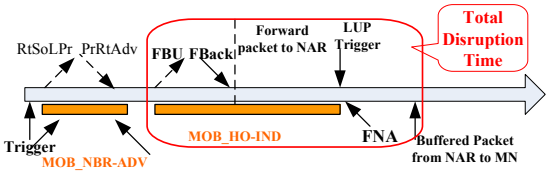

Figure 5. Handover disruption time and delay period

Related to Figure 5, we can calculate the disruption time of CLFS and conventional way are derived below.

$$D_{CLFH} = T_{L2(o)} + T_{MN\_NAR} \quad \textbf{(5)}$$

$$D_{FMIPv6} = T_{L2(c)} + T_{MN\_NAR} \quad \textbf{(6)}$$

4.2 Simulation Results

We now present the results based on previous analysis. To evaluate the schemes, we assume the parameters as the below table. The NAR and PAR are assumed the same distance from the HA. We assume $T_{hop} = T_{frame} + 0.5ms$, and the DAD time is chosen from Poisson distribution: [400ms, 600ms].

The simulation results are divided into two parts. The first part is mainly related to the handover latency and the second part is related to the service disruption time for the proposed scheme and the conventional scheme.

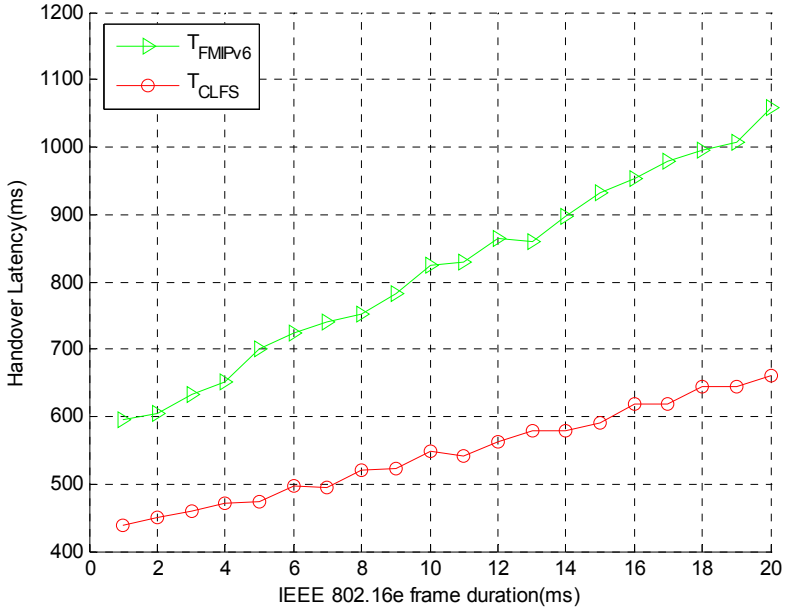

Figure 6. Handover latency for different frame durations

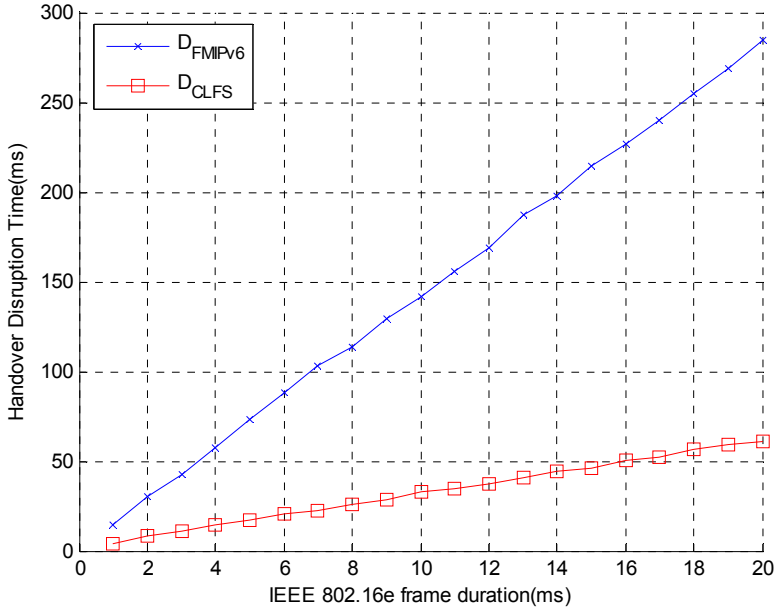

Figure 7. Handover disruption time for different frame durations

Figure 6 compares the handover delay of the proposed CLHS and the conventional scheme. It's noted that the delay time is mainly reduced in CLHS mechanism. The reason is that our scheme needs less number of messages and L2 and L3 signaling messages are properly arranged for parallelism. When performing handover, the CLHS mechanism can greatly reduce the handover latency and optimize the performance.

In Figure 7, we can find the same situation as Figure 6. When the frame duration increases, the FMIPv6 disruption time grows sharply, whereas our scheme only has a slight increase. It's mainly because that no more registration procedure and authorization procedure are needed in this optimized scheme. Therefore, optimized L2 handover scheme reduce the disruption time.

Table 2. Simulation parameter setting

Parameter	Value	Parameter	Value
N_{PAR_NAR}	6	T_{NAR_CN}	10
N_{NAR_HA}	8	$T_{tunnel\ a\_b}$	10 msec

5. Conclusions

In this paper, we have proposed a cross-layer optimization with F-HMIP for WiMAX. Our CLHS mechanism reduces the number of signaling messages by combining L2 and L3 messages and parallelizing L2 and L3 signaling messages. In our CLHS mechanism, we use an optimized L2 handover scheme with a Fast_DL_MAP_IE message to enhance the performance and reduce network entry messages. In addition, we compare our scheme with the previous scheme through exhaustive simulations. However, the selection mechanism of an appropriate BS is not within our consideration for simulation simplification. So future research will extend the concept of cross layer to cover the complete handover procedure and optimize the utilization of network resources.

REFERENCES

[1] BEHESHTI B D. Software implementation and performance analysis of the LTE physical layer blocks on a next generation baseband processor platform. 2008 IEEE Long Island, May 2008, 1-1.

[2] WANG F, GHOSH A, SANKARAN C, FLEMING P, HSIEH F, BENES S. Mobile WiMAX systems: Performance and evolution. IEEE Communications Magazine, Oct. 2008, 46(10): 41-49.

[3] KOODLI R. Mobile IPv6 fast handovers. IETF RFC5268, June 2008.

[4] SOLIMAN H, CASTELLUCCIA C, MALKI K E, ET AL. Hierarchical mobile IPv6 mobility management (HMIPv6). IETF RFC5380, Oct. 2008.

[5] JUNG H Y. Fast handover for hierarchical MIPv6. IETF Internet-draft, draft-jung-mobopts-fhmipv6-00.txt, 2005.

[6] CHOI S, HWANG G H, KWON T, LIM A R, CHO D H. Fast handover scheme for real-time downlink services in IEEE 802.16e BWA system. VTC 2005-Spring, 3: 2028-2032.

[7] IEEE 802.16e. Amendment 2: Physical and medium access control layers for combined fixed and mobile operation in licensed bands and corrigendum 1. Feb. 28, 2006.

[8] JANG H J. Mobile IPv6 fast handovers over IEEE 802.16e networks. IETF RFC5270, June 2008.

Communications and Network, 2009, 42-45
doi:10.4236/cn.2009.11006 Published Online August 2009 (http://www.scirp.org/journal/cn)

A Study of Multi-Node and Dual-Hop Collaborative Communication Performance Based on Harmonic Mean Method

Tingting YANG[1], Shufang ZHANG[2]
College of Information Engineering, Dalian Maritime University, Dalian, China
Email: [1]*xinxi*2004*jiuye*@163.*com*; [2]*sfzhang@dlmu.edu.cn*

Abstract: Closed form expressions for the PDF and MGF of the harmonic mean of two independent exponential variates are cited and derived, and then applied to study the performance of cellular multi-node and dual-hop cooperative communication systems with non-regenerative relays over flat Rayleigh fading channels. We derive the probability density function (PDF) and asymptotic symbol error rate (SER) expression with MRC scheme. Then we use Matlab to simulate the performance.

Keywords: harmonic mean, cooperative communication, multi-node, dual-hop, MGF

1. Introduction

MIMO technique has been regarded as the essential technique for beyond 3G mobile cellular networks. The Benefits of MIMO system have been extensively studied by researchers in both academic and industry. It successfully meets the rapidly growing demand for high rate, voice and especially for multimedia services [1].

In wireless cellular networks, base station can be equipped with multiple antennas and keeps them spatially separated. Unfortunately, it is hardly to fix multiple antennas in portable mobile terminals (also called as mobile terminals or users) due to insufficient antenna space, energy, and price, etc. So, the bottleneck of capacity is limited and the diversity technique of mobile terminals could not be realized from the traditional end-to-end transmission systems. In order to break this embarrassing situation, a novel concept, namely cooperative communication (or user cooperative diversity) was introduced by Sendonaris *et al*. [2].

Mazen O Hasna *et al*. in [3,4] firstly applied the harmonic mean to the cellular multi-node and dual-hop cooperative communication systems. They respectively derived the probability density function (PDF), the cumulative distribution function (CDF) and the moment generating function (MGF) of the expression. It's a new train of thought of cooperative diversity scheme. This paper applied the method of the harmonic mean to derive PDF and MGF of two independent exponential variates are cited and derived to study the performance of cellular multi-node and dual-hop cooperative communication systems with non-regenerative relays over flat Rayleigh fading channels.

2. Harmonic Mean of Exponential Variates

2.1 Definitions

1) Harmonic Mean

Given two numbers X1 and X2, the harmonic mean of X1 and X2, $\mu_H(X_1, X_2)$ is defined as the reciprocal of the arithmetic mean of the reciprocals of X1 and X2 [3] that is:

$$\mu_H(X_1, X_2) = \frac{2}{\frac{1}{X_1}+\frac{1}{X_2}} = \frac{2X_1X_2}{X_1+X_2} \quad (1)$$

2) Exponential RV

X follows an exponential distribution with parameterβ > 0 if the PDF of X is given by $p_X(x) = \beta e^{-\beta x}U(x)$, where $U(\cdot)$ is the unit step function.

2.2 Derive the Moment Generating Function

MGF of the Harmonic Mean of Two Exponential RVs Given a RV X ~ E(β), the PDF of Y = 1/X can be evaluated with the help of [9].

Then, $p_Y(y) = \frac{\beta}{y^2}e^{-\frac{\beta}{y}}U(y)$, $M_\gamma(s) = E_\gamma(e^{-sy})$, K_v (X)= K_{-v} (X)

According to [5], we can get:

$$\int_0^\infty x^{v-1}e^{-\frac{\beta}{x}-\gamma x}dx = 2\left(\frac{\beta}{\gamma}\right)^{\frac{v}{2}}K_v\left(2\sqrt{\beta\gamma}\right)[R_e\beta>0, R_e\gamma>0]$$

$$M_\gamma(s) = E_\gamma(e^{-sy}) = \int_0^\infty p_\gamma(y)e^{sy}dy = \int_0^\infty \frac{\beta}{y^2}e^{-\frac{\beta}{y}}e^{sy}dy$$

$$= M_y(s) = 2\sqrt{\beta s}K_1(2\sqrt{\beta s})$$

When X= $\mu_H(X_1, X_2)$, we can get:

$$M_X(s) = E_X\left(e^{-sx}\right) = \int_{-\infty}^{+\infty} e^{-sx}\frac{1}{2}\beta_1\beta_2 e^{-\frac{x}{2}(\beta_1+\beta_2)}$$

$$\left[\left(\frac{\beta_1+\beta_2}{\sqrt{\beta_1\beta_2}}\right)K_1\left(x\sqrt{\beta_1\beta_2}\right)+2K_0\left(x\sqrt{\beta_1\beta_2}\right)\cdot U(x)dx\right]$$

$$=\int_0^{\infty} e^{-sx}\frac{1}{2}\beta_1\beta_2 e^{-\frac{x}{2}(\beta_1+\beta_2)}\left[\left(\frac{\beta_1+\beta_2}{\sqrt{\beta_1\beta_2}}\right)K_1\left(x\sqrt{\beta_1\beta_2}\right)+2K_0\left(x\sqrt{\beta_1\beta_2}\right)dx\right]$$

$$=\int_0^{\infty} e^{-sx}\frac{1}{2}\sqrt{\beta_1\beta_2}xe^{-\frac{x}{2}(\beta_1+\beta_2)}\cdot(\beta_1+\beta_2)K_1\left(x\sqrt{\beta_1\beta_2}\right)dx+$$

$$\int_0^{\infty} e^{-sx}\beta_1\beta_2 xe^{-\frac{x}{2}(\beta_1+\beta_2)}K_0\left(x\sqrt{\beta_1\beta_2}\right) \quad \textbf{(2)}$$

where K0(•) is the zero-order modified Bessel function of the second kind defined in [11].

Where $K_1(x)$ is the first order modified Bessel function of the second kind defined in [11].

Here, we find the Formula (2) can be constituted with ① + ②, according to [5].

$$\int_0^{\infty} x^{v-1}e^{\alpha x}K_v(\beta x)dx =$$

$$\frac{\sqrt{\pi}(2\beta)^v}{(\alpha+\beta)^{\mu+v}}\frac{\Gamma(\mu+v)\Gamma(\mu-v)}{\Gamma\left(\mu+\frac{1}{2}\right)}F\left(\mu+v,v+\frac{1}{2},\mu+\frac{1}{2},\frac{\alpha-\beta}{\alpha+\beta}\right)$$

Then, we can get:

① $\mu=2$, $\alpha=s+\frac{1}{2}(\beta_1+\beta_2)$; $v=1$, $\beta=\sqrt{\beta_1\beta_2}$

② $\mu=2$, $\alpha=s+\frac{1}{2}(\beta_1+\beta_2)$, $v=0$, $\beta=\sqrt{\beta_1\beta_2}$

$$M_X(s)=\frac{16\beta_1\beta_2}{3\left(\beta_1+\beta_2+2\sqrt{\beta_1\beta_2}+s\right)^2}$$

$$\left[\frac{4(\beta_1+\beta_2)}{\left(\beta_1+\beta_2+2\sqrt{\beta_1\beta_2}+s\right)}*_2F_1\left(3,\frac{3}{2};\frac{5}{2};\frac{\beta_1+\beta_2-2\sqrt{\beta_1\beta_2}+s}{\beta_1+\beta_2+2\sqrt{\beta_1\beta_2}+s}\right)\right.$$

$$\left.+_2F\left(2,\frac{1}{2};\frac{5}{2};\frac{\beta_1+\beta_2-2\sqrt{\beta_1\beta_2}+s}{\beta_1+\beta_2+2\sqrt{\beta_1\beta_2}+s}\right)\right]$$

3. Scheme of Cellular Multi-Node and Dual-Hop Cooperative Communication Systems with Non-Regenerative Relays over Flat Rayleigh Fading Channels

3.1 System Model

Consider an uplink wireless cooperative communication system with only one source, one destination and arbitrary N relays (from mobile terminals to base station). The source terminal transmits Mary phase-shift keying (M-PSK) modulation signals to destination terminal through a direct path along with N dual-hop paths. The channel is assumed to be quasi-static with flat fading. Furthermore, perfect channel state information is assumed available at the receivers, but the channels are unknown at the transmitters. There are two transmission phases. Firstly, the source broadcasts signals to destination and relays. Secondly, the relays which can successfully decode the signals will retransmit them to destination. Otherwise, they remain idle and do not participate in the cooperation.

Figure 1 is the system model of multi-node and dual-hop cooperative communication system. S is the moving terminal, D is the base station. This paper research the MPSK modulation of non-regenerative relay over flat Rayleigh fading channels, and the noise is the additive white Gaussian noise (AWGN). We suppose there are m relays on the uplink, and the gains are Gi. Assume that terminal S is transmitting a signal S(t) which has an average power normalized to 1.

3.2 Performance Analysis

Assume that in the EPA mode, where Ps=Pr=1. In the situation of non-regenerative relay and the MRC receiving mode, the receiving signal are respectively:

$$S_{R_1}(t)=h_1s(t)+n_1(t)$$

$$S_{d_1}(t)=g_1G_1\left(h_1s(t)+n_1(t)\right)+n_2(t)$$

When $G_i=\sqrt{1/h_i}$ can according with the harmonic mean format, as

$$\gamma=\frac{2\frac{h_1^2}{N_0}\cdot\frac{g_1^2}{N_0}}{\frac{h_1^2}{N_0}+\frac{g_1^2}{N_0}}$$

which can use the method of harmonic mean to calculate.

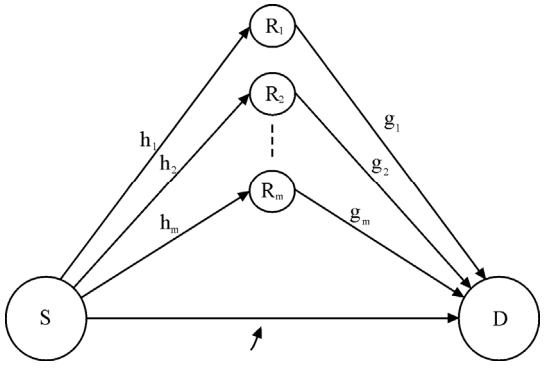

Figure 1. System model

We define $\overline{\gamma_i}$ and $\overline{\gamma_{g_i}}$ are respectively instantaneous SNR of the ith channels. The total SNR is:

$$r = r_f + \sum_{i=1}^{m} r_i$$

According to [4], we can achieve the cumulative distribution function (CDF) of the instantaneous SNR $\overline{\gamma_i}$ of the Multi-node and dual-hop Collaborative Communication channels:

$$F_{r_i}(r) = 1 - \prod_{i=1}^{m} p(r_{h_i} > r) p(r_{g_i} > r)$$

$$F_{r_i}(r) = 1 - \prod_{i=1}^{m} r(\bar{r}_{h_i}\bar{r}_{g_i})^{-1/2} e^{-r/2[(\bar{r}_{h_i})^{-1}+(\bar{r}_{g_i})^{-1}]} K_1[r(\bar{r}_{h_i}\bar{r}_{g_i})^{-1/2}]$$

The probabilitydensity function (PDF) of the instantaneous SNR $\overline{\gamma_i}$ of the Multi-node and dual-hop Collaborative Communication channels:

$$\mathrm{P}_\Gamma(\gamma) = \sum_{i=1}^{m} \frac{2\gamma e^{-\gamma\left(\frac{1}{\overline{r_{h_i}}}+\frac{1}{\overline{r_{g_i}}}\right)}}{\overline{r_{h_i}}\cdot\overline{r_{g_i}}} \left[\frac{\overline{r_{h_i}}+\overline{r_{g_i}}}{\sqrt{\overline{r_{h_i}}\cdot\overline{r_{g_i}}}} K_1\left(\frac{2\gamma}{\sqrt{\overline{r_{h_i}}\cdot\overline{r_{g_i}}}}\right) + 2K_0\left(\frac{2\gamma}{\sqrt{\overline{r_{h_i}}\cdot\overline{r_{g_i}}}}\right) \right] U(\gamma)$$

The Outage Probability

$$Pout = P[\gamma \le \gamma_{th}] = \int_0^{\gamma_{th}} P_\Gamma(\gamma)\, d\gamma$$

On the assumption that the average SNR $\overline{\gamma_i}$ when $\overline{\gamma_{h_i}} = \overline{\gamma_{g_i}} = \overline{\gamma_i}$, can obtain the moment generating function (MGF) of the instantaneous SNR $\overline{\gamma_i}$ of the Multi-node and dual-hop Collaborative Communication channels[4][8]:

$$M_\Gamma(s) = \left(1 - s\overline{\gamma}_f\right)^{-1} \prod_{i=1}^{M} {}_2F_1\left(1, 2; \frac{3}{2}; -\frac{\overline{\gamma}_i}{4}s\right)$$

$$= \frac{1}{\pi} \sum_{K=0}^{N} \frac{(1+K)!\left(\frac{1}{2}\right)!}{1\cdot 3\cdot 5\cdot 7\cdots(2K-1)\left(-\frac{1}{2}\right)!} \left(\frac{\overline{\gamma}}{2}\right)^K \sin^{2k}\left(\frac{\pi}{M}\right) \int_0^{(M-1)\pi/M} \sin^{-2K}\theta\, d\theta$$

This formula can't get it's closed-form, but we can get the asymptotic expression expressed as:

$$M_\Gamma(s) \approx \sum_{K=0}^{N} \frac{(1+K)!\left(\frac{1}{2}\right)!\left(\frac{\overline{\gamma}_i}{2}\right)^K}{\left(-\frac{1}{2}\right)!(2K-1)!} \times \frac{\sin^{2K}\left(\pi/M\right)}{1+\sin^2\left(\pi/M\right)}$$

The upper limit of average SER of the Multi-node and dual-hop channels is:

$$\mathrm{P}_s(E) \le \frac{\mathrm{M}-1}{\mathrm{M}}\left(1 - s\overline{\gamma}_f\right)^{-1} \prod_{i=1}^{m} \mathrm{M}_\gamma\left(-g_{psk}\right)$$

$$\mathrm{P}_S(E) \le \frac{\mathrm{M}-1}{\mathrm{M}} \left(\frac{\sin^2\theta}{\sin^2\theta + \overline{\gamma}_f \sin^2\left(\frac{\pi}{\mathrm{M}}\right)} \right)$$

$$\prod_{i=1}^{m} \left(\frac{(1)!(2)!}{\left(\frac{3}{2}\right)!(1)!}\left(\frac{\overline{\gamma}_i}{4}\right)^1 \sin^2\left(\frac{\pi}{\mathrm{M}}\right) + \frac{(1)!(2)!}{\left(\frac{3}{2}\right)!(2)!}\left(\frac{\overline{\gamma}_i}{4}\right)^2 \sin^4\left(\frac{\pi}{\mathrm{M}}\right) + \cdots \right)$$

$$\le \frac{\mathrm{M}-1}{\mathrm{M}} \left(\frac{\sin^2\theta}{\sin^2\theta + \overline{\gamma}_f \sin^2\left(\frac{\pi}{\mathrm{M}}\right)} \right) \sin^{2m}\left(\frac{\pi}{\mathrm{M}}\right)$$

$$\prod_{i=1}^{m} \frac{\overline{\gamma}_i}{4} \left(\frac{(1)!(2)!}{\left(\frac{3}{2}\right)!(1)!} + \frac{(1)!(2)!}{\left(\frac{3}{2}\right)!(2)!} + \cdots \right)$$

When $\frac{\overline{\gamma}_i}{4} \le 1$,as $i \in (1, m)$

$$P_S(E) \le \frac{\mathrm{M}-1}{\mathrm{M}} \left(\frac{\sin^2\theta}{\sin^2\theta + \overline{\gamma}_f \sin^2\left(\frac{\pi}{\mathrm{M}}\right)} \right)$$

$$\sin^{2m}\left(\frac{\pi}{\mathrm{M}}\right) \left(\prod_{i=1}^{m} \frac{\overline{\gamma}_i}{4}\right) \cdot \sum_{k=0}^{N} \frac{(1)_K (2)_K}{\left(\frac{3}{2}\right)_K K!}$$

4. Numerical Results and Performance Analysis

In this paper, we will respectively simulate and analysis the PDF of instantaneous SNR $\overline{\gamma_i}$ of about different situation the Multi-node and dual-hop Collaborative Communication channels. We research the M-ary phase-shift keying (M-PSK) modulation, M=4,8; the number of relays m=4,10. We respectively simulate the situation of high SNR and low SNR with 20 sampling nodes.

Figure 2 is the compare of PDF about different sampling ranks and different relay numbers. From this figure,

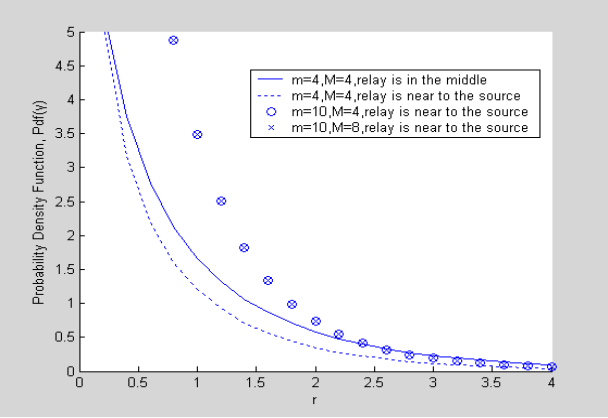

Figure 2. The compare of PDF about different sampling ranks and different relay numbers

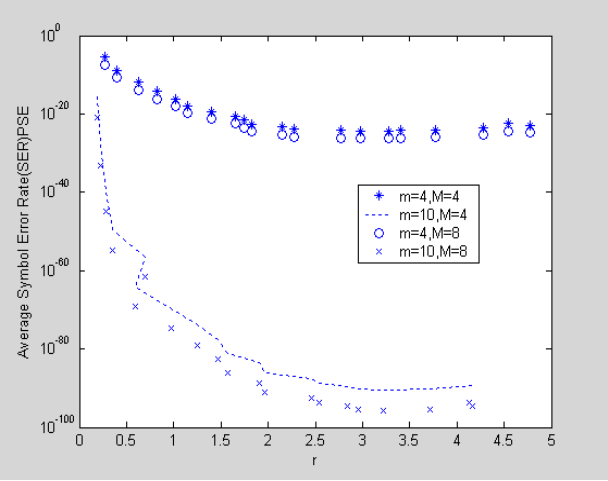

Figure 3. The compare of error symbol rate (SER) about the different sampling ranks and different relay numbers

we can find on the same SNR, the performance is better when the relay number is more. On the same relay nodes, the performance is almost the same when the high sampling ranks and low sampling ranks.

Figure 3 is the compare of error symbol rate (SER) about the different sampling ranks and different relay numbers. We respectively simulate the situation of m=4,10, M=4,8, with 20 sampling nodes. Because of the little SER, we adopt the logarithmic scale coordinate method. We can find on the same SNR, the performance is better when the relay number is more. When the same sampling nodes, the performance is better which is adopt with the high rank modulation. It's also approved that the performance of Multi-node and dual-hop Collaborative Communication can be improved when adopt the high rank modulation while the user's number is definite.

5. Conclusions

This paper applies the method of the harmonic mean to derive PDF and MGF of two independent exponential variates which are cited and derived to study the performance of cellular multi-node and dual-hop cooperative communication systems with non-regenerative relays over flat Rayleigh fading channels.

We derive the probability density function (PDF) and asymptotic symbol error rate (SER) expression. These numerical results indicate that the number of relay is more, the performance is better. It also indicates the ascendance performance of cooperative diversity.

REFERENCES

[1] YIN Q Y, ZHANG Y, DING L. A new space diversity technology. Transactions of Xi'an Jiaotong University. 2005, 39(6): 551-557.

[2] SENDONARIS A, ERKIP E, AAZHANG B. Increasing uplink capacity via user cooperation diversity. IEEE Int. Symp. on Information Theory, Cambridge, MA, Aug. 1998, 156-156.

[3] HASNA M O, ALOUINI M-S. Harmonic mean and end-to-end performance of transmission systems with relays. IEEE Transactions on Communications, 52(1): Jan. 2004.

[4] HASNA M O, ALOUINI M-S. Performance analysis of two-hop relayed transmission over Rayleigh fading channels. Proc. IEEE Vehicular Technology Conf. (VTC'02), Vancouver, BC, Canada, Sept. 2002, 1992-1996.

[5] GRADSHTEYN I S, RYZHIK I M. Table of integrals, series, and products. San Diego, CA: Academic Press, 5th Ed., 1994.

[6] ABRAMOWITZ M, STEGUN I A. Handbook of mathematical functions with formulas, graphs, and mathematical tables. New York, NY: Dover Publications, 9th Ed., 1970.

[7] IKKI S, AHMED M H. Performance analysis of cooperative diversity wireless networks over nakagami-m fading channel. IEEE Communications Letters, Apr. 2007, 11(4).

[8] SIMON M K, ALOUINI M-S. Digital communication over fading channels: A unified approach to performance analysis. New York: Wiley, 2000.

Communications and Network, 2009, 46-50
doi:10.4236/cn.2009.11007 Published Online August 2009 (http://www.scirp.org/journal/cn)

A Novel Scheme with Adaptive Sampling for Better Spectrum Utilization in Cognitive Radios

Qun PAN, Xin ZHANG, Ruiming ZHENG, Yongyu CHANG, Dacheng YANG
Beijing University of Posts and Telecommunications, Beijing, China
Email: *lionheartpq@gmail.com*

Abstract: In cognitive radio (CR) networks, cognitive users need continuously monitor spectrum to decrease or avoid interference to primary users, yet attain a reasonable throughput. In this paper, we exploit a scheme to dynamically change the detection time duration to gain maximum throughput. Meanwhile the average detection time is kept as small as possible. The advantages of our approaches are approved by the deductions. Also the simulation results enable us to recognize the improved performance of our scheme over those ones with fixed detection time assignment.

Keywords: cognitive radio, cooperative sensing, average detection time, channel utilization ratio

1. Introduction

With the rapid development of wireless communication technology, the demand of spectrum resource is growing. The spectrum resource becomes rare due to the popularity of various new wireless applications. However, the recent survey shows a low spectral efficiency in the licensed band. The spectral holes in licensed band can be sensed and used to transmit information by employing cognitive radios technology [1]. The extra system throughput can be provided by cognitive radios without additional spectrum resource allocation. So the Federal Communications Commission (FCC) has recommended cognitive radio (CR) as the candidate for enhancing overall spectral efficiency. Cognitive radio [1] enables CR users (unlicensed users) to obtain the frequency bands with minimal interference to active primary users (licensed users) when they observe the bands allocated to the primary user are vacant and meanwhile detect the continuous spectrum sensing in CR networks. Therefore, as the heart of the cognitive radio techniques, the spectrum sensing is so critical that it determines the throughput and the agility of the CR networks.

One of the challenges of CR system's application is how to detect the primary user's signal quickly and correctly in order to avoid interference to the licensed network. The other is how to fully occupy the spectrum resources acquired by CR network. In this paper, a novel scheme is proposed to use the spectrum holes more efficiently. Meanwhile the interference to licensed network is controlled within an acceptable range. Our proposed scheme could increase spectrum efficiency in full extent in an applicable CR network. We consider the detection performance in the more practical scenario based on IEEE 802.22 WRAN system which uses cognitive radio technology as its key feature. The fast sensing and fine sensing process which utilize energy detection technology and feature detection technology respectively are both considered in our study. The cooperative sensing technology which can increase the sensing performance significantly is also involved in. The approaches of cooperative sensing technology [2-5] all use diversity technologies to improve effective SNR for essential.

The rest of this paper is written as follows. In Section 2, we model the conventional detection scheme in mathematic way. In Section 3, we analyze the influence to channel utilization ratio made by time scheduling, and we propose a novel scheme of maximizing the channel utilization ratio. At last, we will conclude our study in Section 4.

2. System Model

A practical sensing scheme is shown in Figure 1 [6]. There are two types of detection in the figure: the fast sensing (energy detection) and the fine sensing (feature detection). During these two types of detection time, all the CR users should cease their transmission in order to achieve high definition detection. Therefore, these detection periods are also called quiet periods.

The fast sensing processes are triggered periodically, and all the detection information from all CR users is summarized to give a final judgment. If the detection indicates that no primary user exists, the CR users will wait for next fast sensing process. On the other hand, the fine sensing process will be triggered. Usually, the time duration of fine sensing is much longer than that of fast sensing. Also the veracity of fine sensing is much better. Without loss of generality we assume the veracity of fine sensing is 100% all through the rest of the paper.

2.1 Modeling Individual Detection

The binary hypothesis model is adopted in the study of spectrum sensing.

$$\begin{aligned} \mathcal{H}_0 &: y(t) = n(t) \\ \mathcal{H}_1 &: y(t) = h \cdot s(t) + n(t) \end{aligned} \tag{1}$$

where $y(t)$ is the receive signal by CR user at time t. $n(t)$ is the Additive White Gaussian Noise (AWGN), and we assume $n(t)$ follows a standard normal distribution, which means the expectation is 0 and the variance is 1. $s(t)$ is the primary user's transmitting signal. H_0 denotes the null hypothesis, which means there is no primary user signal in a certain spectrum band. H_1 is the alternative hypothesis, which indicates that there exists primary user signal in that band. h is the channel coefficient.

First, we consider local spectrum sensing (energy detection) at an individual CR user. We assume each energy detection interval contains M samples. j denotes the sampling index. Then the statistic characteristic of the i-th CR user is given by:

$$u_i = \begin{cases} \sum_{j=1}^{M} n_{ij}^2 & \mathcal{H}_0, \\ \sum_{j=1}^{M} (h_i s_{ij} + n_{ij})^2 & \mathcal{H}_1. \end{cases} \tag{2}$$

We can see u_i is the sum of M independent Gaussian random variables' square, whose deviation is unit. So u_i follows a central chi-square distribution with M degree freedom when H_0 becomes true, or else u_i follows a non-central chi-square distribution.

$$u_i \sim \begin{cases} \chi_M^2 & \mathcal{H}_0, \\ \chi_M^2(\eta_i) & \mathcal{H}_1. \end{cases} \tag{3}$$

We defined the Γ_i as the instantaneous SNR of the i-th CR user.

$$\Gamma_i = \frac{1}{M} \sum_{j=1}^{M} \left| h_i s_{ij} \right|^2 \tag{4}$$

The non-centrality parameter $\eta_i = M\Gamma_i$.

If M is large enough, the u_i will approximately follow Gaussian distribution according to the Central Limit Theorem as follows:

$$U_i = \frac{u_i}{M} \sim \begin{cases} N\left(1, \sqrt{2/M}\right) \\ N\left(1+\Gamma_i, \sqrt{2(1+2\Gamma_i)/M}\right) \end{cases} \tag{5}$$

2.2 Modeling Cooperative Detection

Individual detection is not sufficient in a practical scenario due to the lower receive SNR of CR users. Hence, cooperative technology is involved in spectrum sensing as in [2-5]. We adopt a linear combine scheme which sums the different CR users' samples with weights in

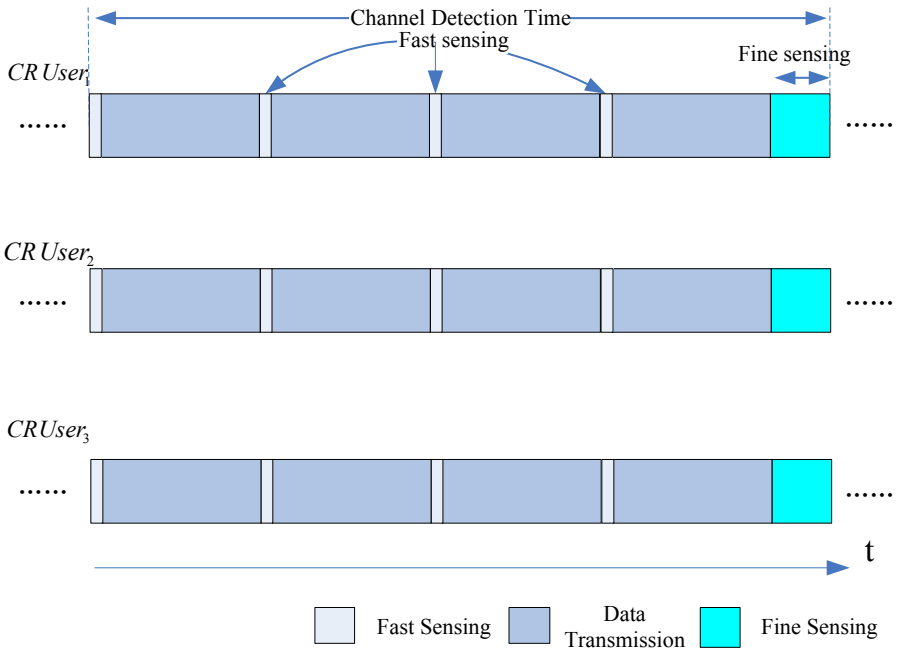

Figure 1. Detection process in cognitive radio network

our cooperative sensing process. The weight coefficient corresponding to the *i*-th CR user is w_i, then the weighted summation is given by:

$$U=\sum_{i=1}^{N} w_i U_i \qquad \left(\sum_{i=1}^{N} w_i^2=1, 0<w_i<1\right) \tag{6}$$

$$U \sim \begin{cases} N\left(1, 2/M\right) & \mathcal{H}_0, \\ N\left(\sum_{i=1}^{N} w_i\left(1+\Gamma_i\right), 2\Big/M\sum_{i=1}^{N} w_i^2\left(1+2\Gamma_i\right)\right) & \mathcal{H}_1. \end{cases} \tag{7}$$

Let λ be the decision threshold of energy detection. Therefore the probability of false alarm P_F, and that of detection P_D are:

$$P_F=\mathrm{Q}\left(\frac{\lambda-\sum_{i=1}^{N} w_i}{\sqrt{2/M\sum_{i=1}^{N} w_i^2}}\right) \tag{8}$$

$$P_D=\mathrm{Q}\left(\frac{\mathrm{Q}^{-1}\left(P_F\right)-\sqrt{M/2}\sum_{i=1}^{N} w_i\Gamma_i}{\sqrt{\sum_{i=1}^{N} w_i^2\left(1+2\Gamma_i\right)}}\right) \tag{9}$$

So the decision threshold and the optimal weight coefficient can be given by (10) and (11) respectively [7]:

$$\lambda=\mathrm{Q}^{-1}\left(P_F\right)\sqrt{2/M\sum_{i=1}^{N} w_i^2}+\sum_{i=1}^{N} w_i \tag{10}$$

$$w_i^*=\frac{\Gamma_i}{\sqrt{\sum_{i=1}^{N}\Gamma_i^2}} \tag{11}$$

3. System Performance Analysis and Proposed Scheme

3.1 Detection Performance

The performance of the cooperative sensing is evaluated by receiver operating characteristics (ROC) which is composed of probability of false alarm and that of detection in plenty of bibliography [7][8]. But these two parameters can only indicate the system performance under some special conditions. Our analysis is shown as follows.

Excellent CR system should exit when the primary user is working on the target channel band, besides sufficiently use the spectrum when primary user is idle. Therefore the two objectives in CR system design are interference avoidance to primary user and full utilization of spectrum holes respectively. In order to decrease or avoid interference to the primary user, the detection sensitivity must be high enough for CR system, i.e. the existence of primary user's signal must be discovered as quickly as possible. If the detection process finds holes in spectrum, the time duration for detection must be as short as possible to leave more resource for data transmission.

We define channel utilization ratio (CUR) as the proportion of time used for data transmission accounting for the whole time when the primary user is idle [9]. ξ_E, ξ_D and ξ_F indicate the probabilities of energy detection, transmission and feature detection. The Markov state transition diagram is shown in Figure 2. So the corresponding Equation (12) is demonstrated as below.

$$\begin{cases} \xi_T\left(1-P_F\right)+\xi_F=\xi_E \\ \xi_T P_F=\xi_F \\ \xi_E+\xi_T+\xi_F=1 \end{cases} \Leftrightarrow \begin{cases} \xi_E=1/(2+P_F) \\ \xi_T=1/(2+P_F) \\ \xi_F=P_F/(2+P_F) \end{cases} \tag{12}$$

So the CUR can be expressed by (13)

$$\eta=\frac{T_T\xi_T}{\xi_E T_E+\xi_T T_T+\xi_F T_F} \tag{13}$$

where T_E, T_T and T_F are the time duration of the three states. Let $T=T_E+T_T$. We define the sampling proportion (SP) as $\alpha=T_E/T$. So (13) can be transformed to (14).

$$\eta=(1-\alpha)T/T+P_F T_F \tag{14}$$

From (14) we can see it is the CUR that not only depends on P_F, but also T and α.

$$P_F=\frac{(1-\alpha-\eta)T}{\eta T_F}>0 \qquad \eta<1-\alpha \tag{15}$$

The average detection time (ADT) [10][11] indicates the average time interval from the primary user's presence until it is found by CR users. We assume the probability of detection in each sensing period is equal to P_D, when the primary user is present. The final H_1 decision must be after feature detection, so the ADT required by CR user to detect the primary user can be given by (16):

$$T_D=T\sum_{k=1}^{\infty} kP_D\left(1-P_D\right)^{k-1}+T_F=\frac{T}{P_D}+T_F \tag{16}$$

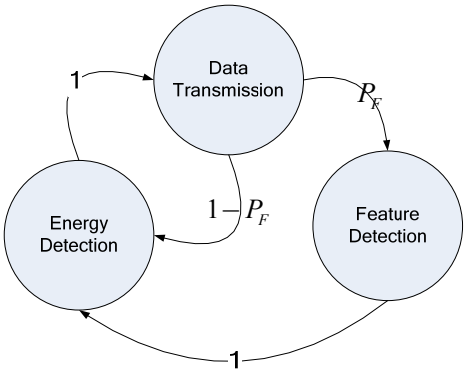

Figure 2. State transition diagram of CR system when no primary user is active

3.2 Maximizing the Channel Utilization Ratio

The interference provided by CR network should be firstly small enough, so that primary user can work normally. In order to limit the interference to primary user, the ADT should have a maximum target. So we will discuss the scheme which can maximize the CUR, and at the same time the target of ADT can be realized.

The sampling number $M = WT_E = WT\alpha$ according to the Nyquist sampling Theorem, where W is the sensing bandwidth. (17) is acquired in terms of (9) and (16):

$$P_F = \mathrm{Q}\left(\sqrt{\sum_{i=1}^{N} w_i^2\left(1+2\Gamma_i\right)}\,\mathrm{Q}^{-1}\left(\frac{T}{T_D - T_F}\right) + \sqrt{WT\alpha}\sum_{i=1}^{N} w_i\Gamma_i\right) \tag{17}$$

The CUR can be given by (18) which is combined by (14) and (17).

$$\eta = \frac{(1-\alpha)T}{\mathrm{Q}\left(\sqrt{\sum_{i=1}^{N} w_i^2\left(1+2\Gamma_i\right)}\,\mathrm{Q}^{-1}\left(\frac{T}{T_D - T_F}\right) + \sqrt{WT\alpha}\sum_{i=1}^{N} w_i\Gamma_i\right)T_F + T} \tag{18}$$

(18) shows that there are too many parameters which could influence the CUR. The bandwidth W is fixed and it depends on the spectrum specification of primary network. The SNR Γ_i of each CR user depends on the radio scenario and the receive equipment of CR user. The time duration of feature detection T_F depends on the character of primary user's signal. Conventionally the frequency of the fast detection $1/T$ is predefined. Therefore, the only parameter which can be adjusted is the α, i.e. the time duration of each fast sensing can be changed to optimize the CUR.

Intuitively if the sensing duration is too short, and simultaneously the ADT can be guaranteed, the probability of false alarm will be raised. As a result, the unnecessary feature detection will be frequently triggered. The unnecessary feature detection will waste a large amount of time which can be used for information transmission. But if the sensing duration is too long, the spectrum resources would be wasted by fast sensing process. Hence, there must be an optimal sensing duration which can maximize the CUR. From all above, it is obvious that the optimal scheme is to integrate information from all CR users, and then calculate the optimal sensing duration to inform each CR user.

To prove the existence of optimal sensing duration, the numerical simulation is brought about in our study. The simulation parameters are shown in Table 1. [6].

In Figure 3 the maximum CUR can be achieved when the sampling number M is at an appropriate value. However, the optimal sampling number is not fixed among

Table 1. The simulation parameters

Parameters	Value
Average Detection Time	0.5s
Sensing Interval	10ms
Feature Detection Time	100ms
Instantaneous SNR	-24dB, -20dB,-16dB, -12dB, -8dB
Sensing Bandwidth	6MHz
CR User Number	5

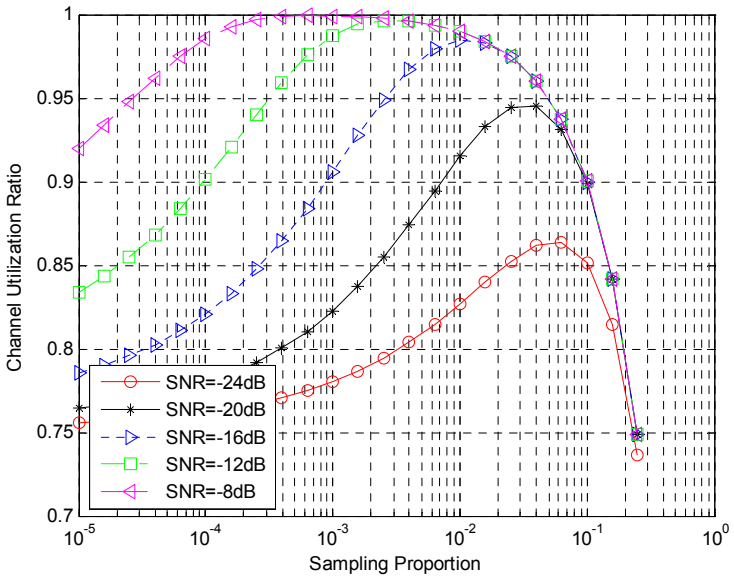

Figure 3. The channel utilization ratio vs. sampling proportion

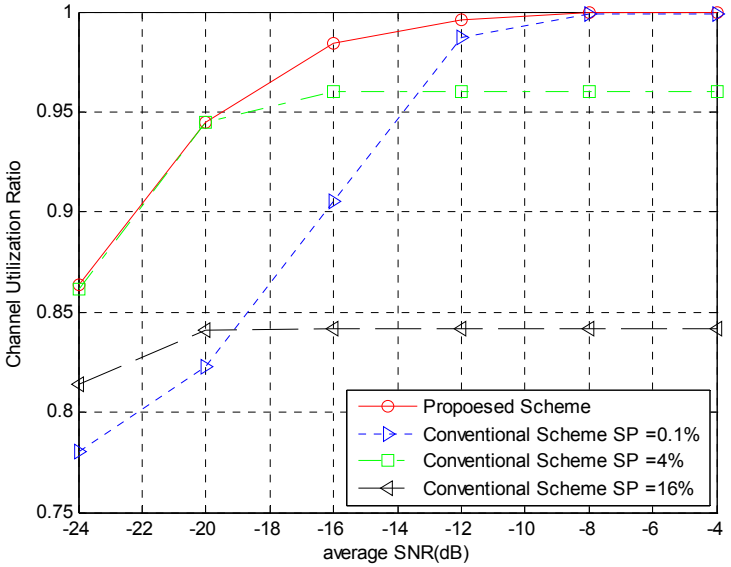

Figure 4. The channel utilization ratio vs. average SNR

different SNR scenarios. Although the optimal sampling number M cannot be calculated easily, the One-dimensional Search Method can deal with the problem. It is clear that in order to utilize the spectrum resource more efficiently, the sampling number must be dynamically adjusted according to the SNRs of CR users. Therefore, we propose a novel sensing time schedule for CR system, which is called dynamic adaptive sensing duration scheme:

At CR BS side:

1. Update the SNRs of all CR users.
2. Considering the target of ADT, calculate the sampling number M which can maximize the CUR.
3. Calculate the threshold λ of energy detection using equation (10)
4. Broadcast the sampling number M to all the CR users.

At CR User Side:

1. Update the sampling number M.
2. Use the updated sampling number M to determine sensing duration and send the sampling results back to BS.

In Figure 4 we compare our proposed scheme with three conventional ones whose sampling numbers are different from each other but not dynamically changed. It is obvious that the conventional scheme can gain a high CUR only when the SNRs are at an appropriate level. However the proposed scheme can always maximize the CUR, in other words the proposed scheme reaches the upper bound of the CUR for detection in CR system.

4. Conclusions

We have focused on how to maximize the CUR and produce interference small enough to primary network. We deduce the relationship between conventional ROC which is composed by Prob. of detection and that of false alarm and our proposed ROC which contains CUR and ADT. Our proposed scheme shows that the CUR can be maximized by optimizing time duration of energy detections according to different SNR conditions.

REFERENCES

[1] MITOLA J and MAGUIRE G Q. Cognitive radio: Making software radios more personal. Personal Communications, IEEE, 1999, 6: 13-18.

[2] GANESAN G and YE L. Cooperative spectrum sensing in cognitive radio, Part I: Two user networks. IEEE Transactions on Wireless Communications, 2007, 6: 2204-2213.

[3] UNNIKRISHNAN J and VEERAVALLI V V. Cooperative spectrum sensing and detection for cognitive radio. In IEEE Global Telecommunications Conference, GLOBECOM'07, 2007, 2972-2976.

[4] ZHI Q, SHUGUANG C, and SAYED A H. Optimal linear cooperation for spectrum sensing in cognitive radio networks. IEEE Journal of Selected Topics in Signal Processing, 2008, 2: 28-40.

[5] WEI Z, MALLIK R K, and LETAIEF K. B. Cooperative spectrum sensing optimization in cognitive radio networks. In IEEE International Conference on Communications, ICC'08, 2008, 3411-3415.

[6] IEEE 802.22-06/0003r3. A PHY/MAC proposal for IEEE 802.22WRAN systems, Part 2: The cognitive MAC. Mar. 2006.

[7] MA J and LI Y G. Soft combination and detection for cooperative spectrum sensing in cognitive radio networks. In Global Telecommunications Conference, GLOBECOM'07, IEEE, 2007, 3139-3143.

[8] TAHERPOUR A, KENARI N M, and JAMSHIDI A. Efficient cooperative spectrum sensing in cognitive radio networks. In

IEEE 18th International Symposium on Personal, Indoor and Mobile Radio Communications, PIMRC'07, 2007, 1-6.

[9] SOOK J W, J. GEUN D, H J AE, K. GWANGZEEN, and SUN S M. An efficient quiet period management scheme for cognitive radio systems. IEEE Transactions on Wireless Communications, 2008, 7: 505-509.

[10] GANESAN G, LI Y, and LI S. Spatiotemporal sensing incognitive radio networks. In IEEE 18th International Symposium on Personal, Indoor and Mobile Radio Communications, PIMRC'07, 2007, 1-5.

[11] GANESAN G, YE L, BING B, and LI S Q. Spatiotemporal sensing in cognitive radio networks. IEEE Journal on Selected Areas in Communications, 2008, 26: 5-12.

Communications and Network, 2009, 52-56
doi:10.4236/cn.2009.11008 Published Online August 2009 (http://www.scirp.org/journal/cn)

The Identification of Frequency Hopping Signal Using Compressive Sensing

Jia YUAN[1], Pengwu TIAN[2], Hongyi YU
Department of Communication Engineering, Institute of Information Technology, Zhengzhou, Henan, China
Email: [1] *hyajia@126.com*; [2] *tpw0802@163.com*

Abstract: Compressive sensing (CS) creates a new framework of signal reconstruction or approximation from a smaller set of incoherent projection compared with the traditional Nyquist-rate sampling theory. Recently, it has been shown that CS can solve some signal processing problems given incoherent measurements without ever reconstructing the signals. Moreover, the number of measurements necessary for most compressive signal processing application such as detection, estimation and classification is lower than that necessary for signal reconstruction. Based on CS, this paper presents a novel identification algorithm of frequency hopping (FH) signals. Given the hop interval, the FH signals can be identified and the hopping frequencies can be estimated with a tiny number of measurements. Simulation results demonstrate that the method is effective and efficient.

Keywords: compressive sensing, frequency hopping signal, identification

1. Introduction

With so many good advantages such as anti-jam, anti-interception, high security and so on, the technique of frequency hopping spread spectrum (FHSS) has been extensively applied in many areas, especially in military domain. The detection and interception of FH signals can be addressed in several methods of which wide band or channelized receiver, time-frequency distribution, and cyclostationary processing are typical ones [1-4]. For all the methods above, the extremely large requirement of measurements is one of the most serious disadvantages, which can be a bottleneck in the application of identification of high speed wide band FH signals. Recently, there have been some active attempts on signal processing with the advantage of CS for the sparse or compressive signals [5-8]. However, most of them are limited within the area of statistical inference tasks which need the prior knowledge of the probability density distribution of signals. Besides, it is seldom to be studied on how to develop the potential of CS to make processing of FH signal which is one of the most important sparse or compressive signals.

This paper makes use of the sparsity of FH signals on the local Fourier basis, and then presents a novel identification algorithm of FH signals with the compressive measurements. Given the hop interval, the FH signals can be identified and the hopping frequencies can be estimated without reconstructing the signals.

2. Compressive Sensing Background

2.1 Representation and Sparsity of Signal

Nyquist-rate sampling is the classical method to describe a signal with its bandlimitedness, while CS aims to completely describe a signal with its sparsity or compressibility to reduce the required number of measurements [9].

A signal x can be viewed as an $N\times 1$ column vector in $\mathbb{R}^N$ with elements $x[n], n=1,2,...,N$. Let the matrix $\Psi=[\psi_1,\psi_2,...\psi_N]$ have columns which form a basis of vectors in $\mathbb{R}^N$. And then, any signal x can be expressed as:

$$\mathrm{x}=\sum_{i=1}^{N} s_i\psi_i \quad \text{or} \quad \mathrm{x}=\Psi\mathrm{s} \tag{1}$$

where s is the $N\times 1$ column vector of weighting coefficients $s_i=\langle \mathrm{x},\psi_i\rangle$.

When we say that x is *K*-sparse, we mean that it is well reconstructed or approximated by a linear combination of just K basis vectors from Ψ, with $K\ll N$. That is, there are only K of the s_i in (1) are nonzero and $(N-K)$ are zero.

2.2 Incoherent Measurements

Consider a generalized linear measurement process of a signal x which is *K*-sparse. Let Φ be an $M\times N$ measurement matrix, $M\ll N$ where the rows of Φ

are incoherent with the columns of Ψ. The incoherent measurements can be obtained by computing M inner products between x and the rows of Φ as in $y_j = \langle x, \phi_j \rangle$. It can also be expressed as:

$$y = \Phi x = \Phi\Psi s = \Theta s \quad (2)$$

where $\Theta := \Phi\Psi$ is an $M \times N$ matrix. It is proved that Φ dose not depend on the signal x and it can be constructed as a random matrix such as Gaussian matrix. And the CS theory shows that there is an over-measuring factor $c > 1$ such that only $M := cK$ incoherent measurements are required to reconstruct x with high probability [9-11]. That is, only cK incoherent measurements include all of the salient information in the K-sparse signal x, which provides the theory support on the signal processing only given the incoherent measurements without reconstructing the signals.

2.3 Reconstruction

With the salient information included in the incoherent measurements, there have been several kinds of reconstruction algorithms including l_1 minimization, greedy algorithm, matching pursuit and so on [12-15]. Since this paper is concentrated on FH signal identification without signal reconstruction, we don't discuss reconstruction algorithms in detail here.

3. Compressive Identification for FH Signal

With the good sparsity of FH signals on the local Fourier basis, we now show that incoherent measurements can be used to solve the identification problem without ever reconstructing the signal. In this process, it is able to save significantly on the number of measurements required.

3.1 Compressive Identification Problem Setup

FH signals are sparse in a time-frequency representation as short-time Fourier transform, and they are always wideband when there is no prior restriction on the frequencies of the local sinusoid [16]. Therefore, the measurements obtained with the traditional Nyquist-rate sampling could be excessive and hard to meet with the present ability of hardware instrument.

Now, consider a FH signal which consists of a sequence of windowed sinusoids with frequencies distributed between f_1 and f_2 Hz. The bandwidth of this signal is $B=f_2-f_1$ Hz, which asks for sampling above the Nyquist rate of $2(f_2-f_1)$ Hz to avoid aliasing. However, the expression of the signal at any single hop is extremely simple: it consists of only one sinusoid of which bandwidth is extremely less than B [16]. Hence, CS could make identification of FH signals possible with a sampling rate that is extremely less than the Nyquist rate.

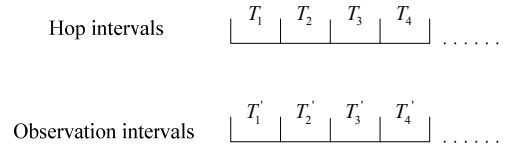

Figure 1. Hop intervals and observation intervals in the condition of 1-sparse

Let the observation interval equal to the hop interval. If the start of the FH signal can be captured exactly, the signal can be observed synchronously as depicted in Figure 1 and it has 1-sparse representation on the local Fourier basis within each of hop interval. Otherwise, as depicted in Figure 2, the signal within each of hop interval will have 2-sparse representation since only two of the hopping frequencies appear in every single observation interval.

We observe $y = \Phi x$ instead of x and our goal is to identify the FH signal and estimate its hopping frequencies with y and its connection with Θ.

3.2 1-Sparse Compressive Identification

The amplitudes of Fourier coefficients of some FH signal within an observation interval have been shown in Figure 3 which dedicates that all the coefficients are almost zero except for only one single large coefficient.

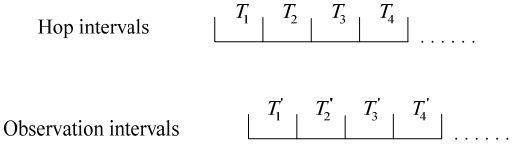

Figure 2. Hop intervals and observation intervals in the condition of 2-sparse

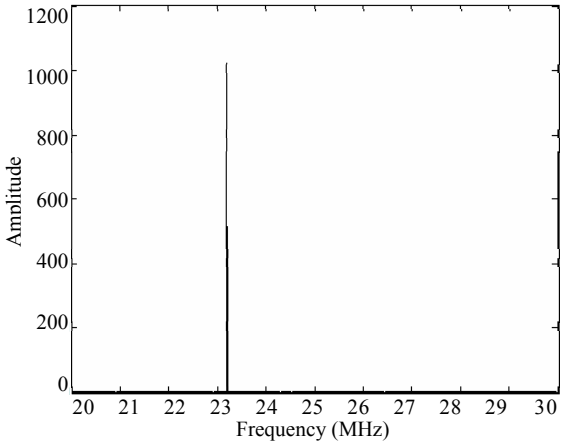

Figure 3. The amplitudes of Fourier coefficients of some FH signal within an observation interval in the condition of 1-sparse

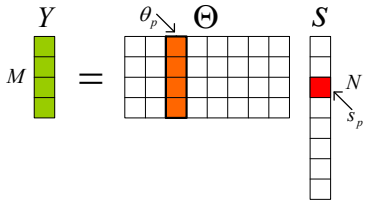

Figure 4. Measurement process in the condition of 1-sparse

The process of 1-sparse compressive measurement is depicted in Figure 4. We aim to find the position of nonzero s_p indicating the hopping frequency of a particular interval.

Since y is obtained by multiplying the nonzero s_p by its corresponding column vector θ_p, the hopping frequency can be estimated given y and Θ. A direct method to estimate the position of nonzero s_p is to search for the position of θ_p which can be decided by calculating the angles between y and each column vector of Θ in the vector space as only the angle between y and θ_p is zero in the ideal condition. Since Θ is also a random Gaussian matrix if Φ is chosen to be a random Gaussian matrix, the angle between y and another column vector of Θ is also zero with extremely low probability. Taking account of the effect of noise, we design the estimation algorithm of hopping frequency as follows:

1) Obtain the incoherent measurements y with Φ.

2) Calculate the cosine of angles between y and each column vector θ_i in the vector space

$$\cos(\theta_i, \mathrm{y}) = \frac{\theta_i^H \mathrm{y}}{\|\theta_i\|_2 \|\mathrm{y}\|_2} \tag{3}$$

where H denotes conjugate transpose.

3) Select the column vector that maximizes $\cos(\theta_i, \mathrm{y})$, and define the position of this vector as estimation of hopping frequency

$$\hat{f} = \arg \max_i \cos(\theta_i, \mathrm{y}) \tag{4}$$

After several intervals of observation and estimation of hopping frequencies, the time-frequency curve of the signal can be obtained and the FH signal has been identified in the condition of 1-sparse.

3.3 2 Sparse Compressive Identification

Different from the condition of 1-sparse, Figure 5 shows that there are two large coefficients within an observation interval as each observation interval covers parts of two hop intervals in the condition of 2-sparse depicted in Figure 2.

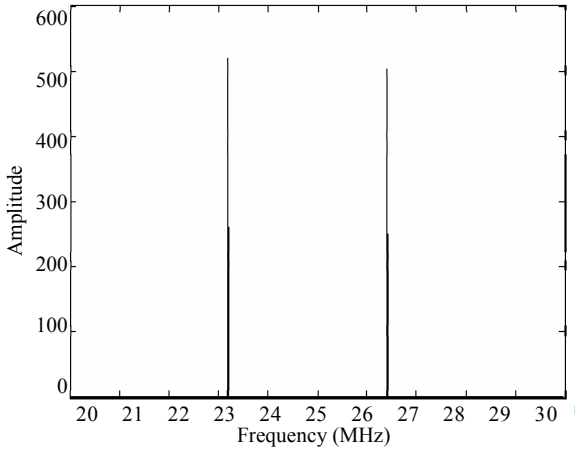

Figure 5. The amplitudes of Fourier coefficients of some FH signal within an observation interval in the condition of 2-sparse

The process of 2-sparse compressive measurement is shown is Figure 3 which dedicates that y is a linear combination of two column vectors θ_{p1} and θ_{p2} corresponding to the two nonzero coefficients s_{p1} and s_{p2} indicating the two hopping frequencies within a particular observation interval. And y is also a linear combination of another two column vectors of Θ with extremely low probability, since Θ is a random Gaussian matrix.

Therefore, the two hopping frequencies can be estimated by deciding the subspace comprised of θ_{p1} and θ_{p2} in Θ. The estimation algorithm is as follows:

1) Obtain the incoherent measurements y with Φ.

2) Calculate the orthogonal projection of y P_y onto the subspace L_{ij} comprised of any two column vectors θ_i and θ_j,

$$P_y = P_{L_{ij}}^{\perp} \mathrm{y} \tag{5}$$

where $P_{L_{ij}}^{\perp}$ is orthogonal projector expressed by:

$$P_{L_{ij}}^{\perp} = V(V^H V)^{-1} V^H \tag{6}$$

where $V = \left[\theta_i, \theta_j\right]$.

3) Select the two column vectors that maximize P_y onto the corresponding subspace, and define the positions of these two vectors as estimation of the two hopping frequencies

$$[\hat{f}_1, \hat{f}_2] = \arg \max_{i,j} (P_{\mathrm{y}}) \tag{7}$$

Taking account of the repetition of hopping frequencies within two consecutive observation intervals in the condition of 2-sparse, we can use the estimation results

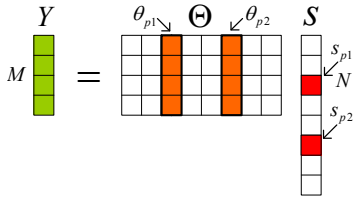

Figure 6. Measurement process in the condition of 2-sparse

of the former interval in the latter one. Only in the first interval, the algorithm is a kind of two-dimensional search as two column vectors have to be selected meanwhile. And in the successive intervals, it can be executed as a one-dimensional search (twice) as one column vector can be confirmed in according to the position information of two selected vectors of the former interval. This iterative processing can effectively reduce the computation, but obviously the error propagation can also be introduced. To solve this problem, an updating window is designed to separate the whole observation time into several segments of intervals. And in the first interval of every updating window, the two-dimensional search is executed all over again.

As the condition of 1-sparse, the time-frequency curve of the FH signal can also be obtained after several observation intervals, and the signal can be identified.

4. Simulation Results

To demonstrate the feasibility and effectiveness of the proposed algorithm, a wideband FH signal submerged in additive Gaussian white noise (AWGN) is considered to make the simulation experiments. This FH signal has ten hopping frequencies which are distributed uniformly between 20MHz and 200MHz, and the hop interval is 1ms, i.e. 1000 hops per second. The other main simulation parameters are as follows: 2048-point local Fourier basis is chosen to be Ψ, random Gaussian matrix is chosen to be Φ, and the number of observation intervals is set to 2000. Each experiment is made in the condition of both 1-sparse and 2-sparse.

First, the estimation performance of hopping frequency is evaluated by normalized mean square error (NMSE) through several intervals of observation, where NMSE is expressed by

$$NMSE = \frac{1}{N_{T'}} \sum_{i=1}^{N_{T'}} \left(\frac{\hat{f}_i - f_i}{f_i} \right)^2 \quad \textbf{(8)}$$

where $\hat{f}_i$ is the estimation of hopping frequency that expressed by f_i in the i th observation interval and $N_{T'}$ represents the number of observation intervals which is set to 2000 here.

Figure 7 and Figure 8 show the performance curves of 1-sparse and 2-sparse respectively.

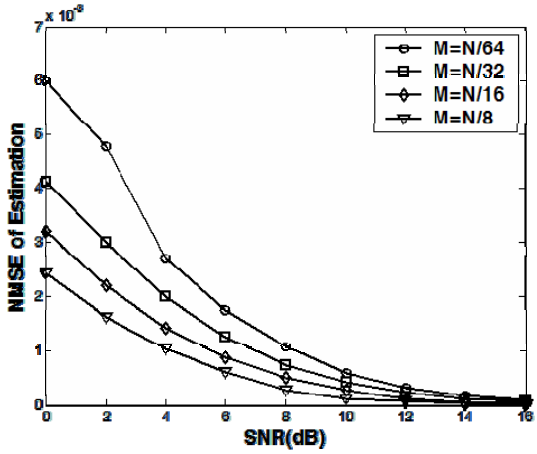

Figure 7. MSE of estimation with SNR in the condition of 1-sparse, where N=2048 and M represents the number of measurements used in this experiment experiments

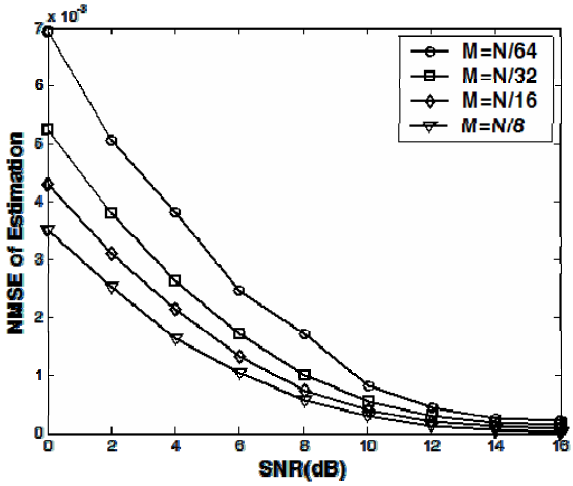

Figure 8. MSE of estimation with SNR in the condition of 2-sparse, where N=2048 and M also represents the number of measurements used in this experiment experiments. And the length of updating window is set to 40

Some conclusions can be demonstrated from Figure 7 and Figure 8. First, the hopping frequencies can be effectively estimated with a tiny number of measurements when SNR is higher than 8dB. Second, the performance of estimation degrades with the decrease of M, especially in low SNR. And finally, the performance of 1-sparse is better than that of 2-sparse.

Next, the estimated time-frequency curves of the FH signal of 1-sparse and 2-sparse are depicted in Figure 9 and Figure 10 respectively when $M = N/16$ and SNR is 10dB.

From the Figure 9 and Figure 10, it is shown that the estimated time-frequency curve is quite close to the real one and the FH signal can be effectively identified, especially in the condition of 1-sparse.

5. Conclusions

Based on CS, this paper provides a novel method for the identification of wideband FH signal with a tiny number of incoherent measurements, which is an inspiration of real-time wideband sparse signal processing. This method can also be of great help for the detection and recognition of wideband signal in the non-cooperative communication.

There are many opportunities for future research. Identification without the information of hop interval, the picket fence effect of Fourier transformation on the performance of identification, and the theoretical bounds of M with a given SNR would be discussed in the future work.

REFERENCES

[1] AYDIN L, POLYDOROS A. Hop-timing estimation for FH signals using a coarsely channelized receiver. IEEE Trans. Communication, Apr. 1996, 44(4): 516-526.

[2] ZHANG X, DU X, ZHU L. Time frequency analysis of frequency hopping signals based on Gabor spectrum method. Journal of Data Acquisition & Processing, Jun. 2007, 22(2): 123-135.

[3] HIPPENSTIEL R, KHALIL N, FARGUES M. The use of wavelets to identify hopped signals. In 1997 Fortieth Asilomar Conf. Signals, System & Computer, 1997, 1: 946-949.

[4] FAN H, GUO Y, XU Y. A novel algorithm of blind detection of frequency hopping signal based on second-order cyclostationarity. Proc. 2008 Image and Signal Processing Congr., 2008, 5: 399-402.

[5] HAUPT J, NOWAK R, YEH G. Compressive sampling for signal classification. In 2006 Asilomar Conf. on Signals, System & Computer, Oct. 2006, 1430-1434.

[6] HAUPT J, NOWAK R. Compressive sampling for signal detection. Conf. Rec. 2007 IEEE Int. Conf. Acoustics Speech and Signal Processing, 2007, 3: 1509-1512.

[7] DUARTE M F, DAVENPORT M A, WAKIN M B. Multiscale random projection for compressive classification. Conf. Rec. 2007 IEEE Int. Conf. Image Processing, 2007, 6: 161-164.

[8] DUARTE M F, DAVENPORT M A, WAKIN M B, BRANIUK R G. Sparse signal detection from incoherent projection. Conf. Rec. 2006 IEEE Int. Conf. Acoustics Speech and Signal Processing, 2006, 3: 305-308.

[9] BRANIUK R. Compressed sensing. IEEE Signal Processing Magazine, Jul. 2007, 24(4): 118-121.

[10] DONOHO D. Compressed sensing. IEEE Trans. Inform. Theory, Apr. 2006, 52(4): 1289-1306.

[11] CANDES E, ROMBERG J, TAO T. Robust uncertainty principles: Exact signal reconstruction from highly incomplete frequency information. IEEE Trans. Inform. Theory, Feb. 2006, 52(2): 489-509.

[12] DONOHO D, TANNER J. Sparse nonnegative solutions of underdetermined linear equations by linear programming. Proc. National Academy Science, 2005, 102(27): 9446-9451.

[13] TTOPP J A. Greed is good: Algorithmic results for sparse approximation. IEEE Trans. Inform. Theory, Oct. 2004, 50(10): 2231-2242.

[14] HAUPT J, NOWAK R. Signal reconstruction from noisy random projection. IEEE Trans. Inform. Theory, Sep. 2006, 52(9): 4036-4048.

[15] CHEN S, DONOHO D, SAUNDERS M. Atomic decomposition by basis pursuit. SIAM J. Sci. Comput., 1998, 20: 33-61.

[16] LASKA J, KIROLOS S, MASSOUD Y, BARANIUK R. Random sampling for analog-to-informaion conversion of wideband signals. IEEE Dallas/CAS Workshop on Design, Application, Integration and Software, Oct. 2006, 119-122.

The 6th International Conference on Wireless Communications, Networking and Mobile Computing

September 23–25, 2010, Chengdu, China
http://www.wicom-meeting.org/2010

Call For Papers

WiCOM serves as a forum for wireless communications researchers, industry professionals, and academics interested in the latest development and design of wireless systems. In 2010, **WiCOM** will be held in **Chengdu**, China. You are invited to submit papers in all areas of wireless communications, networking, mobile computing and applications.

Wireless Communications

- B3G and 4G Technologies
- MIMO and OFDM
- UWB
- Cognitive Radio
- Coding, Detection and Modulation
- Signal Processing
- Channel Model and Characterization
- Antenna and Circuit

Network Technologies

- Ad hoc and Mesh Networks
- Sensor Networks
- RFID, Bluetooth and 802.1x Technologies
- Network Protocol and Congestion Control
- QoS and Traffic Analysis
- Network Security
- Multimedia in Wireless Networks

Services and Application

- Applications and Value-Added Services
- Location based Services
- Authentication, Authorization and Billing
- Data Management
- Mobile Computing Systems

IMPORTANT DATES

Paper due:	March 10, 2010
Acceptance Notification:	May 10, 2010
Camera-ready due:	May 31, 2010

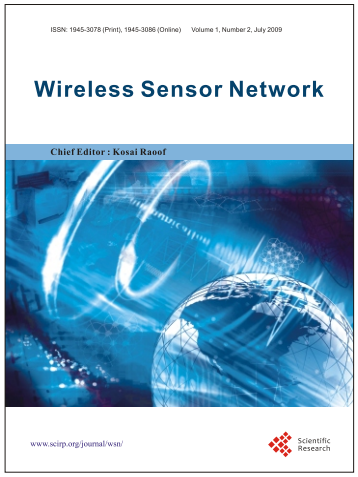

Wireless Sensor Network (WSN)

Call For Papers

http://www.scirp.org/journal/wsn

ISSN 1945-3078 (Print) ISSN 1945-3086 (Online)

WSN is an international refereed journal dedicated to the latest advancement of wireless sensor network and applications. The goal of this journal is to keep a record of the state-of-the-art research and promote the research work in these areas.

Editor-in-Chief

Dr. Kosai Raoof , GIPSA LAB, University of Joseph Fourier, Grenoble, France

Subject Coverage

This journal invites original research and review papers that address the following issues in wireless sensor networks. Topics of interest are (but not limited to):

- Network Architecture and Protocols
- Self-Organization and Synchronization
- Quality of Service
- Data Processing, Storage and Management
- Network Planning, Provisioning and Deployment
- Integration with Other System
- Software Platforms and Development Tools
- Routing and Data Dissemination
- Energy Conservation and Management
- Security and Privacy
- Developments and Applications
- Network Simulation and Platforms

We are also interested in short papers (letters) that clearly address a specific problem, and short survey or position papers that sketch the results or problems on a specific topic. Authors of selected short papers would be invited to write a regular paper on the same topic for future issues of the WSN.

Notes for Intending Authors

Submitted papers should not have been previously published nor be currently under consideration for publication elsewhere. Paper submission will be handled electronically through the website. All papers are refereed through a peer review process. Authors are responsible for having their papers checked for style and grammar prior to submission to WSN. Papers may be rejected if the language is not satisfactory. For more details about the submissions, please access the website.

Website and E-Mail

http://www.scirp.org/journal/wsn

Email: wsn@scirp.org

Communications and Network, 2009, 01-56
Published Online August 2009 in SciRes (http://www.scirp.org/journal/cn).

TABLE OF CONTENTS

Volume 1, Number 1, August 2009

 CN

ISSN: 1949-2421
9771949242001 01